Solidification Phenomena In Steel Weld Metal.

SOLIDIFICATION PHENOMENA IN STEEL WELD METAL

by

Harold Samuel Gurev

A Dissertation

Presented to the Graduate Faculty

of Lehigh University

in Candidacy for the Degree of

Doctor of Philosophy

Lehigh University

1962

Approved and recommended for acceptance as a dissertation in partial fulfillment of the requirements for the degree of Doctor of Philosophy.

5-31-62
(Date)

R S Stark
(Professor in Charge)

Accepted, 5/31/62
(Date)

Special committee directing the doctoral work of Mr. Harold S. Gurev

F. H. Black
(Chairman)

Ivan V. Latshaw

Walter D Bleyaty

R S Stark

Acknowledgements:

The author expresses his sincere appreciation to the individuals who have inspired and directed his introduction to the study of metallurgy. Special thanks are due to Professor R. D. Stout for suggesting and guiding this dissertation investigation. The Linde Company generously supported this investigation through the Linde Company Graduate Fellowship.

Table of Contents

	Page No.
Certificate of Approval	ii
Acknowledgements	iii
List of Tables	v
List of Figures	vi
List of Illustrations	vii
Abstract	1
Introduction	3
Experimental Procedure	12
Welding Procedure	12
Metallographic Examination	13
Alloy Additions	15
Results and Discussion	17
Weld Width	27
Weld Reinforcement Height	28
Reinforcement Area	29
Plate Preheating	32
Weld Crater Length	37
Grain Size	43
Segregation and Freezing Patterns	45
Conclusions	51

List of Tables

Table		Page No.
I	Chemical Analyses of Weld Materials	55
II	Weld Addition Analyses	56
III	Weld Nugget Geometry Date	57
Iv	Chemical Analyses of Weld Metal Drillings	60

List of Figures

Figure		Page No.
1.	Schematic Illustration of Bead on Plate Weld	62
2.	Weld Penetration as a Function of Welding Current at Two Voltage Levels	63
3.	Weld Penetration as a Function of Travel Speed at Five Different Amperage Levels	64
4.	Efficiency Factor E_2 $\frac{\text{Energy to Melt Weld Metal}}{\text{Energy Supplied to Arc}}$ As a Function of Travel Speed	65
5.	Weld Penetration as a Function of Effective Heat Input (E.H.I.)	66
6.	Maximum Penetration as a Function of Power Supplied to Welding Arc	67
7.	Effect of Voltage on Penetration at Travel Speed of 20 Inches per Minute	68
8.	Schematic Illustration of Separation of Penetration into Elliptical Weld Pool Depth, A, and Finger Height, B, as well as Two Representative Weld Bead Cross Sections Indicating Extreme A/B Ratios.	69
9.	Elliptical Pool Depth A, as a Function of E.H.I. at Different Amperage Levels	70
10.	Penetration Finger Height, B, as a Junction of Voltage at 20 Inches per Minute and the Current Levels Indicated.	71
11.	Finger Height, B, as a Function of Welding Current at 20 Inches per Minute and at Two Voltage Levels	72
12.	Finger Height, B, versus Travel Speed	73
13.	Finger Height, B, as a Function of Effective Heat Input	74
14.	Penetration Ratio (Finger Height/Elliptical Pool Depth) versus Travel Speed	75

List of Figures - Continued

Figure		Page No.
15.	Penetration Ratio, B/A, as a Function of Voltage at 20 Inches per Minute and Current Levels Indicated.	76
16.	Weld Width as a Function of Travel Speed. Dotted Lines Indicate Width of Melted Hole in Base Plate for Cases of Undercutting	77
17.	Weld Bead Width as a Function of Effective Heat Input	78
18.	Weld Bead Width versus Voltage at 20 Inches per Minute	79
19.	Weld Reinforcement Height Versus Travel Speed	80
20.	Weld Reinforcement Height as a Function of Effective Heat Input	81
21.	Weld Reinforcement Height as a Function of Voltage at 20 Inches per Minute	82
22.	Weld Reinforcement Height versus Current Level at Two Set Voltages	83
23.	Reinforcement Volume (per inch of weld) as a Function of Travel Speed	84
24.	Reinforcement Area as a Function of Effective Heat Input	85
25.	Reinforcement Area as a Function of Current Level	86
26.	Reinforcement Area as a Function of Welding Voltage at 20 Inches per Minute	87
27.	Reinforcement Area as a Function of Lineal Heat Input	88
28.	Volume of Base Plate Melted (per inch of weld) as a Function of Lineal Heat Input	89
29.	Base Plate Area Melted as a Function of Welding Voltage at 20 Inches per Minute	90
30.	Total Area of Weld Nugget as a Function of Lineal Heat Input	91

List of Figures - Continued

Figure		Page No.
31.	Nugget Area as a Function of Current Level	92
32.	Nugget Area as a Function of Welding Voltage at 20 Inches per Minute	93
33.	Melting Ratio (Base Plate Melted/Total Nugget Area) as a Function of Lineal Heat Input	94
34.	Melting Ratio as a Function of Welding Current	95
35.	Melting Ratio as a Function of Voltage	96
36.	Increase in Penetration as a Function of $\Delta H_T/\Delta H_{1900^\circ K}$ (Ratio of Enthalpy Supplied by Preheat to Enthalpy Required to Melt and Superheat Weld Metal)	97
37.	Effect of Preheat Temperature on Weld Contours Produced at 410 Amperes, 28 Volts, 30 Inches per Minute(7X, Nital Etch)	98
38.	Weld Bead Width as a Function of Preheating Enthalpy Parameter	99
39.	Base Plate Area Melted as a Function of Preheat Enthalpy Parameter	100
40.	Reinforcement Area as a Function of Preheat Enthalpy Parameter	101
41.	Weld Reinforcement Height as a Function of Preheat Enthalpy Parameter	102
42.	Reciprocal of Base Plate Area Melted as a Function of $\Delta H_{1900^\circ K} - \Delta H_{\text{Preheat Temperature}}$ to Indicate Hyperbolic Relation Between B.P.M. and $\Delta H_{1900^\circ K-T}$	103
43.	Maximum Travel Speed Producing Weld Bead Free of Undercutting as a Function of Current Level Employed	104
44.	Minimum Width of Base Plate Melted as a Function of Arc Power	105
45.	Bath Length, as Measured in Crater, as a Function of Travel Speed	106

List of Figures - Continued

Table		Page No.
46.	Bath Length, L, as a Function of Arc Power at Two Voltage Levels	107
47.	Bath Length as a Function of Preheat Temperature Parameter	108
48.	Average Weld Bead-Base Plate Contact Angle e as a Function of Travel Speed	109
49.	Weld Bead Contact Angle e as a Function of Preheat Enthalpy Parameter	110
50.	Austenite Grain Size, as Measured at Lateral Extremities of Weld in Direction to Heat Flow, as a Function of $\sqrt{\text{Heat Input}}$	111
51.	Representative Transverse and Longitudinal Macrographs	112
52.	Map Locations of Minima Noted in Microhardness Traverses of Weld A-2.	116
53.	Macrostructure of Weld M32, Prepared by Welding Over 4% C Iron Powder.	117
54.	Sulphyr Prints of Welds Prepared by Welding Over Iron Sulphide Powder	118
55.	Effect of Travel Speed on Proportion of Penetration Which is Sulphur-free "Dead Zone"	119

Abstract:

The mechanical properties of weld metal are a direct result of the action of the welding arc conditions on the base plate-electrode combination selected through alterations of the deposit geometry, chemistry and thermal history. The present experimental study, conducted on the consumable electrode, inert gas shielded (M.I.G.) welding of mild steel, investigated several facets of this weld metal property dependence.

Such geometric parameters of practical interest as weld width, height, penetration depth, nugget area and reinforcement area were correlated to the effect of current and travel speed on net heat input as corrected for changing arc efficiency. Discontinuities were noted in weld geometry at voltages and current levels associated with the spray-drop transfer mode transition. Under conditions of spray transfer, voltage increases produced increased weld width, yet significant decreases in weld height, penetration, and reinforcement area.

This anomalous decrease in weld penetration, noted generally in several welding processes, was found to be caused by the decrease in depth of the characteristic finger penetration associated with the M.I.G. process.

New insight into the phenomena of undercutting is provided by experimental observations of the width of base plate melted under independent variations of travel speed. It was shown that, with increasing travel speed, this gouged width rapidly approaches a constant value which was a linear function of power input to the arc. From these observations it was concluded that the lateral range of oscillation of the cathode

spot is independent of travel speed and increases with power input giving rise to this minimum melted width. Hence undercutting will occur when the weld metal lacks sufficient fluidity to fill this groove width.

Variations in weld heat input without alteration in welding arc conditions were achieved by preheating weld plates. Such beads exhibited increases in geometry which were proportional to the enthalpy supplied the plate by the preheating. Thus penetration, to cite the parameter of greatest practical importance, is a linear function of heat input if arc conditions are maintained constant. It was also observed that preheating prevented undercutting by increasing bead width and not by decreasing gouged width.

Segregation in the weld bead was found to be strongly influenced by weld geometry. Such segregation, accentuated by intentional additions of carbon and sulfur to the weld plate in the path of the arc, was most pronounced under conditions where a well defined narrow finger penetration was produced. Microhardness surveys, sulphur printing and microscopic observation revealed both layering of segregated strata parallel to the fusion line, as well as presence of alloy-poor regions at the finger tip.

A general study of the austenite grain orientation and austenite grain size in weld beads indicated that freezing patterns were significantly different as each variation of weld parameter produced a different weld contour.

Introduction:

The mechanical properties of a metal structure depend on the chemical analysis, thermal and strain history of the various portions of the structure. Thus one might predict the service behavior of a welded structure if one knew the composition, mechanical and thermal history at each point in the body.

Determination of such data for the nonfused portions of welded specimens (the heat affected zone) has constituted a major effort in welding research in recent years. The present study will look at variations in such chemistry and thermal treatment of the weld metal itself, seeking to establish a rational basis for forecasting the structure, and hence the mechanical behavior of weld metal.

The most fundamental approach to such a correlation of welding conditions and weld properties would be the calculation of the time-temperature relationships in any given portion of a weld by application of basic principles of heat transfer, followed by the experimental verification of such relationships. The chemical analysis of any point could then be calculated on the basis of known reaction rates and such predicted analyses verified by microchemical analysis. The high thermal fluxes associated with the welding process, as well as the relatively small volumes of metal affected by such fluxes, have combined to raise serious experimental obstacles to such determinations of microchemistry and micro-thermal history.

Temperatures in the welding process have been predicted by Rosenthal(1)+, Rykalin(2), and Wells(3)+, among others, but experimental verifications, though accurate away from the weld pool, develop gross deviations there. Basic shortcomings of such overly simplified mathematical models lie in assuming the weld arc, a finite region where complex chemical and electrical phenomena occur, to be a point or line source of heat, and in failure to consider the release of heat of fusion on solidification.

In consumable electrode welding, the electrode metal is melted and crosses the arc to the work under the propelling electrical, magnetic and gravitational forces. The retarding forces on a given drop include the surface tension forces associated with the formation of the free surface of the globule. Such globules on entering the weld pool give up heat to the cold mass of surrounding base plate and receive heat from the action of the passing arc.

Though any given portion of the weld metal experiences rapid transient thermal effects, a quasi-steady state exists for temperatures considered with reference to the arc itself. Predictions of shape and location of isotherms below the melting range, which describe the heat affected zone, have been experimentally verified and correlated to metallurgical structural changes encountered in practice.

+ Figures in () refer to Bibliography at end of dissertation.

However, experimental results describing isotherms in the weld metal pool are almost nonexistent and even measurements of peak pool temperatures are both sparse and in poor agreement. For the case of steel weld metal, Erokhin(4) reported the temperature of globules leaving steel electrodes to be between 2000° and 2400° C, a value considered too high by Jackson(5), who states that globule temperatures are not expected to be much above the melting point of the electrode. Calorimetric measurements of mild steel weld pools produced by the submerged arc process indicated an (apparently mean) temperature of 1770° C. Christensen and Chipman(6), after failing to obtain reproducible thermocouple readings of covered electrode weld pools, calculated a maximum temperature of nearly 2000° C on the basis of chemical analyses of slag-metal reactions in the process. Christensen(7) attempted further measurements by thermocouples and could conclude only that "liquid weld metal temperatures above 2000° C may be expected in the case of steel....directly beneath the arc only".

An indication of the magnitude of thermal gradients which exist within the limited confines of a weld pool may be found in the work of Rabkin(8), who performed such measurements in welds of aluminum, an element exhibiting much higher thermal conductivity than iron. Rabkin found temperatures ranging from 1600° C beneath the arc to 1100° C

at the sides of a weld puddle produced under automatically controlled conditions. Similar measurements were made by Frumin(9) for steel welding, whose results are not yet available to the author.

Lack of more complete thermal data has prevented much quantitative analysis of chemical changes produced by the welding process. However, some largely qualitative evidence has appeared, again primarily in the Russian language, to indicate that a variety of anomalous chemical inhomogeneities can be produced under certain welding procedures.

Since freezing rates in weld pools are generally quite high, interdendritic spacing would be expected to be much smaller than commonly encountered in other cast structures and hence microsegregation caused by partition of impurities into interdendritic interstices would be on a much finer scale in welds. However, several types of macrosegregation are noted in weld metal which are unique to the highly dynamic freezing conditions produced by the passage of such intense heat sources over massive base plates which quench effectively through intimate liquid-solid contact. Such evidence of segregation is at variance with commonly held opinions that weld beads are homogeneous in alloy content by virtue of the drastic mixing action of the arc and the high degree of superheat received by the pool.

Livshits(10), Bruk(11) and Petrov(12) have presented microchemical analyses, metallographic and autoradiographic evidence of the formation, during the welding process, of a pair of narrow zones at the fusion line, which can differ quite drastically in carbon content if the base plate and weld metal contain widely different amounts of elements which are strong carbide formers. The degree of this highly localized impoverishment and enrichment can extend well beyond the range of gross carbon content of base plate and weld metal. To trace one possible case of such segregation, consider a base plate-electrode combination which under a given set of welding conditions yields weld metal whose average carbon content is less than the base plate and whose content of such alloying elements as vanadium, chromium, titanium, etc., is also less than the base plate. During the welding process, these elements in the strip of base plate in the heat affected zone at the fusion line will deplete the thin zone of liquid weld metal in contact with it of carbon, producing movement of carbon in a direction opposite to the concentration gradient of that element. Such action, leaving a zone of carbon enriched metal below the fusion line and carbon impoverished metal above, would be accentuated by any subsequent heat treatment process which would allow additional time for the carbon atoms to seek the carbide forming elements.

Makin(13) has presented autoradiographic evidence of the formation of narrow zones, depleted in phosphorus, at the weld bead extremities in the welding of fully austenitic stainless steel, which he has ascribed to rejection of this element to the center of the weld puddle during freezing. No evidence of such a segregation of sulphur under these conditions was found by Makin.

A more general mode of macrosegregation has been noted by Makara and Rossoshinskii(14), Petrov(12), Bruk(11), Movchan(15), Poznak(16), and Makin(13) for the heterogeneous distribution of carbon, sulphur and phosphorus in the freezing of steel weld metal. Such investigators report the formation of series of thin layer lines, alternately enriched and impoverished in the elements listed above, extending parallel to the fusion line and persisting well into the weld bead. Such stratification is finely spaced near the fusion line and becomes progressively coarser toward the top of the weld bead, and is most frequent for welding conditions which produce high rates of cooling and a sharp temperature gradient in the weld pool before the solidification front.

Explanations of the mechanism of formation of such strong, highly localized concentration gradients all ascribe them to the discontinuous nature of the freezing of weld metal. Such discontinuity may arise from rapid fluctuations in heat and mass transferred by the arc setting up wave-like action in the pool and/or by the release of latent heat of fusion by solidifying metal. The nature of such freezing

interruptions has been described as either simple thermal arrest while excess heat is dissipated or even remelting of some metal.

Observations of such layering under conditions where freezing occurred subsequent to cutting off the source of heat, as in craters of arc welds or in weld nuggets produced by spot welding, leads to the conclusion that layering can result just from thermal imbalance produced by release of latent heat of fusion, though fluctuations in the heat source may serve to magnify the effect.

During such arrests in the solidification process, time is available for diffusion of such elements as carbon, sulphur and phosphorus, from the solid layer to the liquid metal in contact with it. This enriched layer will be constrained from freezing immediately both by the need for dissipation of the heat of solidification of the solid layer it is in contact with, and the fact that such enrichment serves to depress the freezing range of the liquid. The process will be repeated after this layer freezes and seeks to release its latent heat. Thus it can be reasoned that a high cooling rate will encourage layering by increasing the rate at which the latent heat of fusion is released, while a high temperature gradient in the liquid metal before the solidification front will increase the period of the thermal arrest and augment segregation.

Muir(17) studied the chemical heterogeneity of welds by depositing mild-steel wire on 18-8 austenitic stainless steel base plate by the metal arc inert gas shielded (MIG) process. The pattern of mixing in the weld pool could then be studied by macro-etching of weld sections. (The welding conditions this investigator used produced a well defined finger at the base of the weld bead penetration, a phenomenon which is generally observed in MIG welding of steel with monatomic gas mixtures.) A zone of heterogeneity at the base of the beads was found and termed layering. Such layering did not take the form of continuous, thin, alternate layers of enriched and impoverished metal, but was composed of islands of base plate composition, seemingly entrapped by the turbulence of the weld bead and frozen before diffusion could take place. Increasing voltage and decreasing oxygen content in the cover gas had the simultaneous effects of increasing the severity of the finger penetration and the extent of island layering described above. To support the theory that such islands were formed as described above, alterations in the degree of turbulence produced by varying the angle of inclination of welding torch to the travel direction resulted in corresponding changes in the amount of layering exhibited.

The examples presented above illustrate how the complex thermal processes act with the initial base plate geometry, and plate-electrode chemistry to determine weld structure,

chemistry and hence properties. Welding parameters influence properties through a rather involved set of interactions producing changes in the complex modes of heat and mass transfer through the arc. Thus a change in a weld parameter will produce alterations in the characteristics of the arc; i.e., its length, width, temperature, mode of metal transfer, etc. Such arc events, and their dependence on electrical conditions has been studied extensively (primarily in non-consumable electrode welding to reduce variables operative) and have been summarized by Jackson(5) and Lesnewich(18).

The tie between such arc events and corresponding thermal patterns set up in the weld pool is a crucial link in the welding process which, because of extreme experimental difficulties, has received little attention in the past. Direct investigation of these relationships is not within the scope of the present dissertation. The present work is concerned with direct measurements of the effects of these thermal patterns on weld metal structure and chemistry, the final link in the dependence of weld properties on weld process parameters. It is expected, however, that through just such systematic observations of the effects of arcs on weld metal, conclusions may be reached as to the probable nature of the arc event-thermal pattern interactions.

Experimental Procedure:

The investigations carried out in the course of this dissertation can be divided into three major experimental programs.

The first stage was the preparation of a series of single pass, bead on plate, metal arc shielded inert gas consumable electrode welds (MIG), over a wide range of welding conditions with subsequent macro and microanalysis of the weld metal so produced through measurements of hardness, chemical analysis, weld bead geometry, and grain structure.

A second program involved the preheating of plates and their subsequent welding at plate temperatures as high as 1600° F. Resultant weld beads were examined to note how the preheat condition had altered their geometry and structure.

In the third phase, alloying elements in the form of crushed powders were added to the weld metal by welding over the powders arranged in a shallow groove on the base plate. The primary interest of this program was the determination of the location of such alloying elements in the weld nugget as an indication of segregation tendencies of the welding process.

Welding Procedure:

All welding was performed with a Linde SWM-3 inert gas metal arc controller and an H-16 MIG torch. The inert gas mixture employed, at a total flow rate of 55 cubic feet per

hour, was 'M-5', which contains 95% argon and 5% oxygen for increased arc stability. All welding was performed by direct current, reverse polarity (by this convention the weld wire is positive.) The welding wire employed was 1/16 inch diameter Oxweld 65 and the base plate was one inch thick ABS-B mild steel. Their analyses are presented in Table I.

The torch was mounted on a Linde type OM-48 Machine Carriage whose travel speed (S) could be varied by an electronic governor over the range of 3 to 90 inches per minute. The base plate was held by grounding clamps to a stationary bed during welding. Welding power was supplied by a Westinghouse "Rectarc" rectifier set rated at 800 amperes. Welding current (I) and voltage (V) were varied in turn over a range from 235 to 450 amperes and from 18 to 40 volts, though, as noted in the Results Section, arc stability could not be maintained at all possible combinations of these two parameters utilized.

Bead-on-plate welds were laid along the longitudinal axis of 6-inch by 12-inch by 1-inch plates which had been prepared by surface grinding and cleaned of adherent oil and dirt.

Metallographic Examination:

Transverse sections were sawed from all welds prepared. The desired section, selected randomly from any part of the weld length except the first and last two inches, were surface ground and polished metallographically. These sections

were then etched by immersion in a 5% nital solution and examined.

A studio-type macrocamera, capable of from 6x to 15x magnification, was employed to photograph each weld section. These macrophotographs, enlarged 2x, were studied to determine the parameters illustrated by Figure 1:

a. penetration - p

b. weld width - w

c. weld height - h

d. reinforcement area - R

e. area of base plate melted - B.P.M.

f. contact angle of weld bead on flat base plate - θ

Linear dimensions were calculated by measurement of a calibrating inch scale photographed with each specimen. The areas noted were determined by planimetry, using the average of at least five readings for each value reported.

To determine the degree to which the random transverse sections selected for study were actually representative of the geometry of the entire weld established between initial starting transient conditions, and formation of the end crater, four weld beads were selected at random and sectioned transversely at four or five evenly spaced intervals. The linear dimensions of each of these sections were found to vary by less than 2% for any one weld bead. Thus it was felt that the single random sampling method provided valid information about the geometry of the weld beads prepared.

The contact angles noted were measured on the macrographs by drawing a tangent to the weld bead at the base plate with the aid of a 3x hand magnifier. The contact angle e was then read with a protractor to the nearest 1/2° interval.

Alloy Additions:

The base plates previously described were prepared for welding with single alloying element addition by machining, on the longitudinal axis, a circular groove of 5/8 inch radius and 0.060 inch depth. Into this groove was placed either carbon or sulphur bearing powder prepared by crushing, screening and rejecting all particles larger than 50 mesh. For carbon additions, chips of a 4% C cast iron were utilized, and FeS powder was added when S was desired. Chemical analyses of these two powders are presented in Table II.

The powders were weighed into one gram lots, and placed into the groove at the rate of one-half gram per inch of groove length. The powders were held in place by application of Microbraze, a proprietary brazing cement. Subsequent holding of the plates at 350° F for two hours prior to welding drove off the organic binders in the cement, and the remainder of the Microbraze vaporizes, without residue, in the heat of the welding process.

Plate Preheating:

Several series of welds were prepared by welding over plates preheated as high as 1600° F. For such experimental conditions, smaller plates (3 inches by 6 inches by 1 inch) were selected for convenience, since the plates were preheated in an air furnace to a temperature above the weld plate preheat level desired, transferred to the welding table and then welded when at the desired temperature. Plate temperature was read with a chromel-alumel thermocouple imbedded into the center of the plate. (It was determined experimentally by comparison of room temperature weld geometry, that there was no significant difference in weld size between the subsize and normal plates for the relatively rapid welding speeds employed in the preheating study.)

RESULTS AND DISCUSSION:

Penetration:

Weld penetration, defined as the maximum extent of the weld nugget into the thickness of the plate relative to the original base plate surface, was found to vary, in different modes, with changes in the three welding parameters studied. Such a definition of penetration has practical value, for it describes the ability of a welding process to provide a fusion zone of sufficient depth to bond components into a mechanically integral weldment. Yet penetration so measured is actually the sum of the crater depth below the base plate surface and fusion depth below the crater. For a basic understanding of the effect of welding conditions on events occurring in the weld pool, separation of penetration into these components is essential, since the crater is the liquid surface level which the arc contacts.

Unfortunately measurements of crater level during various welding conditions are almost non-existent in the literature, owing to the extreme experimental difficulties associated with such studies. It has been hypothesized(5) that crater level may vary from plate level to the entire penetration level depending, of course, on conditions employed.

Reported penetration data was analyzed by Jackson(19), who found that such penetration was proportional to an empirical welding technique performance factor which he calculated to be $\sqrt[3]{\frac{I^4}{SV^2}}$. This relation was found to hold for

available data on covered electrode welding, submerged arc, and MIG welding(5), the constant of proportionality varying with the particular process and welding materials employed.

In the present investigation, the variation with current was most direct; Figure 2 indicates that, with other conditions constant, penetration is linearly proportional to current over the range studied. Furthermore, the parallelism of the plots at the two voltages studied indicates the simplicity of the increase in penetration as higher heat inputs are produced by augmented current. (The current level of the discontinuity in the data obtained at 24 volts coincides with the transition current from spray to drop transfer at lowering currents as observed during the welding operations, and is in agreement with Lesnewich(18).)

Increasing travel speeds, as shown in Figure 3, cause a general decrease in penetration with the exception of extremely low speeds at the lower current levels, where an anomalous increase in penetration was measured. At such extremely low speeds, a relatively thick layer of molten weld metal builds up beneath the impinging arc, thus cushioning the deep penetrating argon arc. With slightly higher speeds, the protective layer of melt thins out to allow the arc to act more fully on the solid plate.

The depth of this molten layer below the arc was measured by Rabkin(8) in the automatic welding of aluminum at 390-430 amperes and 34-41 volts. He found this depth fairly

constant at approximately 0.15 inches at speeds below 11 inches per minute, and then decreasing sharply to less than 0.04 inches at 14 inches per minute. (These quantitative results are pertinent, of course, only to the particular conditions investigated, but they do affirm the postulated behavior pattern of this molten layer.)

Intuition might lead one to conclude that changes in travel speed influence penetration, and other weld bead parameters, simply by altering the heat input per unit length. Before exploring the validity of such an assumption, some discussion of the calculation of such heat input is in order. From electrical measurements of current flowing through the circuit, voltage drop between weld wire contact and base plate ground, and arc travel speed, one may compute the energy consumed by the welding process per inch of weld produced. However, energy losses occur in the arc as radiation, metal splatter, etc.

Two methods of determining the efficiency of energy transfer by the arc may be considered. The more direct method would be to measure, by calorimetry, the total energy rise in the base plate and thus compute:

$$E_1 = \frac{q/l}{IV/S}$$

Where q = total energy rise in plate
l = length of weld bead
I = welding current
V = welding voltage
S = travel speed

This method was utilized by Christensen(7), who reported a consistent efficiency, E_1, of 0.66 to 0.69 in MIG welding of mild steel over wide variations of welding conditions.

An alternative method defines melting efficiency as:

$$E_2 = \frac{NA\ (\Delta H)\ 1\sigma}{IV/S}$$

Where NA = nugget area

ΔH = enthalpy required to melt and superheat a unit weight of weld metal

σ = density of weld metal

There are two assumptions implicit in defining this as a measure of the efficiency of energy transfer by the arc. First the weld metal is assumed to have a uniform maximum (or average) temperature, 1900° K, and secondly it is assumed that the rate of heating below the arc is so great that the entire depth and width of any differential volume of the weld is melted instantaneously. As the arc travels, a very steep thermal gradient exists in front of it.

With the limiting assumptions in mind, E_2 was calculated for each bead produced and plotted against travel speed in Figure 4. It is readily apparent that E_2 is strongly dependent on speed but relatively independent of current level.

Effective heat input was defined as $(NA)1\Delta H\sigma$ or E_2 (IV/S) and thus can be seen to be proportional to measured nugget area. Penetration at the various current levels was seen to behave in quite regular modes with this EHI parameter (Figure 5).

Penetration, at low EHI, is independent of current level employed and breaks away from this common behavior at various heat inputs. The travel speed at which each current level series breaks away was calculated from the experimental points closest to the break.

Current	Penetration at breakaway	Travel speed at breakaway
260 amperes	0.120 inches	27 inches per minute
300	0.200	24
350	0.225	23
400	0.330	16

Further observation of Figure 5 shows that each current level rapidly approaches a constant penetration level independent of EHI (and hence of speed) at lower speeds than the above critical speed. This maximum penetration is a linear function of welding power input (Figure 6) and its existence indicates that the blocking molten layer limits the range of utility of the process studied. In passing it should be noted that extremely high heat input welds, beyond the range described, were in excess of the capacity of the equipment employed. Though it may be argued that the quantitative results may be in error at the highest current levels, the maximum penetration levels noted at lower currents are well within the limits to avoid the influence of plate thickness on weld heat flow. A modest extrapolation of Figure 5 to zero EHI leads one to expect zero penetration.

Voltage exerts a most curious effect on penetration (Figure 7). All voltage increases above 24 volts, despite the resultant increased electrical energy consumption, resulted in linear drops in penetration at all current levels studied. Voltage increases below the 24 volt level, at 260 and 390 amperes, however, resulted in penetration increases. These welding conditions produced the only arcs exhibiting drop transfer. (Welds above 300 amperes were all of the spray transfer mode, and attempts to lower their voltage below 24 volts failed to establish a stable arc.)

The above correlations of penetration to independent variations of welding conditions show the pitfalls of seeking a single empirical expression of penetration as a function of all welding parameters, i.e., a uniform increase in voltage may produce a change in penetration whose magnitude and sign will depend on the complete set of parameters of the welding process.

Further inspection of the etched transverse sections revealed a pattern to the geometry of the melted base plate region. This geometric pattern may best be described by the admittedly arbitrary scheme sketched in Figure 8. The fused base plate of all bead on plate welds produced could be divided into two regions: an elliptical region of measured height A, and a "finger" of height B, B being calculated as the difference between total penetration p and height A. In most cases the elliptical bath could be easily constructed

by extrapolation of the weld fusion line's reentrant region. As illustrative examples of the variety of penetration shapes produced, bead A-5 presents a very shallow, but wide elliptical bath and a deep penetration finger, while the penetration in bead L-2 is formed almost entirely by the weld elliptical bath.

The formation of a penetration finger is a rather unique phenomenon associated with the MIG welding process. Breymeier(20) has described the finger penetration in MIG welding of steel as the result of the high velocity and force which the liquid particles achieve while traveling across the welding arc. Baker(21) et al, attribute such penetration to the plasma jets associated with the sharply defined ionization core characteristic of monatomic gas arcs.

Hence the base plate will be fused in two distinct regions, the finger formed by the intense impinging arc action, and the elliptical bath formed with time by the inevitable conduction of heat away from the hot weld bath centered around the oscillating cathode spot in direct current, reverse polarity welding. Thus it would appear reasonable that the elliptical bath's dimensions depend only on the rate of heat dissipation into the plate, while the finger size appears to be more closely related to the actual electrical conditions prevailing in the arc. These hypotheses are borne out by consideration of A and B, heights of the elliptical bath and finger region respectively, as functions of the independently varied weld process parameters.

The height of the elliptical portion, A, increases markedly with voltage rises, but appears relatively insensitive to current changes at this weld travel speed. Even more surprisingly this parameter goes through a maximum with speed variations. These maxima varying as noted:

Amperes	Speed of A maximum
250	45 (Inches per Minute)
300	33
350	35
400	28
450	25

Consideration of A as a function of EHI (or nugget area) in Figure 9 retains, as expected, the maxima at the welding speeds indicated and accentuates the family of curves for the individual current levels investigated, with the exception of the plot for 260 amperes which is displaced to higher values of EHI than would be expected. These maxima in A may be rationalized by consideration of the thermal pattern which apparently is operative during the welding process. Thus, at high speeds, A increases with decreasing speed as more heat is made available per inch of weld to increase total penetration. But as speed decreases further, the molten layer alters the melting pattern to yield a wider, yet thinner elliptical pool but does not alter the dependence of the penetration finger on travel speed, as shown later.

Finger height B shows a marked linear decrease with increased voltage (Figure 10) with the same maxima at 24 volts for 260 and 300 ampere levels as noted in analysis of total penetration in Figure 7. Viewing the two figures referred to above, as well as the effect of voltage in increasing A, establishes that it is the finger height B which is responsible for the anomalous decrease in penetration with voltage increases.

Proceeding to inspection of B as a function of current at the constant speed of 20 inches per minute and at various voltages (Figure 11), it is seen that B increases strongly with current and the rate of such increase is the same for both voltage levels investigated. Combination of this information with the linearity noted in Figure 10 leads one to state that, above 24 volts, B is linearly dependent on current and voltage by the relation:

$$B = -0.0174\ V + 0.110I + \text{constant}.$$

B exhibits general decrease with increased speeds (Figure 12). The higher current level weld series show an abrupt change in slope at around 30 inches per minute, while the lower currents have only a gradual finger shortening to the highest speeds tested. The failure of this family of curves to behave regularly, i.e., their tendency to intersect is not rectified by plotting B against EHI in Figure 13. The pattern of behavior in the relationships between B and speed appear too complex for analysis at this time, though it may be

noted that B does exhibit a tendency to reach maxima at high EHI at each current level.

An appreciation of the relative magnitude of the contributions of the finger and elliptical bath regions to total weld penetration may be gained from Figure 14. Here the ratio B/A is presented as a function of speed variations at each current level. The general behavior of rapid increases in the relative magnitude of finger height with decreasing speed is apparent at all current levels. Indeed it is only at extremely high speeds that the magnitude of A attains significant influence on the magnitude of total penetration.

Figure 15 records the generally linear decrease of the B/A ratio with voltage increases. The relative positions of the plots for each current level indicate that B/A increases with increasing current level.

Thus measurements based on the arbitrary division of each weld bead into an elliptical bath and a finger area cast considerable light on the anomalous dependence of penetration on welding conditions. To summarize the evidence discussed:

1. Except at extremely high travel speeds, finger height dominates the magnitude of the penetration dimension.

2. This finger decreases in height markedly with voltage increases and increases with current. Finger height generally increases with effective heat input rise resulting from lowering of travel speed, these increases soon leveling out at high heat inputs.

3. The depth of the elliptical bath increases as voltage rises. At constant voltage, and speed, depth A is relatively insensitive to current, yet goes through a maximum with speed variations. Despite this generally erratic behavior, these changes in A influence total penetration very little except at extremely high speeds.

Weld Width:

Weld width, defined as maximum width of the weld metal bead (which was always found at the original base plate surface in these bead-on-plate welds) was noted to increase rather uniformly with welding variable changes which promoted increased heat inputs. Thus, Figure 16, increasing speeds resulted in decreasing weld widths. (On these same axes are indicated the maximum width of melted base plate measured in cases of undercutting. The significance of these melted width measurements will be discussed later under the topic of Undercutting.)

Conversion of these speeds to the form of Effective Heat Inputs yielded the family of width-EHI curves in Figure 17. At low heat inputs this family of generally parallel curves forms a series of straight lines which extrapolate to the following approximate widths at zero heat input.

Current (amperes)	Width at zero EHI (Inches)
260	0.15
300	0.12
350	0.08
400	0.03
450	0.00

Since increased current levels were usually accompanied by slightly higher voltages for maximum arc stability, evidence was sought that the inverse relation between width (at constant heat input) and current level, noted in Figure 17, was indeed due to current variations. Observations made at 260 and 300 amperes, where the same voltage could be used for both series of welds, indicated that widths at 300 amperes were consistently lower. Further evidence may be gathered from Figure 18, which indicates that independent increases of voltage produce either increases or no change in weld width. At low amperages, in the range of voltages used in the travel speed variation series (24-31 volts), width is fairly constant with voltage, while at higher amperages, width increases markedly with voltage increases. Since width does decrease steadily with rising current level, the current itself must be exerting such a powerful influence on the processes responsible for weld bead width that it overpowers the slight and erratic changes wrought by the minor accompanying voltage modifications. A possible cause for this weld width decrease will be postulated after consideration of the effect of welding current level on the relative amounts of weld wire and base plate melted during production of the weld bead at a later point in this dissertation.

Weld Reinforcement Height:

The height of weld beads above the original plate surface was found to decrease with increasing travel speed at

each current level investigated. However, these relationships (Figure 19) present rather wide scatter from a family of parallel curves. The direct correlation of height with EHI (Figure 20) is relatively precise and yields just one common curve for all the current levels studied.

Large independent variations in voltage produce changes in height which are inconsistent with the above result. In Figure 21, it can be seen that height decreases erratically with rising voltage. Increasing current (Figure 22), as expected from the results pictured in Figure 20, causes steady increase in weld heights.

Reinforcement Area:

Reinforcement cross sectional area (or reinforcement volume per unit weld length) was shown to vary inversely with speed at each current level investigated (Figure 23). Further insight may be obtained by considering reinforcement as a function of EHI (Figure 24) to yield several interesting conclusions.

1. Reinforcement is a different linear function of EHI at each current level, each such curve exhibiting a change in slope and extrapolating to zero at zero EHI. Reinforcement increases at constant EHI, in inverse relation to current level.

2. Such a plot does not relate two completely independent variables. Since EHI is linearly proportional to the sum of reinforcement and base plate melted areas, the actual function pictured is R/R+ BPM = K (a constant).

Reinforcement shows an increase with current increases as seen in Figure 25. The area of reinforcement also exhibits a general decrease with voltage increases (Figure 26). Consideration of reinforcement area as a function of heat input changed by speed and current yields Figure 27 which indicates a single relation between these two quantities. In addition reinforcement area is a linear function of heat input below approximately 60 kilojoules per inch.

The area of base plate melted, on the other hand, is highly sensitive to the current level selected. Hence Figure 28 indicates the manner in which the base plate melted area increases with heat input. At any given current level, this increase is linear and then undergoes an abrupt decrease in slope with further increases in heat input. The conditions accompanying such slope changes are presented below:

Current (amperes)	Conditions for slope break Heat input (Kilojoules/in.)	Speed In./min.
260	25	15
300	23	19
350	44	12
400	55	12.5
450	55	15

Further study of Figure 28 shows that at a constant heat input, base plate area melted increases with the current level studied. Thus the sharp increase in BPM with current at constant speed and voltage reflects both increased heat input at the higher current as well as an intrinsically

greater base plate melting ability. Figure 29 records the varying effect of voltage on BPM and, in contrast to reinforcement melting, base plate melting increases with voltage except at extremely high voltages.

Combining these two melted areas, we find that total nugget area is a linear function of heat input below a certain breakaway input which increases with current level (Figure 30). Thus at low heat inputs, the reinforcement behavior predominates, while at high heat inputs, the large changes in base plate melting behavior due to current level begin to assert their influence. Hence total nugget area, measured at 20 inches per minute (which is just in the low heat input zone noted above), is a linear function of current (Figure 31) and is relatively insensitive to voltage (Figure 32) except at low amperages, where maxima with voltage noted in reinforcement and BPM behavior act in conjunction.

Analysis of this complex process of melting and depositing weld metal may be simplified by considering the parameter of melting ratio, defined as the ratio of base plate melted area to total nugget area. Thus the influence of travel speed may be seen in Figure 33 where this melting ratio decreases from maxima at low heat inputs produced by speed variations, while it should be noted that melting ratio is quite sensitive to current level studied. As could be intuitively concluded from weld area data previously presented

current level and heat input exert strong influence over the size of the bead as well as the concentration of electrode metal in the weld nugget. Melting ratio generally increases with current (Figure 34) and behaves erratically with voltage (Figure 35), exhibiting maxima at low currents, being constant at an intermediate current, and increasing markedly at a high current level.

Plate Preheating:

From geometry parameter data previously analyzed, it can be seen that variations in amperage and voltage cause significant changes in weld configuration which may not be calculated on the basis of their effects on heat input alone. This result was not surprising in view of the effect of current and voltage on the welding arc. Variations in welding speed also prove, to some surprise, to cause weld geometry changes beyond those which could be related to the effect of these speeds on heat input alone.

It was thus sought to vary the heat input to the weld without changing welding parameters which might alter processes occurring in the weld arc. Since welding speed changes proved to generate alterations in weld bead geometry beyond those expected from heat input considerations, the preheating of weld plates was undertaken as a source of such independent heat input variation.

In calculating a parameter to describe the contribution of the preheating process to the thermal conditions of the weld, several assumptions were made:

1. The weld metal has a mean maximum temperature of 1900° K.

2. The plate temperature has negligible effect on processes occurring in the weld arc.

3. The sole effect of preheat is to decrease the enthalpy needed to melt and superheat the base plate melted metal.

The parameter $\frac{\Delta H_T}{\Delta H_{1900°K}}$ Where: $\Delta H_T = H_T - H_{298°K}$

$\Delta H_{1900°K} = H_{1900°K} - H_{298°K}$

was selected since it represents the fraction of the enthalpy required to melt and superheat the weld metal which is supplied by the preheat process.

Penetration was found to increase linearly with $\Delta H_T/\Delta H_{1900°K}$ for all three welding conditions investigated, namely 300 amperes, 24 volts at 20 and 35 inches per minute, and 410 amperes, 28 volts with 30 inches per minute. As noted in Figure 36, the rate of change of penetration with preheating under all of these diverse welding conditions is constant. Figure 37 presents a series of representative macrosections of weld beads produced with varying amounts of base plate preheating. It may be noted that the dependence of the fused contour of the base plate on preheating is different for the two welding amperage levels studied. At 300

amperes, increasing preheat decreases the relative height of the penetration finger, while at 410 amperes, the finger area and elliptical pool retain their relative proportions of total penetration. It appears that increasing preheating promotes not only increased penetration but increased opportunity for formation of the elliptical weld pool by encouraging the sidewise flow of heat prevented by rapid weld arc travel. At 410 amperes, a large elliptical weld pool already exists when welding at room temperature, hence the ratio of finger to bath height remains unchanged with preheating.

In this regard it is interesting to contrast the relative insensitivity of width to preheating at the 300 ampere level (Figure 38) with the marked widening caused by preheating before welding at 410 amperes. This, coupled with the general increase in base plate area noted under all conditions (Figure 39), indicates that the increased heat in preheated 300 ampere plates is expended in filling out the long, narrow weld contour to the more semicircular shape noted at 400 amperes without preheating, while the preheat enthalpy at the higher current level is available for a general increase in all weld dimensions.

Reinforcement was fairly independent of preheat conditions, to affirm the assumed insensitivity of arc conditions to preheating (Figure 40). Yet some increase in reinforcement

area was noted at the highest preheat temperatures. This anomaly could be perhaps attributed to the oxidized surface of plates, preheated in air, releasing small amounts of elements to the arc atmosphere which increase the burn off rate of the electrode.

Weld height (Figure 41) decreased uniformly with preheat. This decrease in weld height would indicate that the molten reinforcement metal remains hotter longer when in contact with the preheated base plate, and the resultant lower surface tension forces allow formation of a less peaked bead.

To check the validity of the assumption that the sole role of preheat is to raise the enthalpy of the base plate metal melted, ΔH was defined as $H_{1900^\circ K} - H_T$. Then if the above assumption is correct:

$\Delta H_{T_1} (BPM)_{T_1} = \Delta H_{T_2} (BPM)_{T_2}$ Where: ΔH_{T_i} = ΔH at preheat temperature T_i

or $\Delta H_{T_i} = \frac{\text{constant}}{BPM_{T_i}}$ BPM_{T_i} = base plate melted when preheated to T_i

Thus Figure 42, which shows the linearity of 1/BPM as a function of ΔH, affirms the hyperbolic relation postulated on the basis of the assumed role of the preheating process.

Undercutting:

Undercutting, a practical consideration which restricts usable welding speeds, results in the formation of damaging longitudinal grooves alongside the weld bead where a portion

of the melted base plate region has not been filled by the molten weld metal. The relation of maximum travel speed attainable without undercutting is recorded in Figure 43 as a function of electrical conditions during welding. As inspection of this figure will show, the appearance of undercutting does not occur at a constant travel speed nor does it coincide with a set value of heat input, for indeed the heat input for undercutting increases strongly with welding current. Below are the welding conditions noted at first sign of undercutting:

Current (amperes)	Speed (Inches per minute)	Heat Input (Kilojoules per inch)
260	45	8.32
300	33	13.1
350	30	18.9
400	30	23.2
450	25	33.5

An interesting experimental observation on this phenomenon may be gathered from Figure 16, which records melted width as a function of weld travel speed. The width of the hole melted in the base plate, at speeds where undercutting is seen, rapidly levels off with speed and approaches a minimum value. These limiting undercut widths are plotted in Figure 44 and seen to be proportional to the electrical power of the welding arc. This width behavior may be related to the transverse amplitude of oscillations which the cathode spot has been reported to undergo in reverse polarity welding.

This cathode spot travel width, being independent of travel speed, apparently increases linearly with weld power and is thus responsible for the minimum weld width here reported.

Hence undercutting may be viewed as being caused by the weld metal lacking sufficiently high fluidity to fill, at high speeds, the constant width weld groove. This cause of undercutting is also considered by Lesnewich(18) who postulates that localized heat generated by cathode sputtering action develops a gouge near the arc and undercutting is produced if sufficient metal is prevented from flowing into these regions.

Weld plate preheating was found to relieve this undercutting by supplying more heat to the base plate, thus aiding to fill these gouges. Thus on preheating an increment of heat input is added to the weld by the preheated base plate and the appearance of undercutting is retarded, without altering welding parameters. Examination of width of preheated welds (Figure 38) indicates that the minimum width of the undercut hole is not changed by the preheating treatment, hence the fluidity of the weld metal is the factor affected.

Weld Crater Length:

The length of the weld bath can be measured only at the weld crater, formed at interruption of the welding arc. The depression in the weld bead at the crater is formed partially by the lack of further molten metal to compensate for metal

shrinkage and partially by the weld pool's height being some distance below the weld bead height under the steady state conditions of welding.

Rykalin, through a theoretical consideration of thermal processes during welding, concludes that the length of the weld pool is proportional to the product of welding voltage and amperage and that such length is independent of travel speed of the arc. From Figure 45, it may be seen that at the two constant electrical conditions considered, only minor variations exist in bath length as a function of travel speed, yet these minor variations follow the same distinct saw tooth pattern for both conditions. Consideration of bath length as a function of voltage indicates a near constancy in bath length except at the low amperages, which again exhibit the discontinuous behavior below 24 volts previously associated with transition in arc transfer mode.

Though Rykalin presents experimental measurements of weld craters for the submerged arc and covered electrode processes, he does not consider MIG welding directly. For the processes he did investigate, crater length increased with arc power at the rate of 0.67 to 0.92 inches per kilowatt.

To test Rykalin's relationship directly, bath lengths at a variety of amperages are presented in Figure 46 as a function of arc power. Though linearity is noted, the curves are separated at the two voltage levels considered and extrapolate to a predicted weld length at zero power, not of

zero as predicted by Rykalin, but of approximately 0.6 inches. The curves thus have the form:

$L = K\,(IV) + A$ Where:

K = constant= 0.9 inches/kilowatt

A = constant= 0.6 inches

Thus the rate of change in bath length with arc power predicted by Rykalin has been verified experimentally as long as only current variations are considered. The invariance with voltage and the anomalous extrapolation to zero power must be considered in the light of the several ways the physical process of welding differs from its mathematical model. Thus the latent heat of solidification and actual position, width and temperature of the cathode spot require further experimental and theoretical consideration.

Another approach to verification of Rykalin's relation lies in variation of the effective temperature elevation for melting through preheating. Thus in the postulated relation:

$$L = \frac{q}{2\pi\lambda T_s}$$ Where: q = power input

λ = thermal conductivity

T_s = melting point of base plate

the factor T_s is reduced by each preheat temperature, T_h, and L should be proportional to the factor $1/T_s - T_h$ with variations in temperature. As Figure 47 records, L does indeed follow this inverse relation with the exception of a sharp rise in bath length at 300 amperes at the highest preheating temperature. It is interesting to note that all this increase occurs in the bath length behind the arc, for the length of the

bath in front of the arc remains constant with preheating in agreement with Rabkin's observations in the preheating of aluminum weldments. This experimental observation would lead one to surmise that the process creating the forward bath contour, being insensitive to plate temperature, may either be radiation from the nearby arc or erosion by highly superheated ($>1900°$ K) weld metal propelled directly under the arc.

Weld Contact Angles:

The high thermal gradients in the molten weld pool, which have made experimental observations of the freezing process difficult, are least severe in the lateral extremities of the weld pool. Here, where weld metal, base plate and atmosphere meet in line contact, an attempt was made to assess weld metal surface tension through contact angle measurements. The experimental results are limited in several ways:

1. Surface contraction on freezing cannot be compensated for to yield actual liquid-solid contact angles.

2. Though all plates were prepared in the same manner prior to welding, gas coverage on the area in question differed with bead width.

3. Temperature gradients and degree of undercooling in the various beads could not be determined.

4. The magnitude of hydrostatic and magnetic forces operative on the liquid weld metal in contact with solid base plate was unknown.

The correlation between the wetting angle, e, and welding speed at the various current levels studied is similar for all the conditions presented in Figure 48. Wetting of the base plate by the weld metal is poor at low speeds, and then goes through a maximum at intermediate speeds. The advent of undercutting and the wetting maxima occur at roughly the same speeds at each current level. Thus the decrease in wetting at high speeds coincides with the increasing extent of undercutting, though measurement of wetting in undercut beads is rather difficult. However, the wetting angle data presented does lead one to conclude that the appearance of undercutting at high travel speeds cannot be ascribed to a lack of wetting action between bead and plate, for it is at precisely those speeds that the wettability is maximized.

A possible cause for the increase in e at low speeds may be the effect of slow travel speeds on the temperature distribution in the lateral extremities of the weld pool. Since the surface tension of liquid metals decreases generally with temperature increases, the decreased wetting at low speeds can be ascribed to a lower local bath temperature. Though the fusion line, at all speeds, represents an isothermal (liquidus temperature) condition; the temperagradient in the bath adjacent to this line is a function of the bath width and thickness.

Evidence presented earlier of the minimum melted width indicated that the cathode spot travel range has a finite width dependent only on electrical conditions in the arc.

Assuming that arc temperatures are independent of travel speed would mean that the temperature gradient near the fusion line would become increasingly flat at low travel speeds. Hence the weld contour in the vicinity of the liquid-solid-gas intersection would be expected to reflect this decreased mean melt temperature at low travel speeds.

Proceeding on this basis, it may be argued that the thermal gradient in the weld pool near the fusion line is also lowered by the plate preheating operations. Thus it would be predicted that higher preheating temperatures would tend to produce higher contact angles, indicating lower wettability. This was borne out experimentally quite strongly, as plotted in Figure 49, and since θ increases monatomically with the ΔH parameter to values of 90° at preheating temperatures above 1400° F, with relative lack of dependence on the particular welding condition employed.

It should be noted that this increase in surface tension at the lateral extremities of the weld pool occurring with preheating is a local condition peculiar to such weld areas, for the general change in shape in the reinforcement of such welds produces wider and lower beads with increased preheating. This appearance variation would indicate that any increase in surface tension in the extremities of the weld bead plays a negligible role in determining weld contour compared to the large alterations in thermal pattern induced by the preheating process, primarily manifested as large increases in solidification time.

Grain Size:

Mechanical properties of two alloys of similar chemical analysis and phase composition may be altered markedly by relative size or preferred orientation of grains. Since steel is a complex alloy which undergoes several phase changes during its thermal history, a brief discussion of the meaning of grain size of such steel weld metal is in order.

Though any Fe-C alloy with less than 0.5% carbon cooled from the liquid state, under equilibrium conditions, will first solidify out δ ferrite prior to a peritectic transformation to austenite, such a δ ferrite grain size has little meaning for steel weld metal due to its rapid freezing rate and the high atomic mobility at the peritectic temperature wiping out traces of prior grains. It is the austenite grain size, delineated by proeutectoid transformation products, which plays a prime role in behavior of the structure, both by influencing transformation kinetics and morphology, and by the areas of weakness represented by the segregated proeutectoid. The grain size of the transformation product itself will play an important role in determining mechanical behavior.

For the specific case of steel weld metal, austenite grain size as measured at the fusion line was seen to change markedly with welding conditions. These grain sizes, measured perpendicular to the major axis of the dendritic grains,

are plotted in Figure 50 as a function of the square root of linear heat input, q/S .

Since the complex sequence of transformation in such a steel effectively limits the detection of segregation which would delineate the interdendritic interstices by metallographic means, the relation between such austenite grain size formed by solid state transformation and interdendritic spacing formed during solidification must await further investigation with methods more sensitive to chemical inhomogeneities, such as autoradiography. However, comparison of the behavior of these two structural parameters with welding conditions does reveal similarities.

Brown and Adams(22) studied the MIG welding of a single phase, aluminum alloy which exhibits no solid state transformations. The interdendritic spacings were measured from the resultant segregation pattern and the investigators found them to be a linear function of the square root of the lineal heat input in agreement with behavior predicted from theoretical consideration of the constitution supercooling process and analyses of heat transfer rates in weld pools.

$$L^2 = \frac{8\, D\Delta T\, t}{M(1-k)\, C_o}$$

Where: L = dendrite spacing
ΔT = degree of constitutional supercooling
M = slope of liquidus line
C_o = overall solute concentration
$1-k$ = segregation coefficient
t = solidification time

$$t = \frac{Hq}{2\ K\ C_p\ S(T_m-T_o)^2}$$

Where: H = heat of fusion
q = welding arc power
K = thermal conductivity
C_p = specific heat of solid
S = arc travel speed
T_o = initial plate temperature
T_m = liquidus temperature

Combination of these two equations leads to the predictions that

a. $L^2 = A\ (q/S)$, when welding conditions are varied at a set plate temperature, and

b. $L^2 = B\ (1/T_m-T_o)^2$, when plate temperature is varied at constant welding conditions, A and B being material constants of the alloy being welded.

Since austenite grain size does follow the behavior pattern a. above, with some variance noted at extremely high heat inputs, it might be expected that the predicted behavior with plate temperature would be obeyed during the preheating experimental series. However, measurements of austenite grain width in such weld beads revealed mixed results, with welds produced at 300 amperes and 20 ipm showing the predicted increased width with higher plate temperatures, while welds of the other two experimental conditions studied remained fairly constant in austenite width with temperature.

Segregation and Freezing Patterns:

Metallographic examination of etched weld cross sections revealed a tendency, increasing with travel speed, to formation of bands of chemical inhomogeneity running roughly paral-

lel to the weld fusion line. Reference to longitudinal sections of the same weld beads reveals that these lines are transverse intersections of curved surfaces appearing to originate at the weld root and fading away in intensity in the reinforcement area. Figure 51 depicts the occurrence of such layer lines in a series of weld beads prepared with variations in weld travel speed and a series in which welding voltage was the variable.

As outlined in the Introduction, it has been proposed that such layer lines are the result of brief interruptions in the freezing of steel weld metal associated with the time lag required to dissipate the head of solidification. Such thermal buildup causes a thermal arrest, or even remelting of portions of the bead, thus allowing such rapidly diffusing elements as carbon, sulphur and phosphorus to remove themselves from the solid weld metal, cross the solid-liquid interface, and enter the liquid phase, which offers greater solubility for them. When this enriched liquid subsequently freezes on resumption of the solidification process, another pair of alternately impoverished and enriched layers has been created in the weld bead.

Note that at higher speeds, the layer lines become more accentuated and assume a greater proportional depth. In the upper portions of the welds, grains grow close to vertically, indicating the heat flow direction exerted by the base plate, but in the weld finger, heat is abstracted from the narrow sides of the bead also, giving rise to the varied

patterns seen. A general effect noted at low travel speeds is the 'bending' of the austenite grains near the surface in the direction of arc travel, a result perhaps of a skin cooling effect augmented by the cooling of the trailing cover gas stream.

Various types of crater appearances were noted in the longitudinal sections. A-7 illustrates a crater where the leading wall of the melted hole is bare of deposited weld metal and thus apparently was fused solely by radiation from the arc and not by the latent heat of superheated electrode drops. While such 'clean' craters were noted at the higher travel speeds, lower speeds produced craters lined with weld metal to indicate that either a different mechanism of crater formation is operative or that the electrode metal, at higher travel speeds, does impinge on the leading wall but fails to wet it.

Several curious effects were noted in macrographs of welds deposited at various voltage levels. At the lowest voltage, an extremely deep finger was produced that lead to formation of two distinctive freezing patterns as the upper weld section froze vertically, while austenite grains formed in the finger strongly inclined towards the welding arc. The boundaries of such grains in the finger region are almost perpendicular to the weld pool boundary lines as delineated as layer line segregation. Thus it would appear that, here on the center line of such welds, heat is abstracted by

the weld pool wall in a unique pattern, reflecting perhaps the low degree of superheat in the finger. At higher voltages, the decrease in penetration documented previously can be traced in the decrease in the finger freezing mode zone. The lack of sufficient mixing between reinforcement and base plate metal manifests itself in deep finger penetration beads by the entrapment of small islands of higher carbon metal (from fused base plate) in the fusion line area as seen in beads L-1 and L-5.

Surveys of the microhardness of a number of welds prepared in the present study revealed a correlation, in specimens exhibiting marked layering, between the location and periodicity of hardness minima or maxima and the pattern of chemical inhomogeneity delineated by metallographic treatment. As an illustration, Figure 52 traces the contour lines of hardness minima observed in a series of traverses of the cross section of weld bead A-2, whose layering is quite apparent in Figure 51. Noting that the spread in hardness between minima and maxima was from roughly 250 DPH to 350 DPH respectively, it may be concluded that such hardness variations are due to strong segregation of carbon over the short distances between layer lines.

In addition to such highly localized carbon segregation across layer lines, gross segregation in the weld pool was noted and accentuated in welds made over the 4% carbon cast iron powder previously cemented in the arc travel path. One

such specimen, M-3, welded at 300 amperes, 24 volts and 30 inches per minute over such carbon enriching powder exhibited gross differences in etching characteristics in various areas of its macrostructure (Figure 53). From observation of this figure, the cross sectional area of the bead may be divided into three distinct zones. Zone A, at the fusion line, possessed the characteristic pearlitic-acicular ferritic microstructure observed in unalloyed beads. The very dark macroetching of the uppermost zone C was explained by its bainitic microstructure, whose appearance suggested that this zone had the structural proportions expected from a 0.40 to 0.50% carbon steel. Zone B was seen to be intermediate between the others in etching characteristics as well as apparent carbon content based on microstructural observation. Microhardness measurements of this weld nugget showed that Zone A had an average characteristic hardness of 73 on the 15-N scale, Zone B, 78, and Zone C, 82. Chemical analyses of chips removed from each one of these zones substantiated the inferred macrosegregation of carbon, for Zone A contained 0.14% carbon, Zone B 0.24%, and Zone C 0.42% as listed in Table IV.

Segregation patterns, similar to those described above for the case of carbon as solute, were clearly delineated by welding over iron sulphide powder placed over defined lengths of the grooved centerline of base plates. Subsequent sulphur printing of longitudinal sections of such weld beads allows experimental observation of the mode of sulphur distribution

as a function of welding parameters. Figure 54 presents such prints of two typical specimens studied. M-81, welded at 300 amperes, 24 volts and 15 inches per minute, and S-62, welded under the same conditions but at only 6 inches per minute, provided several observations of interest. The spatial relationships in such sulphur prints may be easily established if one differentiates the characteristic 'salt and pepper' pattern of the relatively coarse sulphides in the base plate from the general darkening of the sulphur enriched weld metal. Due to the inherent fineness of sulphide particles in the unenriched weld metal, such areas fail to darken the photographic emulsion.

As seen in M-81, a definite sulphur free volume exists at the finger of penetration attesting to the lack of mixing noted previously in carbon enriched weld metal. This extent of the sulphur free strip goes through a maximum with travel speed at a given welding condition as illustrated in Figure 55. However, even at extremely low travel speeds, such as produced S-62, entrapment of sulphur-poor regions is noticed, indicating the relatively short reaction times of liquid-liquid contact for homogenization in the weld finger. The characteristic layer lines may be noted in both prints by gradations in shading, the analogy to wave-like deposition and solidification of weld metal being strongly suggested by these figures.

Conclusions:

To summarize the correlations found between welding conditions and weld geometry, it may be stated that:

1. Reinforcement area is the one weld geometry parameter which is dependent on heat input without regard to the particular combination of process variables employed. This suggests that the major influence of welding parameters is on the pattern of arc interaction with the base plate rather than on arc power or anode events.

2. Weld parameters strongly influence both the efficiency of melting base plate and the contour of such fused areas. The mechanism causing the inverse relation of penetration to voltage and the failure of penetration to exceed maxima dependent on arc power requires development of further experimental techniques to determine crater height and isotherms in the weld pool. Any analysis of thermal effects in the weld pool must take into account the probable wave-like movements of the heat conducting medium under the arc. On this violent action in the finger must be superimposed the extent of lateral heat flow through perhaps more calm portions of the weld pool.

3. On this basis, the more regular increase in width with weld parameters increasing heat input may be understood as the result of the lateral steady state heat flow removed from the turbulent, very high temperature arc region. In a similar fashion, the dependence of weld height on EHI with-

out regard for the current-speed combinations employed is a result of the height forming at a considerable distance, equal to the crater length, behind the arc as the reinforcement metal, whose volume depends only on heat input, seeks to fill the melted width under the influence of surface tension forces.

4. Weld penetration is a linear function of heat input increases provided by preheating. It was seen that this penetration increase resulted from a larger elliptical weld pool and not from finger length increases.

5. Undercutting of weld beads was demonstrated to be associated with the minimum width of base plate melted at high travel speeds. This lower limit to width, which increases with arc power level, is believed to be a result of the lateral amplitude of oscillation of the cathode spot on the base plate being independent of travel speed, and thus becomes an intrinsic limitation of this particular welding process. It was found that this undercutting is not the result of high travel speeds decreasing weld metal-base plate wetting, for the contact angle θ of weld metal in the vicinity of the undercut region is at a minimum at travel speeds where undercutting is first encountered, which would indicate high weld metal temperatures in these localities. Weld preheating alleviated undercutting not by reducing this minimum width, but by producing a lower, flatter reinforcement area.

Thus undercutting would be expected to reappear at higher travel speeds, even in preheated plates, since the volume of weld metal which seeks to fill the minimum melted width continually decreases with travel speed.

6. Weld crater length was found to agree with theoretically predicted behavior only with variations in current, since the bath length proved to be independent of voltage and dependent on travel speed. The mode of increase of bath length with preheating temperature agreed with theory and the length of the forward portion of the bath (the distance from the arc measured in the direction of arc travel) was independent of preheating.

7. Austenite grain size is a function of $\sqrt{\text{heat input}}$, which indicates that this grain size is a function of solidification time, a characteristic noted in other casting processes studied.

8. Several modes of macrosegregation were noted in the weld beads studied by metallography, microhardness surveys, sulphur printing and chemical analysis, and were accentuated and delineated by intentional additions of C and S to the weld pool. These modes included:

a. The formation of layering, parallel alternate strate of enriched and impoverished weld metal

b. Gross segregation of the weld pool, resulting in the tip of the penetration finger being poor in alloying element added to the pool

c. Entrapment of small pockets of weld metal of base plate composition in the weld bead.

These segregation patterns were seen to vary in definite relation to welding parameters. The layering grew more pronounced and persisted to a greater depth in the weld bead with higher travel speeds. The dead zone, noted above in b. was found to reach a maximum thickness with travel speed at a given current level. Thus this dead zone extended to maxima of 0.06 and 0.08 inches in total penetrations of 0.16 and 0.20 inches respectively for the two current levels studied.

9. Closely tied to such segregation phenomena is the intricate pattern of dependence of pattern of freezing of the weld metal on the welding conditions which dictate contour of weld pool, temperature distribution in the weld pool and distribution of alloying elements. The complex changes in weld geometry which were discussed previously are important in determining the direction of crystal growth in various portions of the pool. For instance, extremely low voltages lead to the formation of a deep finger which chills the pool strongly in a lateral direction. Thus the lateral growth of grains in the finger of such welds contrasts strongly with the almost vertical growth noted in the elliptical pool and the strong chilling action is believed responsible for the creation of the dead zone in the finger.

Table I

Chemical Analyses of Weld Materials

	Welding Wire	Base Plate
C	0.08%	0.26%
S	0.018	0.037
P	0.01	0.015
Mn	1.42	0.76
Si	0.56	0.01
Al	0.06	----
Ti	0.10	----
Zr	0.04	----

Table II

Weld Addition Analyses

	4% C cast iron drillings	Fe-S powder
C	4.02%	0.1%
S	0.019	33.
Mn	0.26	0.16
P	0.036	0.008
Si	1.01	0.64
Ti	0.026	0.012
Fe	balance	64.3

Table III
Weld Nugget Geometry Data

	Current amps	Voltage volts	Arc Speed inches/min.	Penetration inches	Width inches	Height inches	Reinforcement area inches^2	Base Plate Melted in^2
H-6	260	24	3	0.105	0.657	0.155	0.0795	0.0238
H-5	270	25	6	0.154	0.716	0.150	0.0788	0.0377
G-2	260	24	10	0.160	0.683	0.131	0.0630	0.0380
G-8	260	24	15	0.162	0.567	0.113	0.0446	0.0350
G-4	255	24	20	0.139	0.485	0.155	0.0309	0.0274
G-7	260	24	25	0.130	0.388	0.113	0.0265	0.0214
G-3	250	24	30	0.0969	0.339	0.101	0.01975	0.0163
G-6	260	24	35	0.101	0.335	0.0859	0.0184	0.0160
Y-5	260	24	45	0.0996	0.313	0.101	0.0157	0.0156
H-7	260	24	60	0.0333	0.279	0.0614	0.00973	0.00575
P-4	235	24	20	0.0820	0.433	0.0982	0.0262	0.0214
P-1	250	19	20	0.0913	0.359	0.114	0.0271	0.0178
P-2a	260	20	20	0.106	0.414	0.123	0.0323	0.0208
P-2b	250	21	20	0.104	0.444	0.103	0.0316	0.0223
S-4	260	26	20	0.139	0.424	0.103	0.0284	0.0287
P-3	260	28	20	0.123	0.419	0.109	0.0294	0.0245
S-3	255	30	20	0.115	0.462	0.0986	0.0288	0.0244
J-7	300	24	3	0.210	1.01	0.202	0.168	0.0770
A-3	300	24	4.5	0.235	0.970	0.208	0.1603	0.0670
J-6	300	24	6	0.216	0.803	0.160	0.0985	0.0556
J-8	300	24	6	0.207	0.820	0.173	0.108	0.0517
A-5	300	25	10	0.227	0.734	0.136	0.0732	0.0479
A-8	300	24	15	0.207	0.534	0.140	0.0487	0.0384
O-1	300	24	20	0.212	0.468	0.136	0.0403	0.0373
A-7	300	24	21	0.208	0.490	0.145	0.0421	0.0338
A-1	300	24	25	0.163	0.399	0.131	0.0318	0.0273
C-4	300	24	30	0.151	0.385	0.1285	0.0292	0.0244
A-2	300	24	33	0.142	0.362	0.125	0.0249	0.0231

K-3	300	24	45	0.0901	0.312	0.0875	0.0144	0.0139
K-1	300	24	60	0.0735	0.304	0.0670	0.00965	0.01092
F-6	300	20	20	0.148	0.484	0.131	0.0407	0.0300
0-3	300	20	20	0.153	0.411	0.141	0.0398	0.0298
F-5	300	22	20	0.184	0.426	0.154	0.0442	0.0319
0-2	300	26	20	0.193	0.450	0.134	0.0378	0.0357
F-4	300	28	20	0.173	0.434	0.140	0.0374	0.0332
F-3	300	29	20	0.168	0.450	0.140	0.0381	0.0326
F-2	300	30	20	0.147	0.449	0.108	0.0333	0.0288
Y-1	300	32	20	0.150	0.450	0.116	0.0302	0.0280
H-4	350	28	3	0.287	1.090	0.202	0.1893	0.1138
F-1	350	27	6	0.321	0.858	0.183	0.1220	0.0775
A-4	350	27	10	0.308	0.758	0.165	0.1002	0.0724
B-1	350	27	15	0.275	0.619	0.165	0.0688	0.0581
B-5	350	27	20	0.245	0.511	0.155	0.0540	0.0473
B-4	350	27	25	0.220	0.410	0.152	0.0409	0.0383
C-2	350	27	30	0.176	0.388	0.137	0.0304	0.0335
C-3	350	27	30	0.177	0.421	0.140	0.0297	0.0336
B-3	350	27	35	0.173	0.394	0.139	0.0283	0.0322
C-5	350	27	35	0.194	0.390	0.141	0.0291	0.0325
Y-6	350	27	45	0.173	0.347	0.155	0.0273	0.0268
H-2	350	27	60	0.110	0.353	0.110	0.0152	0.0149
G-5	350	24	20	0.257	0.350	0.167	0.0443	0.0425
F-8	350	29	20	0.200	0.497	0.165	0.0485	0.0453
F-7	350	32	20	0.193	0.503	0.143	0.0449	0.0440
Y-2	350	36	20	0.161	0.617	0.127	0.0525	0.0510

J-2	400	29	3	0.418	1.210	0.239	0.2440	0.1720
J-1	400	29	6	0.391	1.000	0.210	0.1564	0.1138
D-2	400	29	10	0.376	0.813	0.185	0.1120	0.0954
D-6	400	29	15	0.313	0.643	0.159	0.0704	0.0733
D-1	400	29	20	0.258	0.514	0.160	0.0555	0.0562
D-3	400	29	25	0.232	0.463	0.133	0.0359	0.0488
D-5	400	29	30	0.232	0.447	0.133	0.0312	0.0416
D-4	400	29	30	0.198	0.435	0.135	0.0324	0.0409
C-1	400	29	35	0.194	0.457	0.139	0.0316	0.0405
J-4	400	29	60	0.139	0.418	0.115	0.0208	0.0245
J-3	400	29	90	0.132	0.383	0.106	0.0150	0.0176
L-4	400	25	20	0.311	0.391	0.199	0.0609	0.0519
L-5	400	28	20	0.271	0.487	0.152	0.0510	0.0579
L-1	400	32	20	0.234	0.528	0.158	0.0522	0.0593
L-2	400	33	20	0.218	0.570	0.139	0.0490	0.0634
L-3	400	35	20	0.190	0.599	0.113	0.0407	0.0542
Y-3	400	36	20	0.209	0.650	0.126	0.0577	0.0653
E-2	450	31	10	0.395	0.813	0.203	0.1230	0.1210
E-4	450	31	15	0.368	0.683	0.189	0.0905	0.0993
D-7	450	31	20	0.302	0.524	0.176	0.0628	0.0680
E-7	450	31	25	0.280	0.516	0.165	0.0525	0.0663
E-1	450	31	30	0.259	0.504	0.161	0.0464	0.0576
E-5	450	31	35	0.248	0.473	0.152	0.0370	0.0504

Table IV

Chemical Analyses of Weld Metal Drillings

	C-4 (300 A, 24V, 30 ipm)	M-3 (300 A, 24 V, 30 ipm)		
		Zone A	Zone B	Zone C
C	0.15%	0.14%	0.24%	0.42%
S	0.027	0.018	0.024	0.029
P	0.012	0.012	0.013	0.013
Mn	1.04	0.95	0.97	1.01
Si	0.27	0.27	0.26	0.25

Figures:

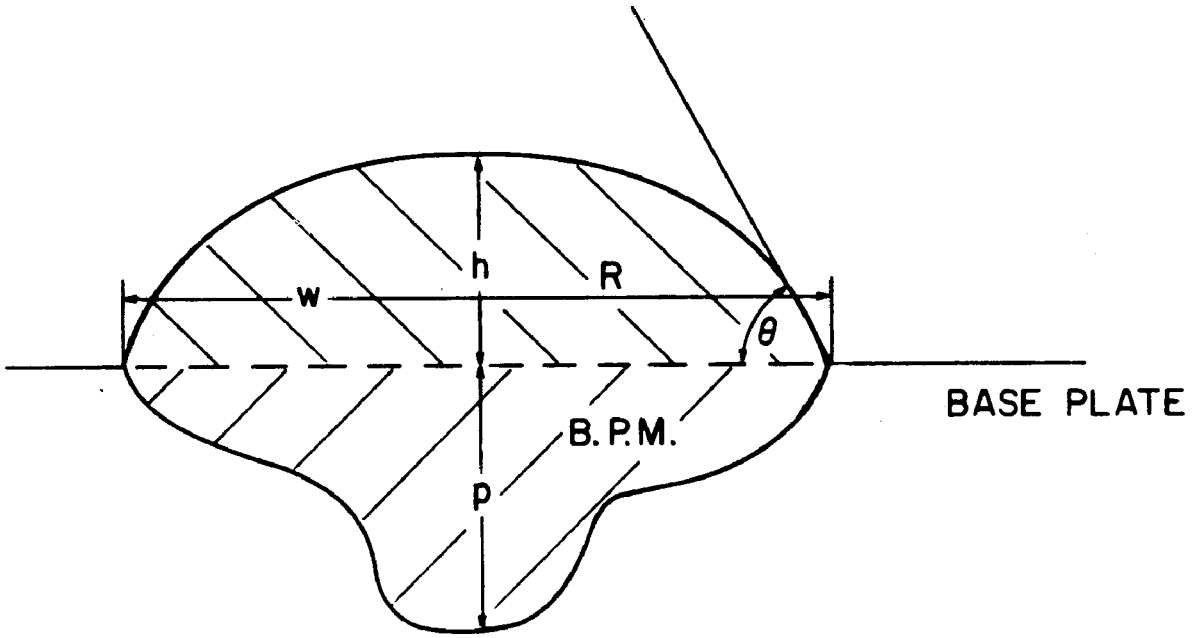

FIG. 1. SCHEMATIC ILLUSTRATION OF BEAD ON PLATE WELD.

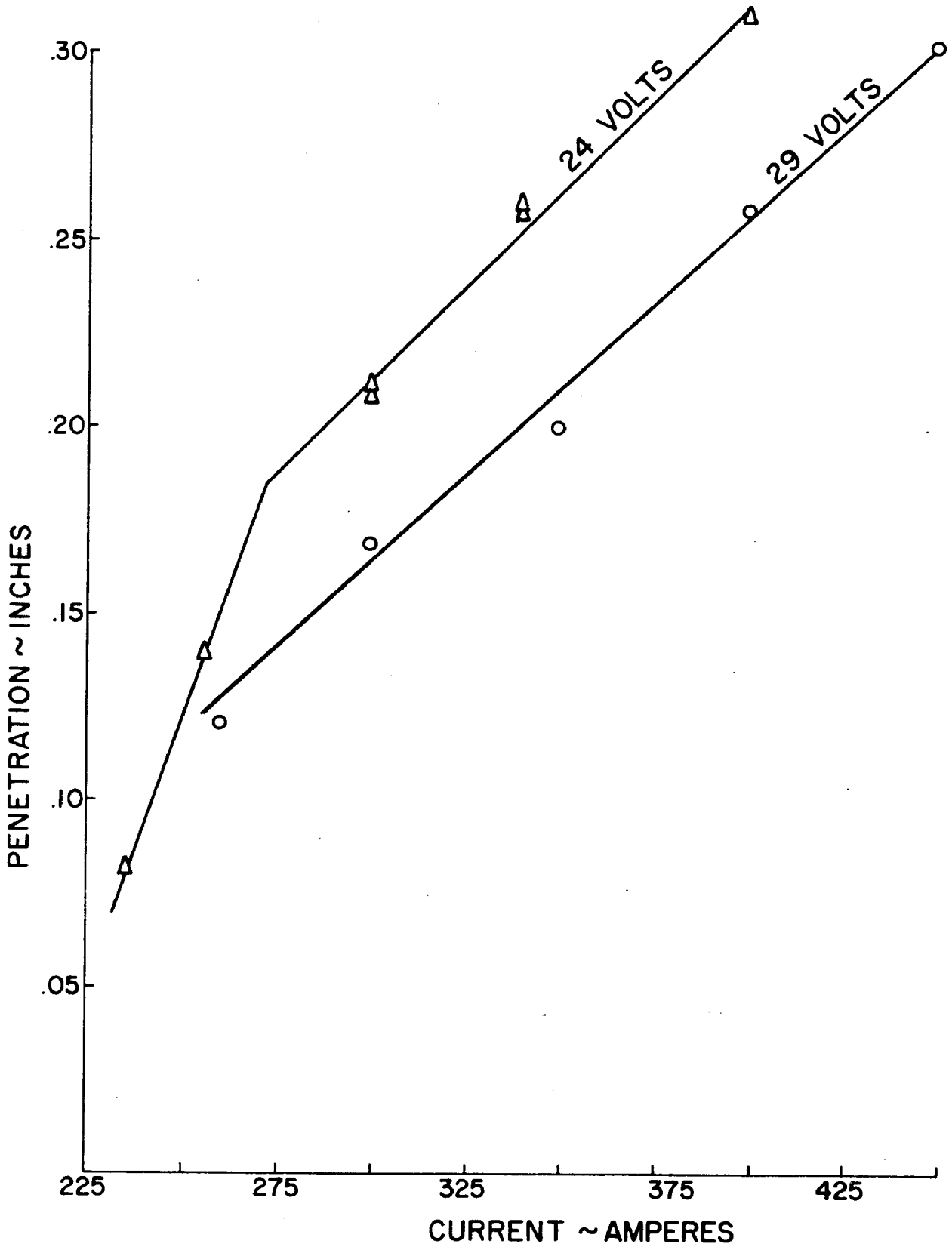

FIG. 2. WELD PENETRATION AS A FUNCTION OF WELDING CURRENT AT TWO VOLTAGE LEVELS.

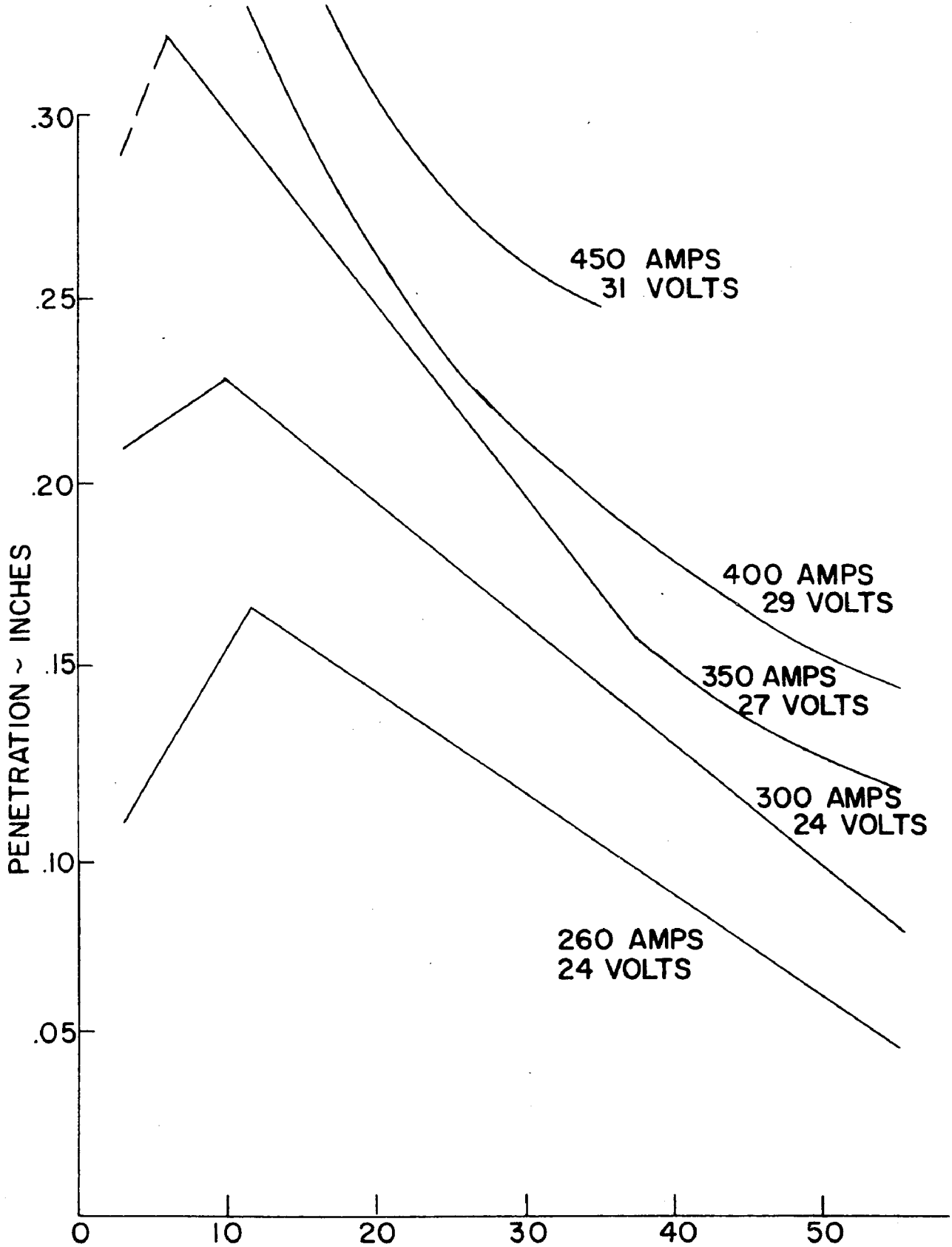

FIG. 3. WELD PENETRATION AS A FUNCTION OF TRAVEL SPEED AT FIVE DIFFERENT AMPERAGE LEVELS.

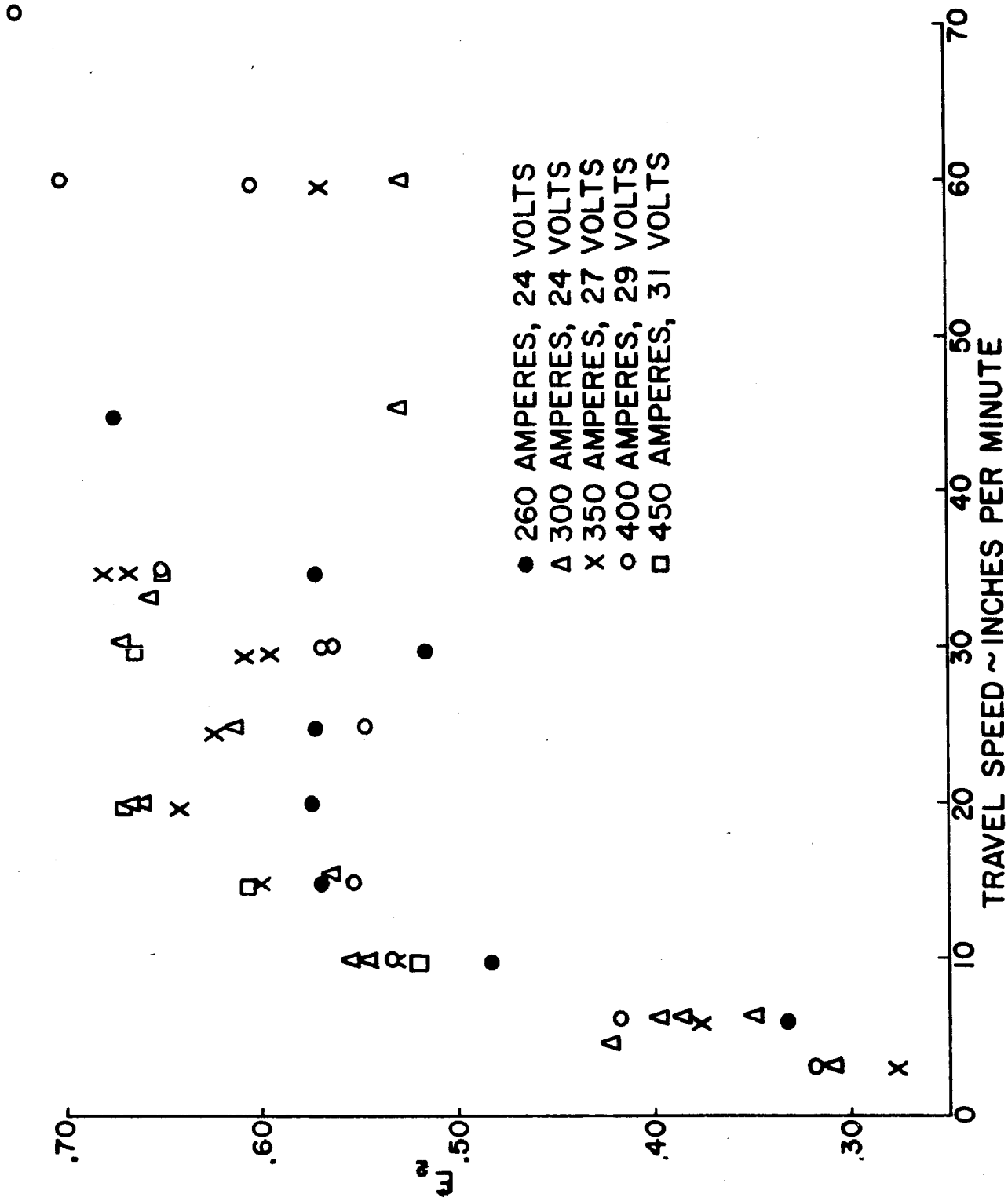

FIG. 4. EFFICIENCY FACTOR $E_2\left(\frac{\text{ENERGY TO MELT WELD METAL}}{\text{ENERGY SUPPLIED TO ARC}}\right)$ AS A FUNCTION OF TRAVEL SPEED.

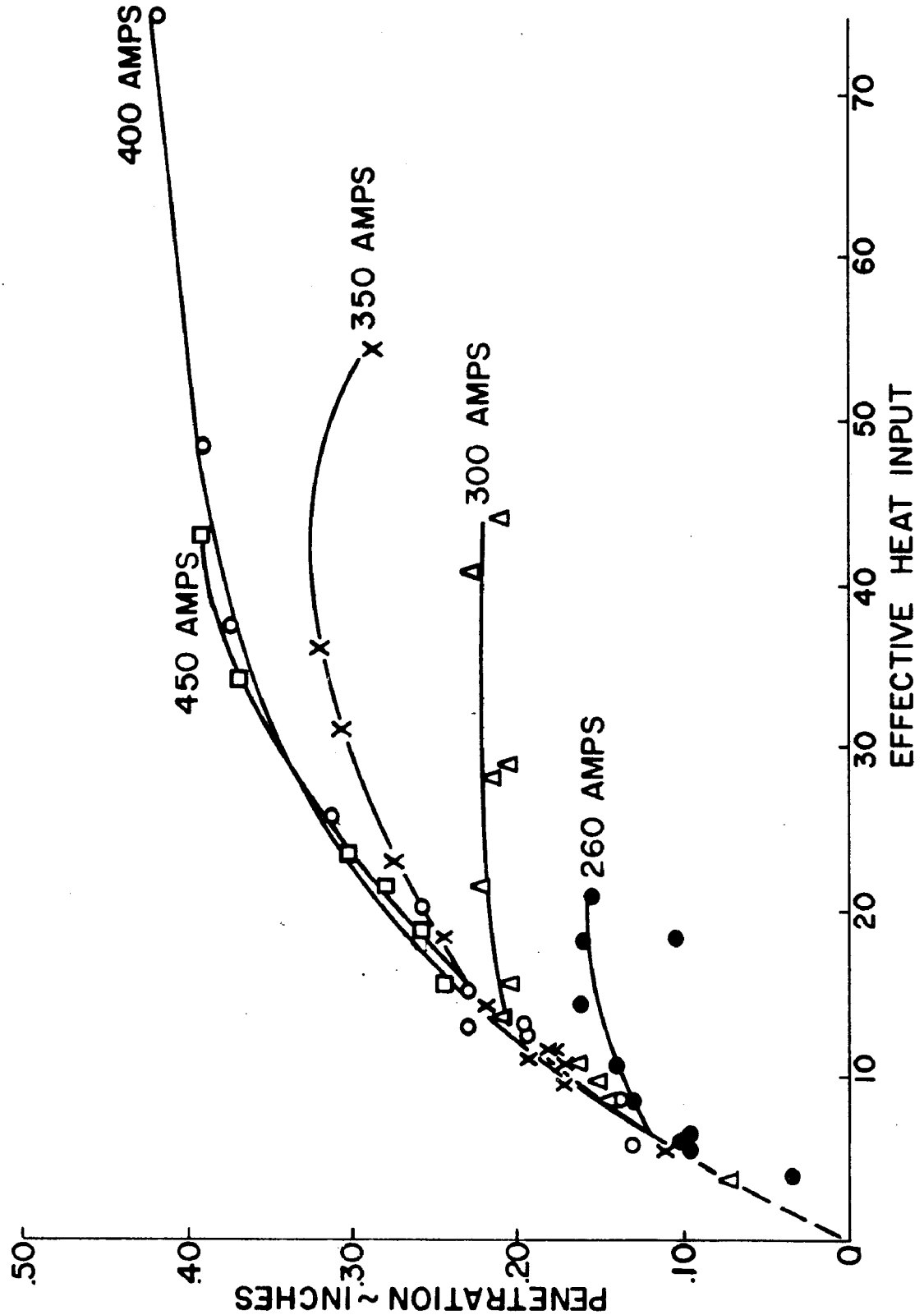

FIG. 5. WELD PENETRATION AS A FUNCTION OF EFFECTIVE HEAT INPUT (E.H.I.)

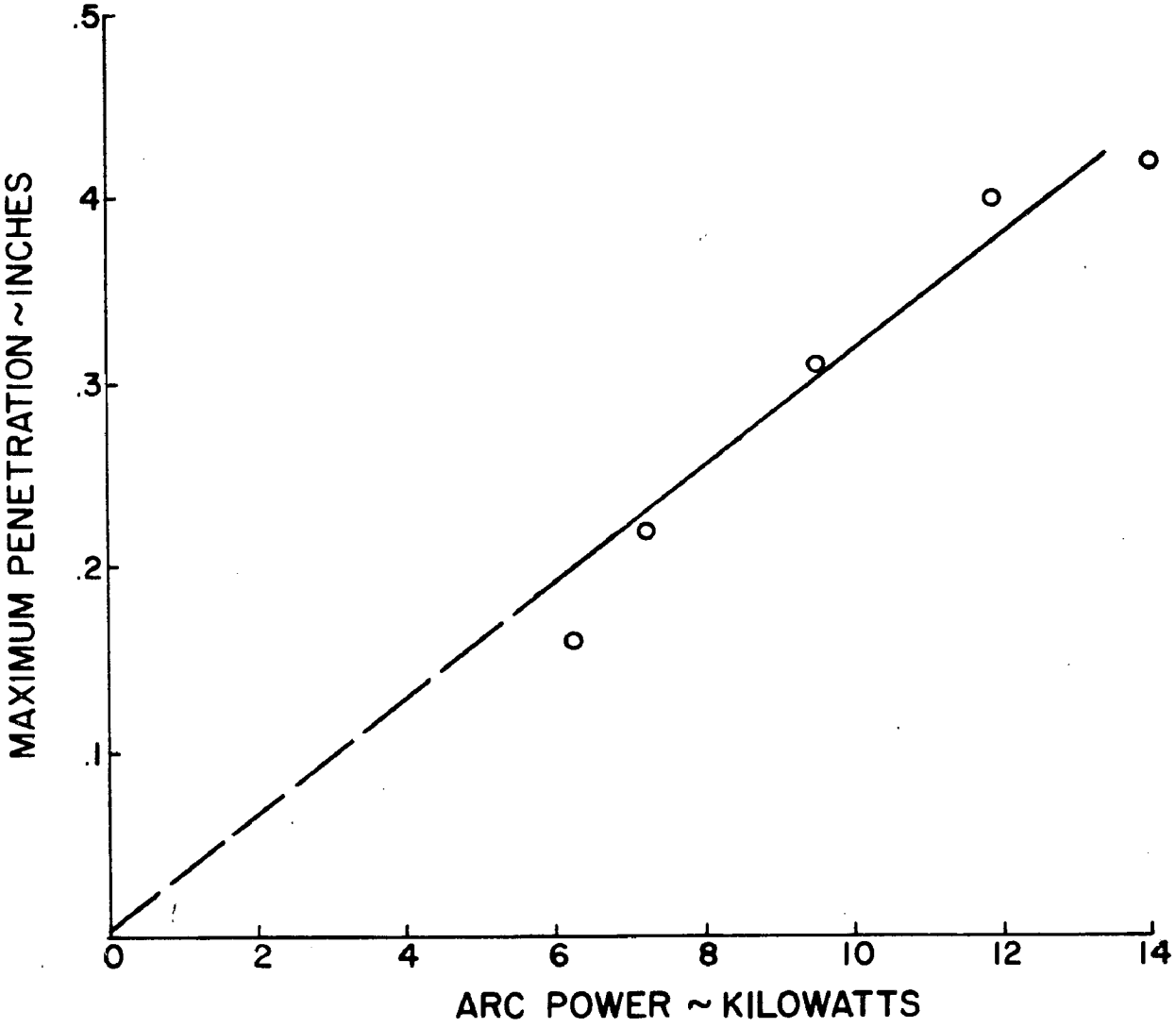

FIG. 6. MAXIMUM PENETRATION AS A FUNCTION OF POWER SUPPLIED TO WELDING ARC.

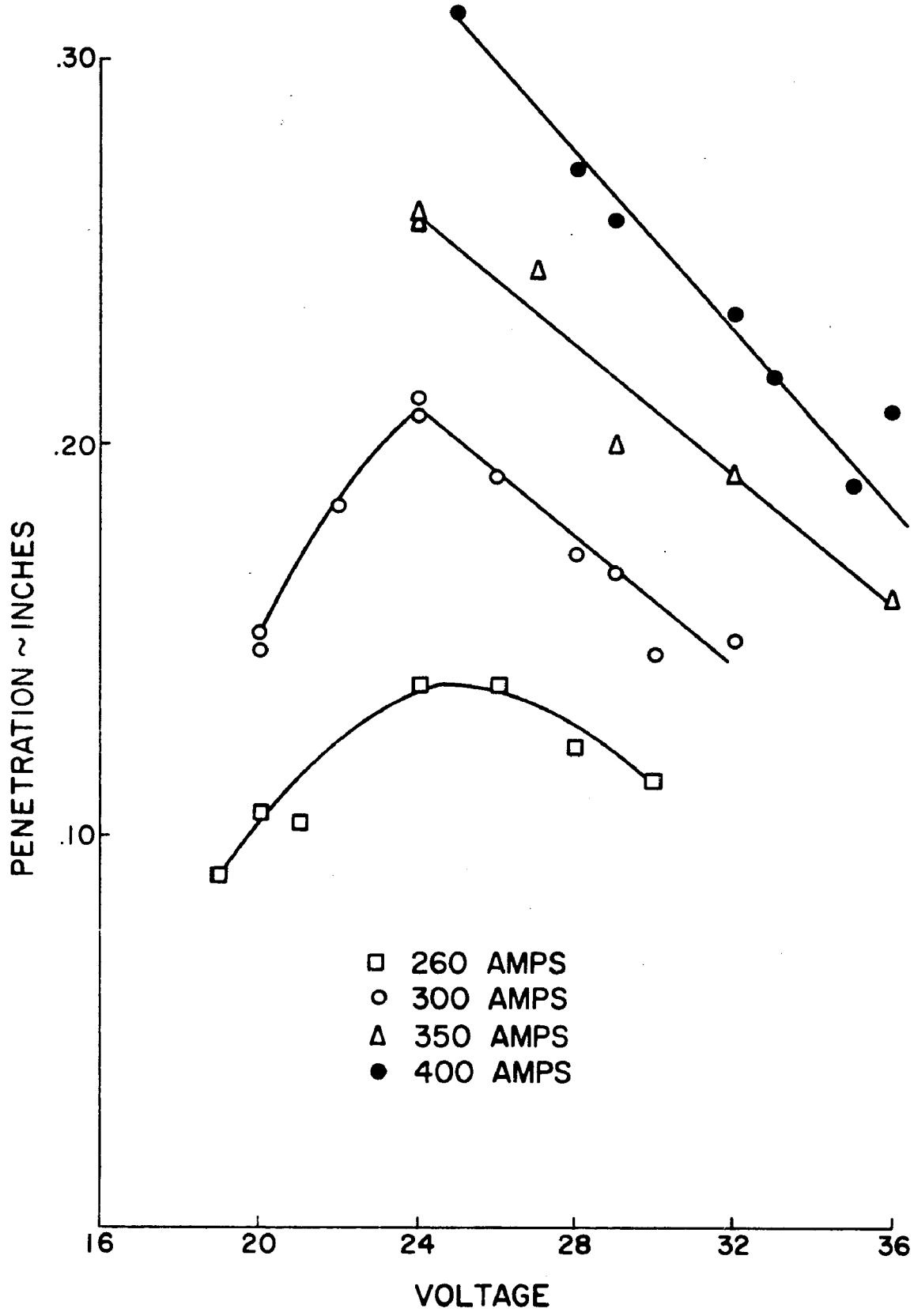

FIG. 7. EFFECT OF VOLTAGE ON PENETRATION AT TRAVEL SPEED OF 20 INCHES PER MINUTE.

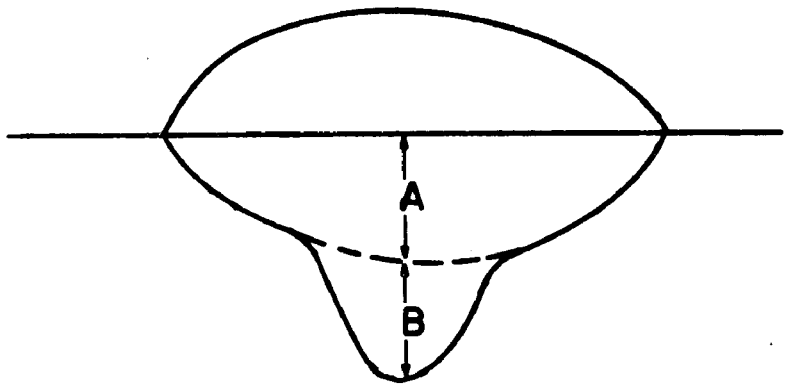

A-5
300 AMPS, 25 VOLTS
10 INCHES PER MINUTE

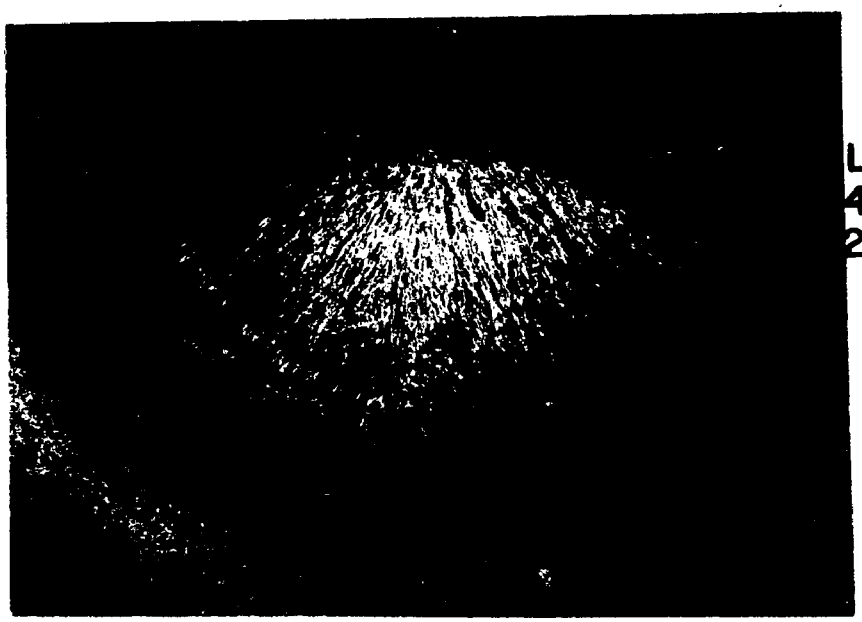

L-2
400 AMPS, 33 VOLTS
20 INCHES PER MINUTE

FIG. 8. SCHEMATIC ILLUSTRATION OF SEPARATION OF PENETRATION INTO ELLIPTICAL WELD POOL DEPTH, A, AND FINGER HEIGHT, B, AS WELL AS TWO REPRESENTATIVE WELD BEAD CROSS SECTIONS INDICATING EXTREME A/B RATIOS.

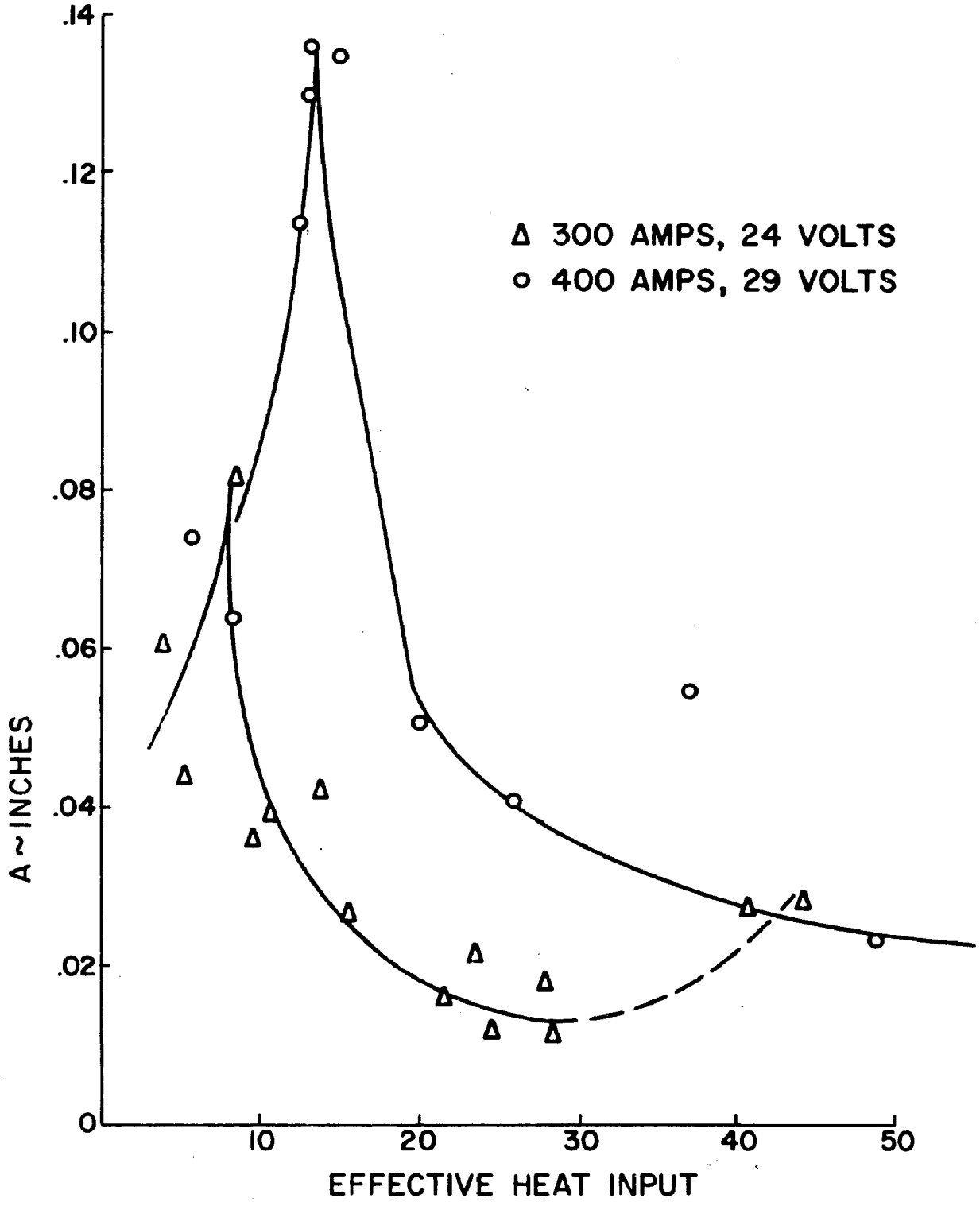

FIG. 9. ELLIPTICAL POOL DEPTH A, AS A FUNCTION OF E.H.I. AT DIFFERENT AMPERAGE LEVELS.

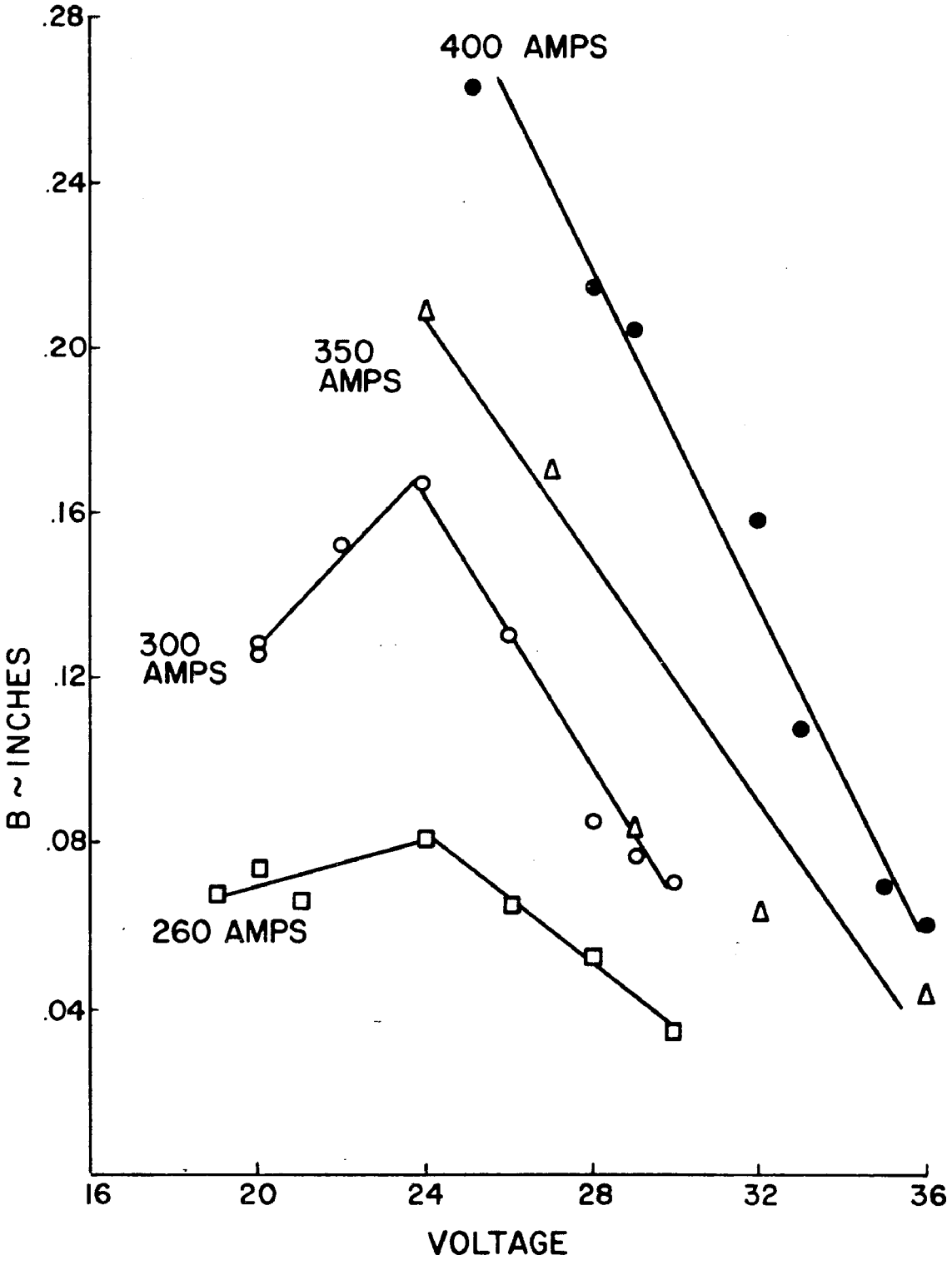

FIG. 10. PENETRATION FINGER HEIGHT, B, AS A FUNCTION OF VOLTAGE AT 20 INCHES PER MINUTE AND THE CURRENT LEVELS INDICATED.

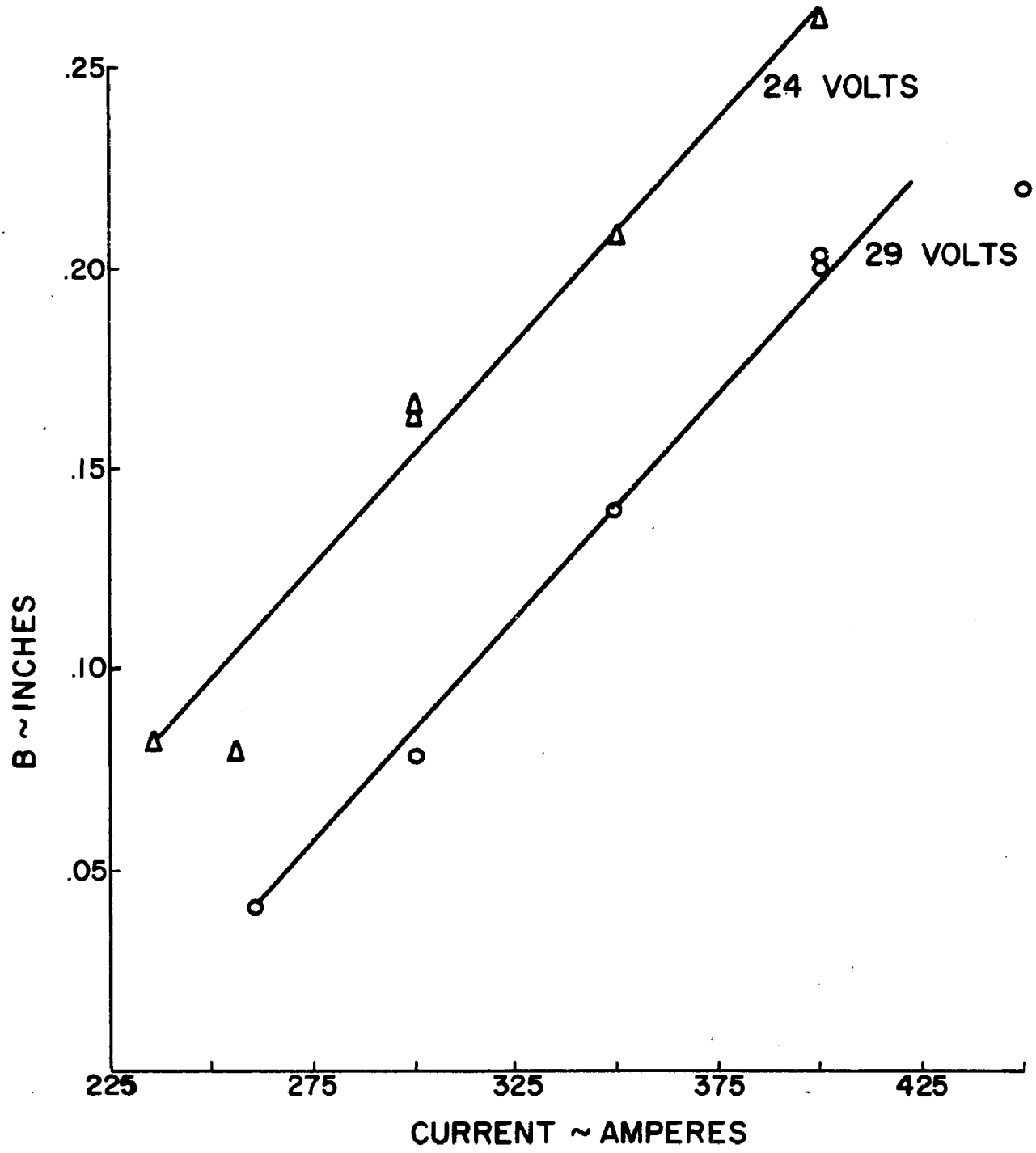

FIG. 11. FINGER HEIGHT, B, AS A FUNCTION OF WELDING CURRENT AT 20 INCHES PER MINUTE AND AT TWO VOLTAGE LEVELS.

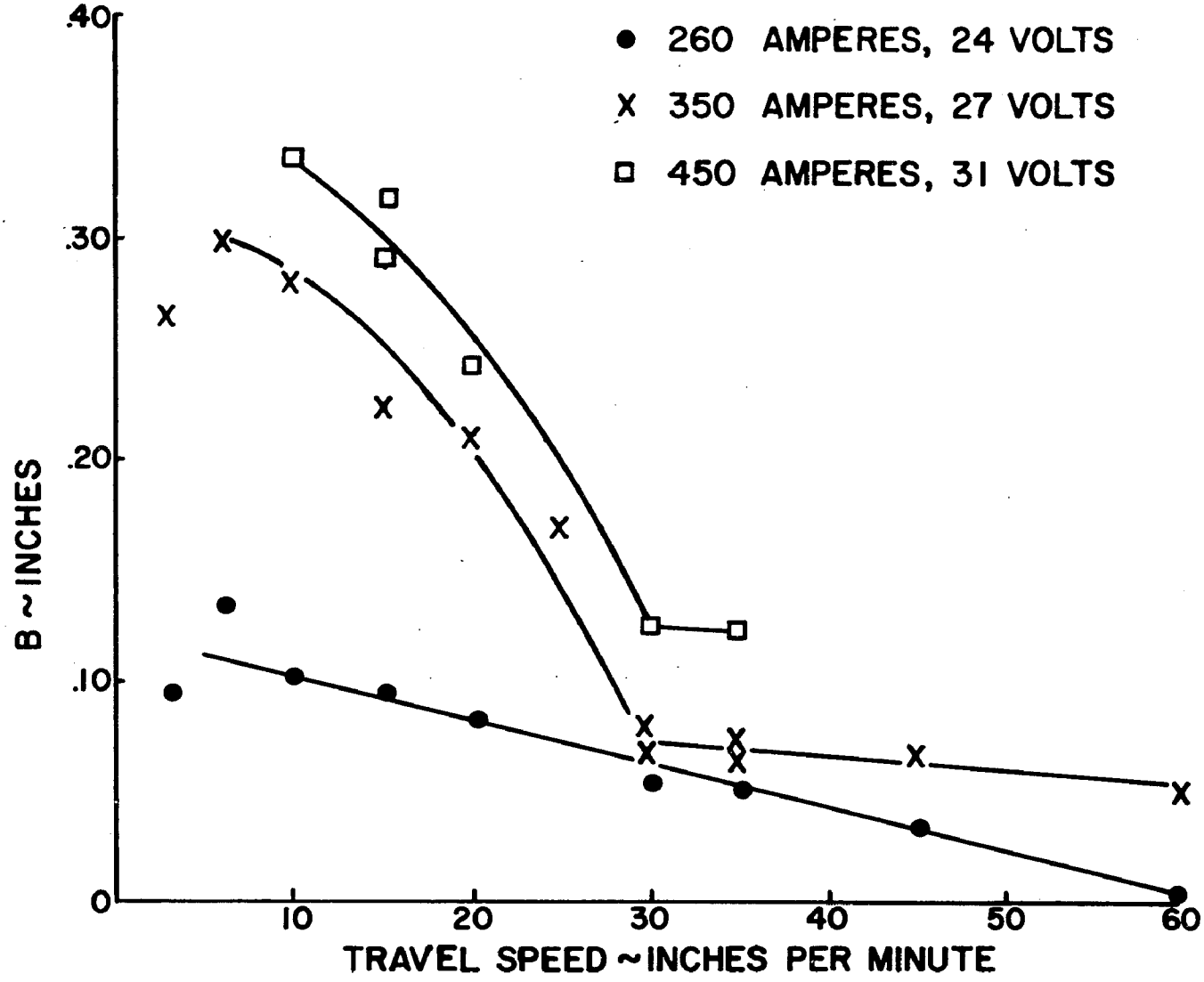

FIG. 12. FINGER HEIGHT, B, VERSUS TRAVEL SPEED.

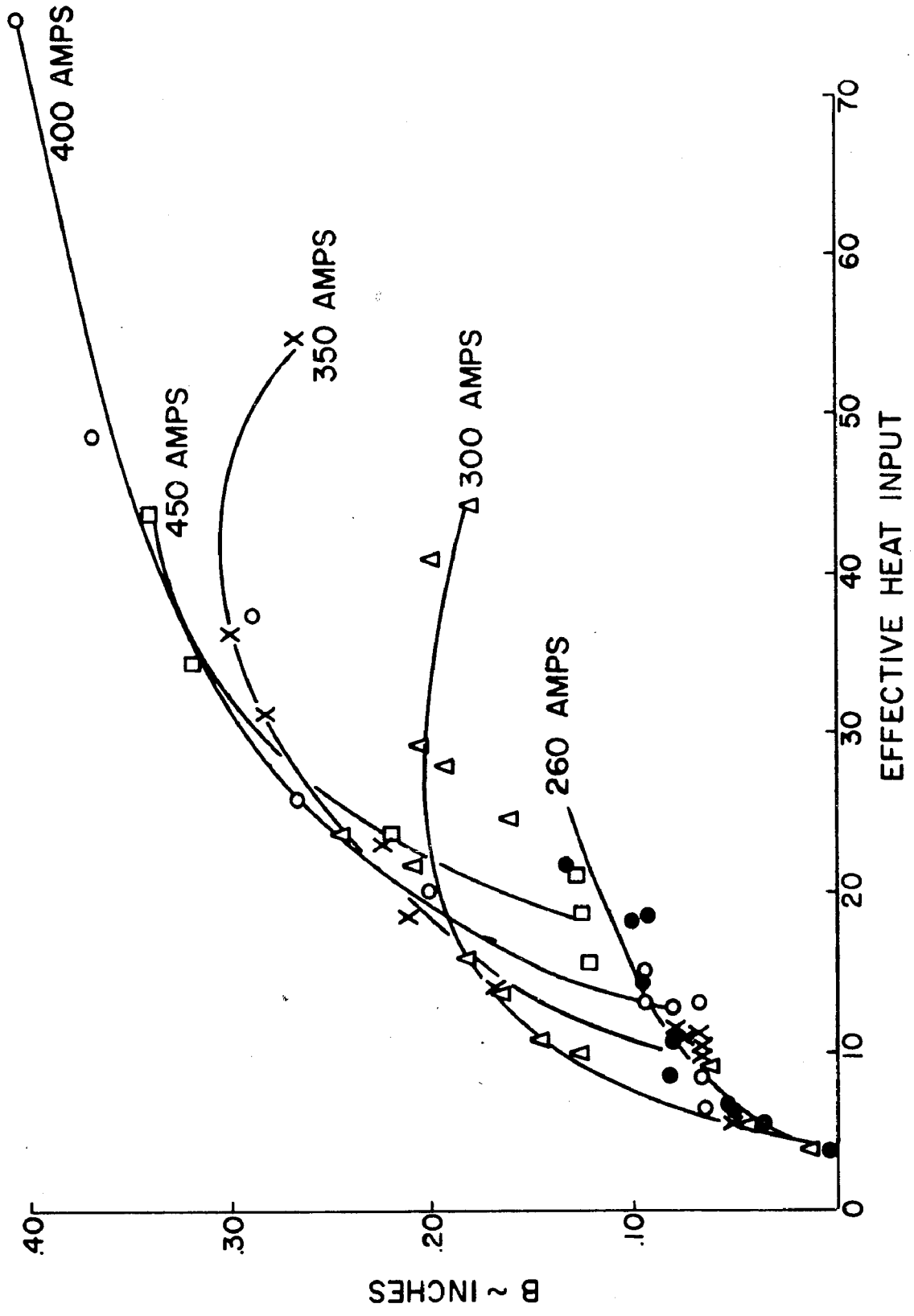

FIG. 13. FINGER HEIGHT, B, AS A FUNCTION OF EFFECTIVE HEAT INPUT.

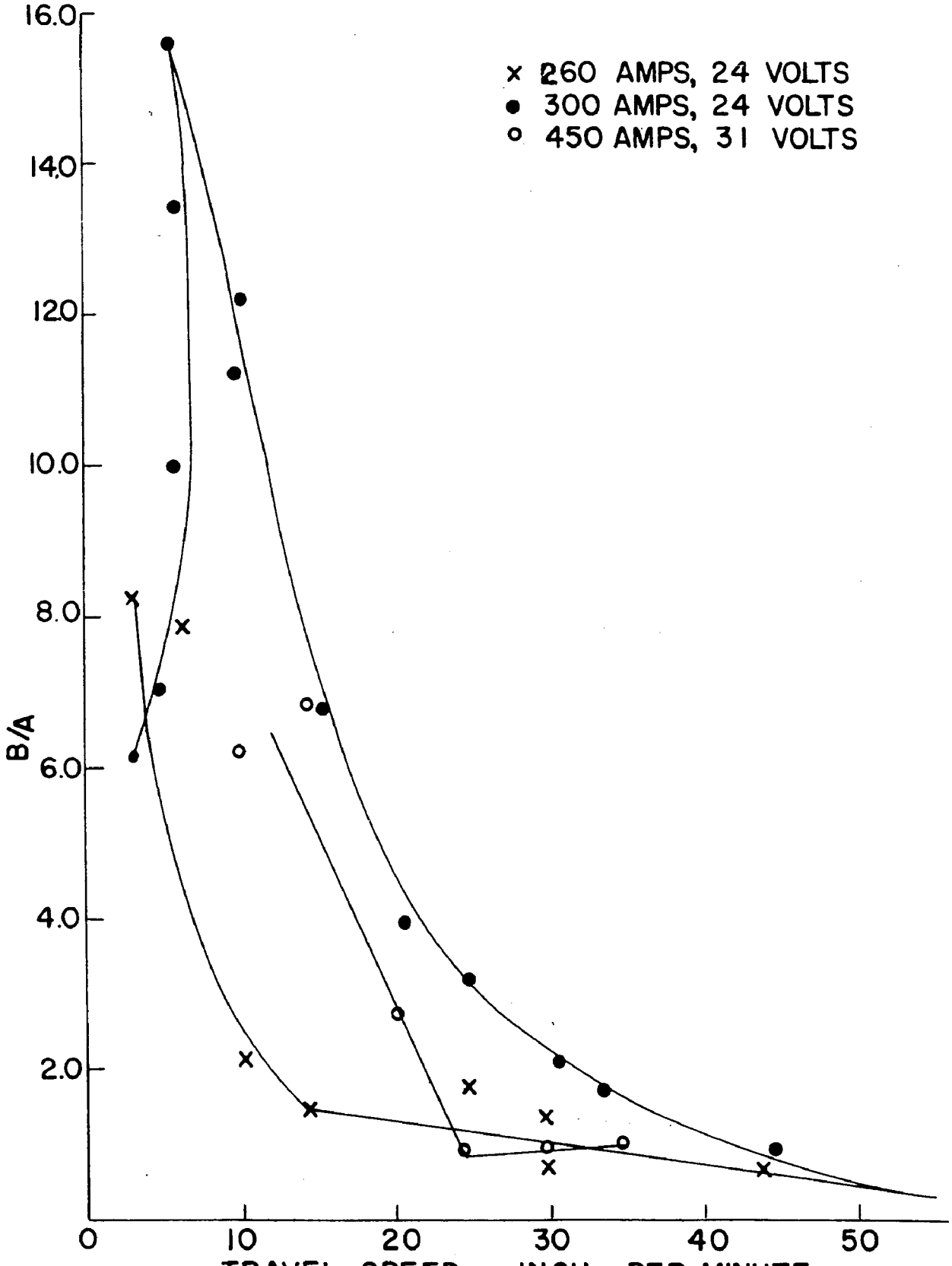

FIG. 14. PENETRATION RATIO (FINGER HEIGHT/ELLIPTICAL POOL DEPTH) VERSUS TRAVEL SPEED.

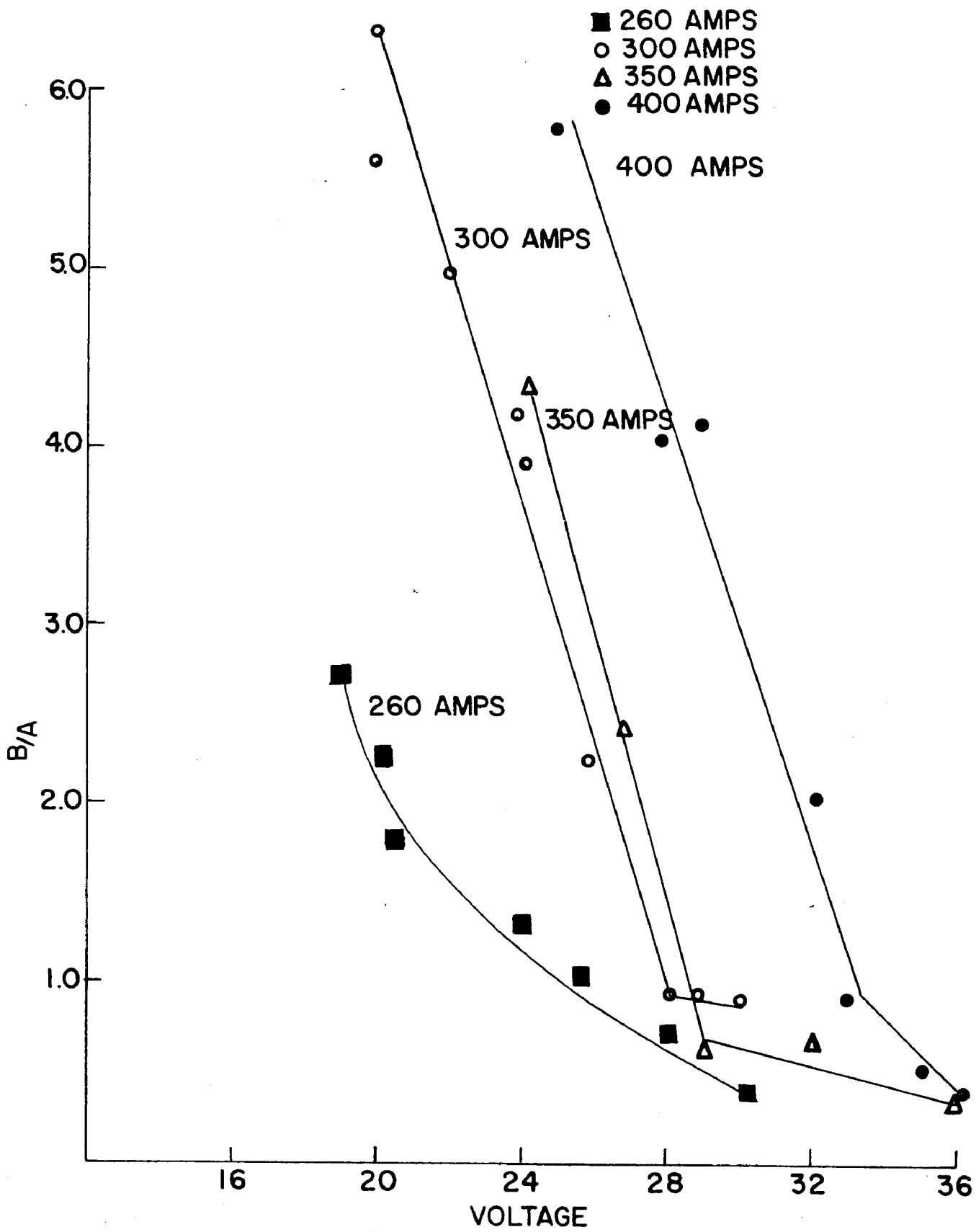

FIG. 15. PENETRATION RATIO, B/A, AS A FUNCTION OF VOLTAGE AT 20 INCHES PER MINUTE AND CURRENT LEVELS INDICATED.

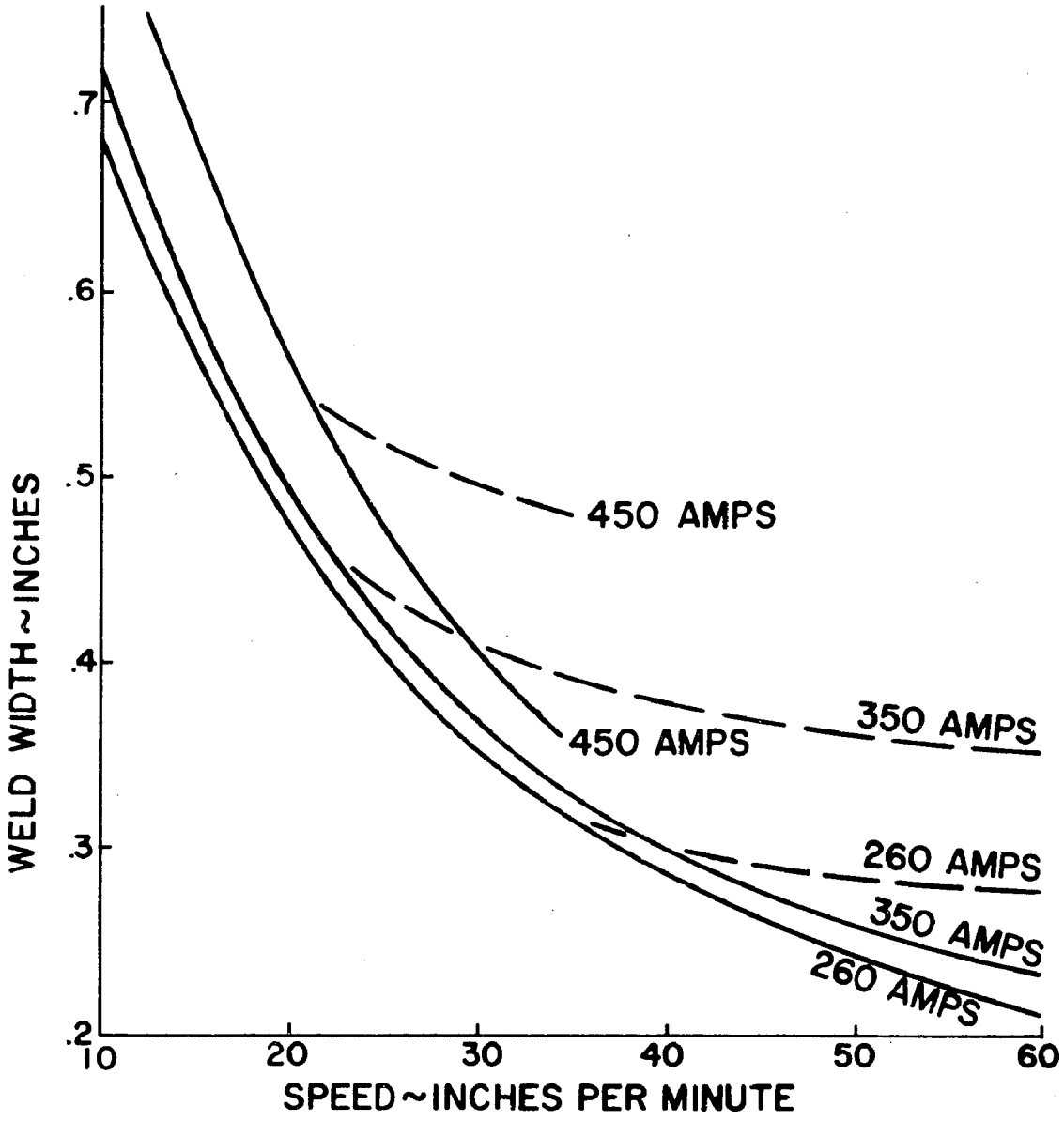

FIG. 16. WELD WIDTH AS A FUNCTION OF TRAVEL SPEED. DOTTED LINES INDICATE WIDTH OF MELTED HOLE IN BASE PLATE FOR CASES OF UNDERCUTTING.

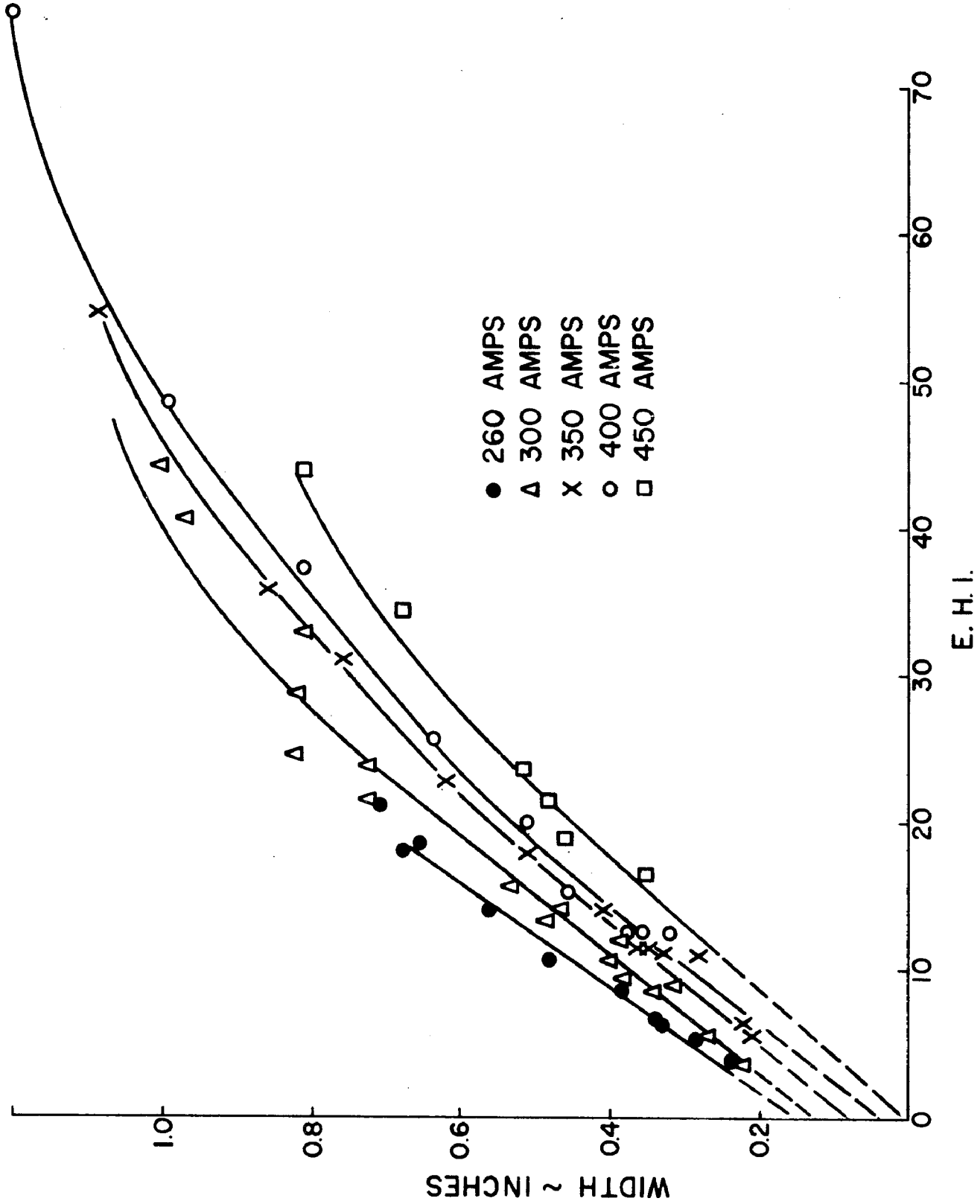

FIG. 17. WELD BEAD WIDTH AS A FUNCTION OF EFFECTIVE HEAT INPUT.

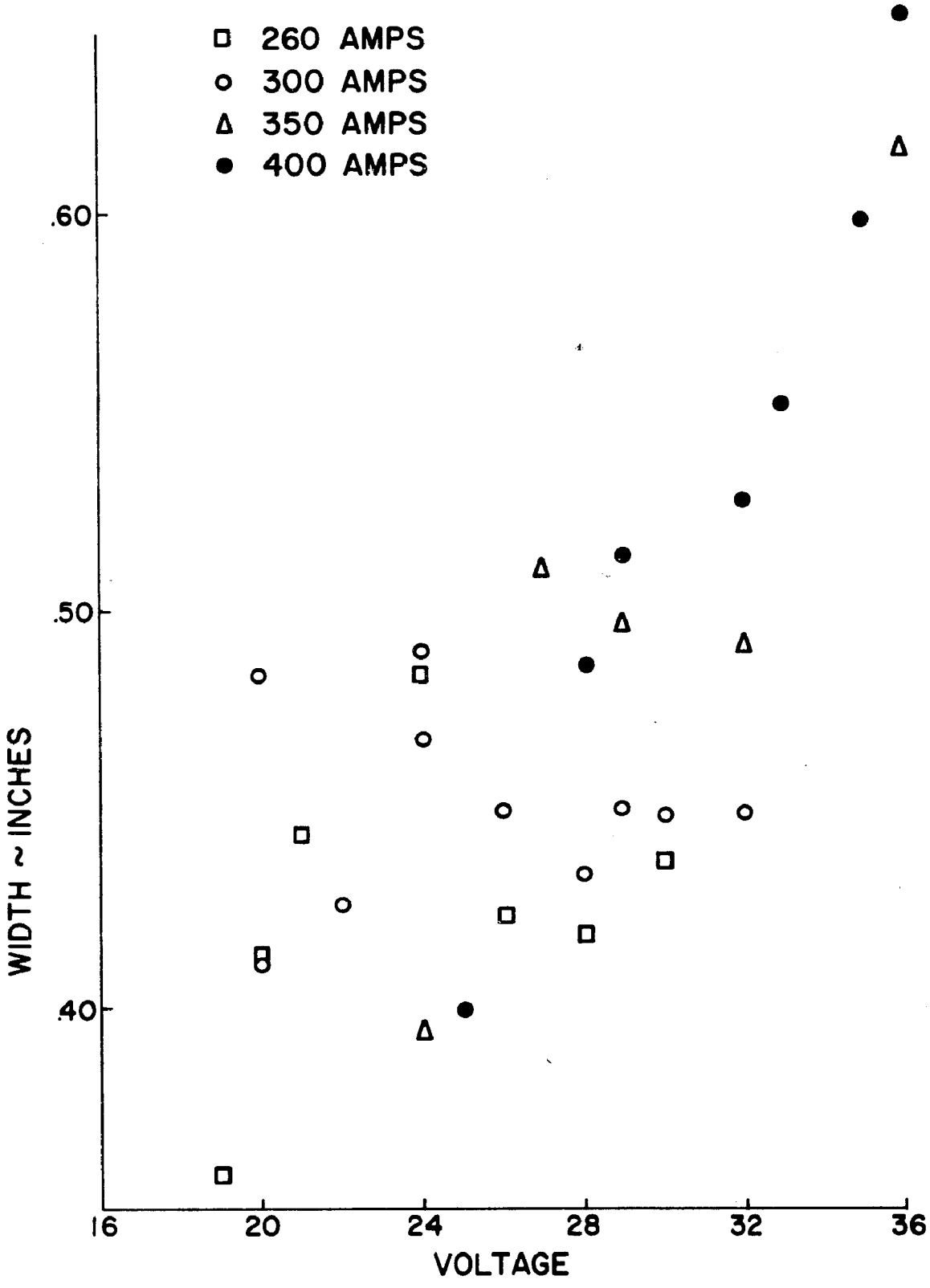

FIG. 18. WELD BEAD WIDTH VERSUS VOLTAGE AT 20 INCHES PER MINUTE.

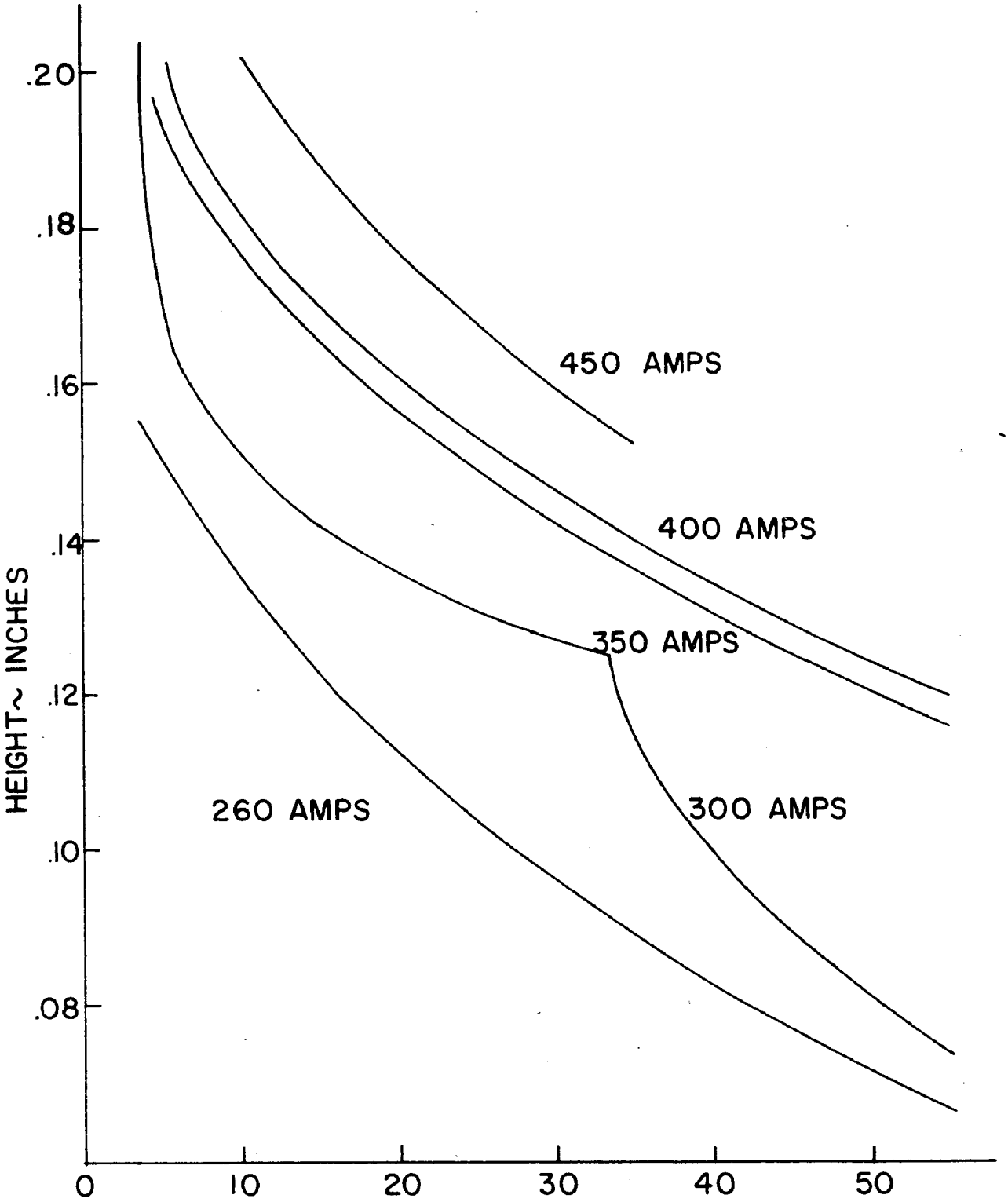

FIG. 19. WELD REINFORCEMENT HEIGHT VERSUS TRAVEL SPEED.

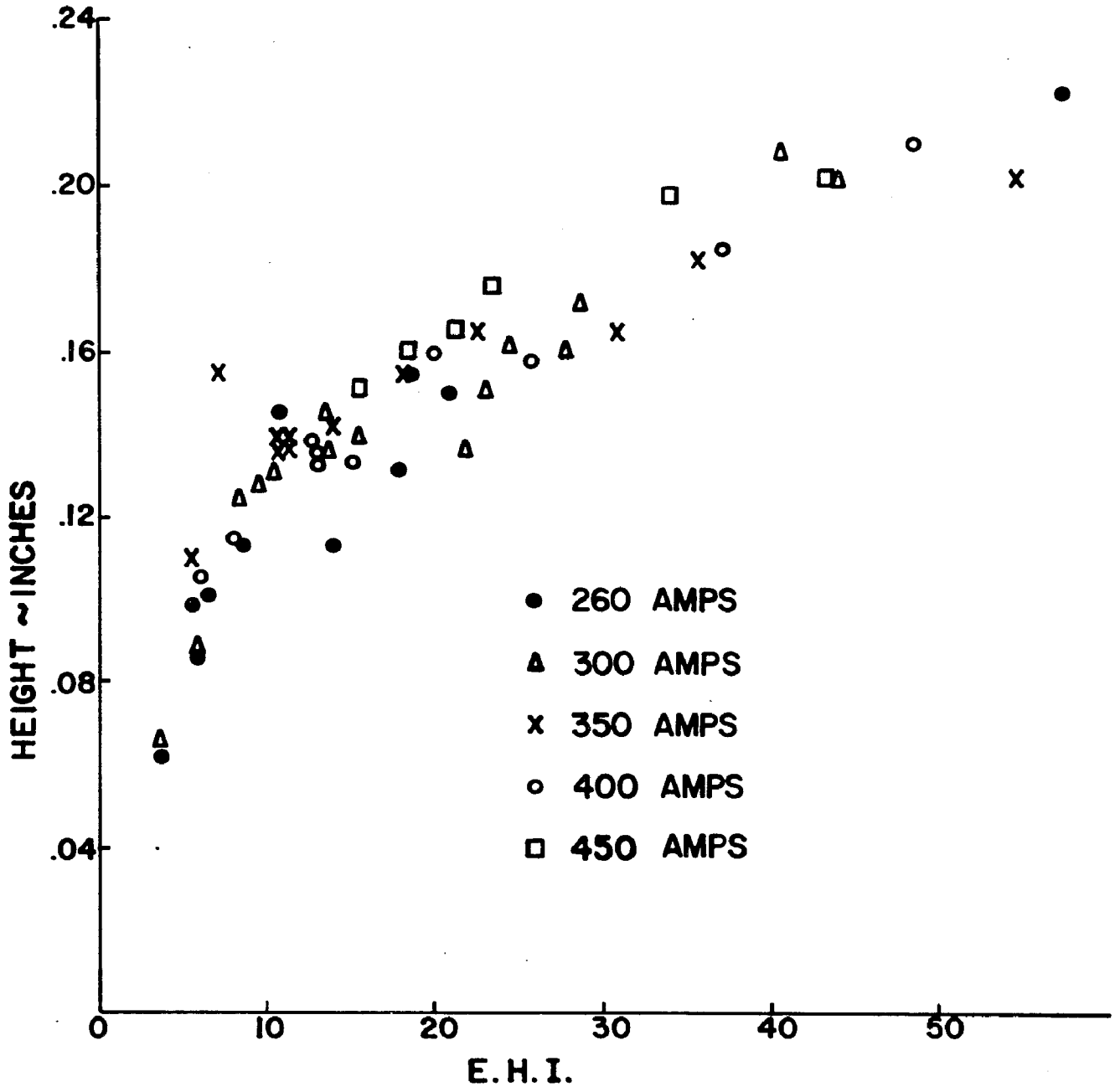

FIG. 20. WELD REINFORCEMENT HEIGHT AS A FUNCTION OF EFFECTIVE HEAT INPUT.

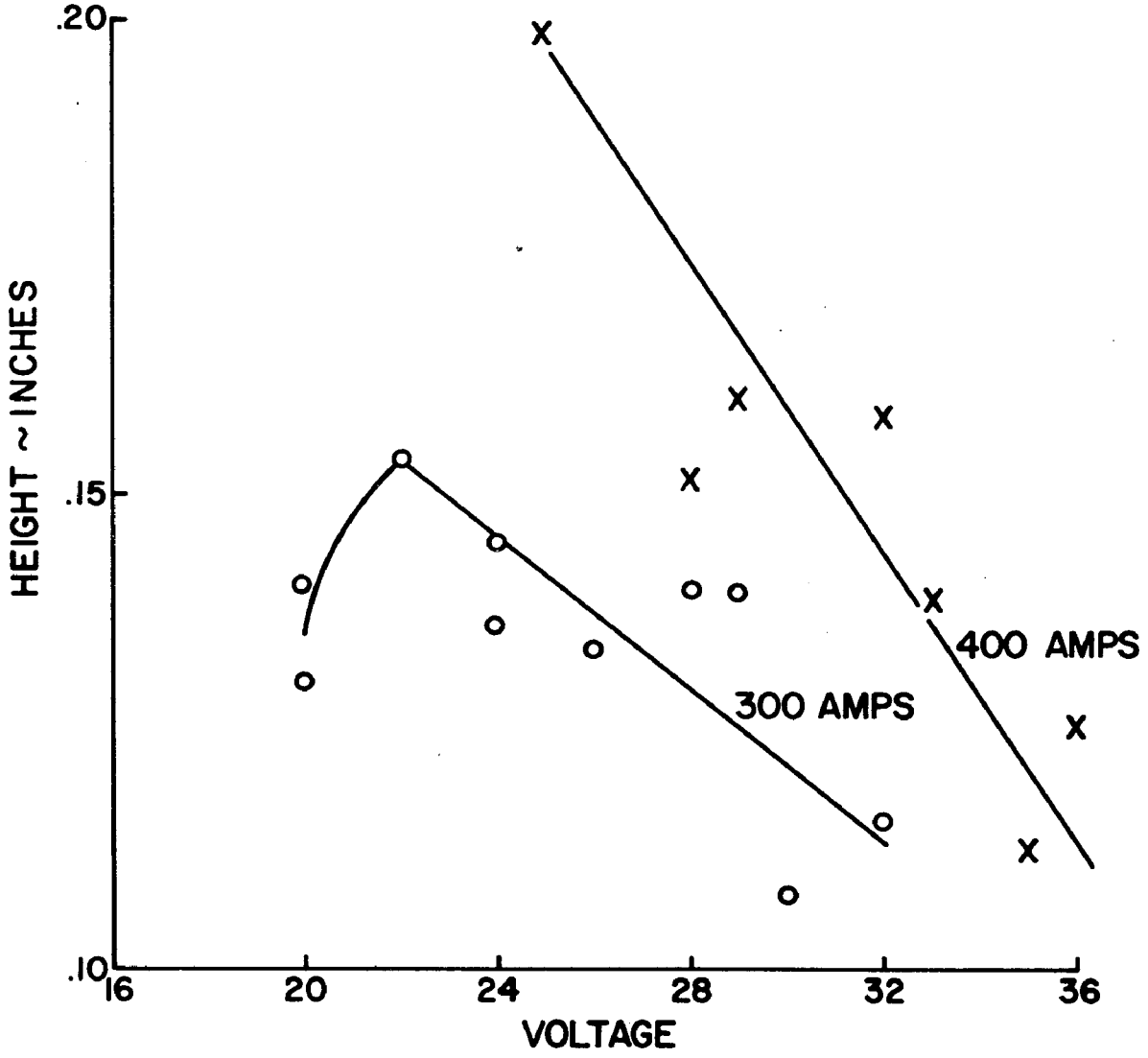

FIG. 21. WELD REINFORCEMENT HEIGHT AS A FUNCTION OF VOLTAGE AT 20 INCHES PER MINUTE.

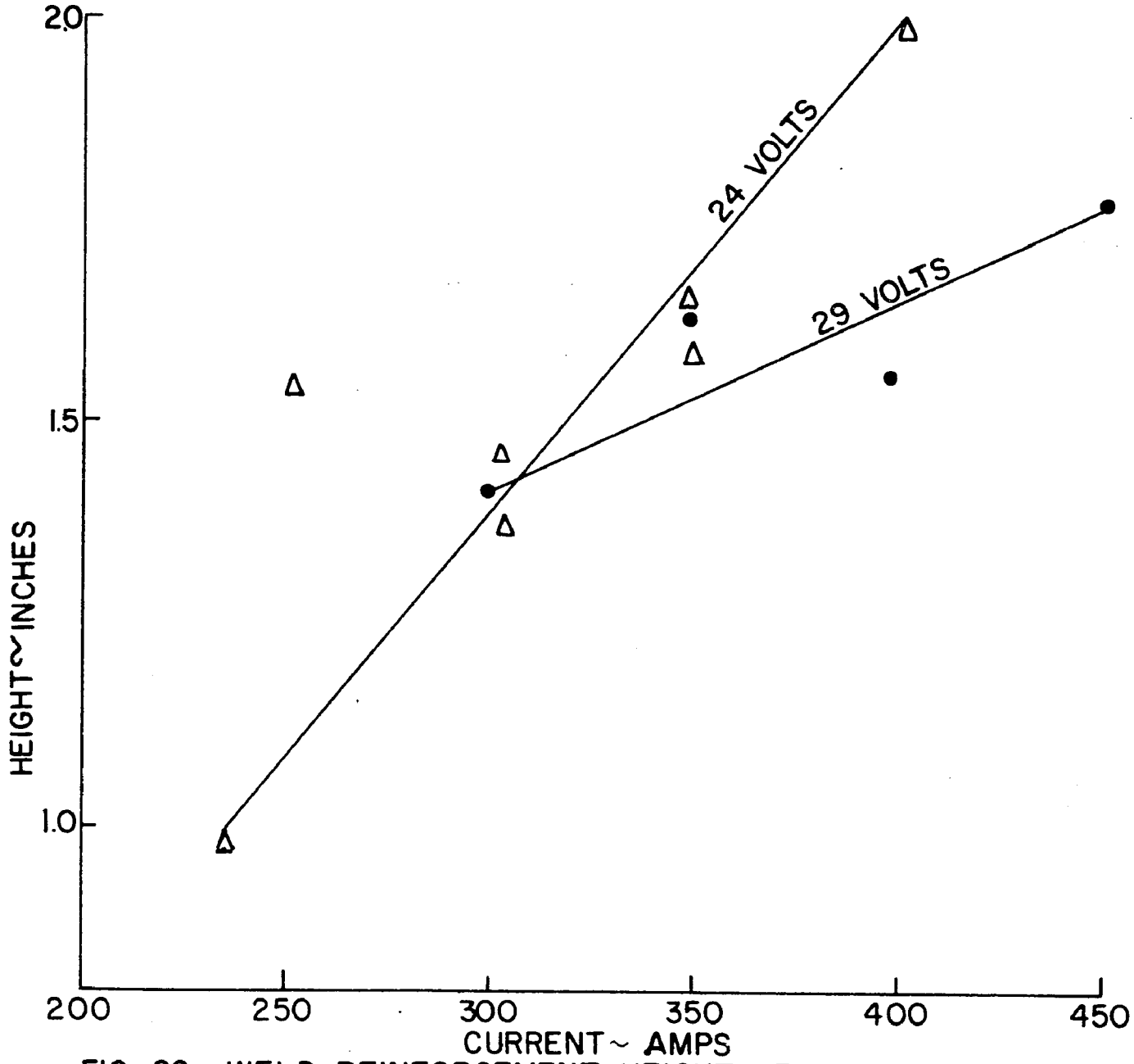

FIG. 22. WELD REINFORCEMENT HEIGHT VERSUS CURRENT LEVEL AT TWO SET VOLTAGES.

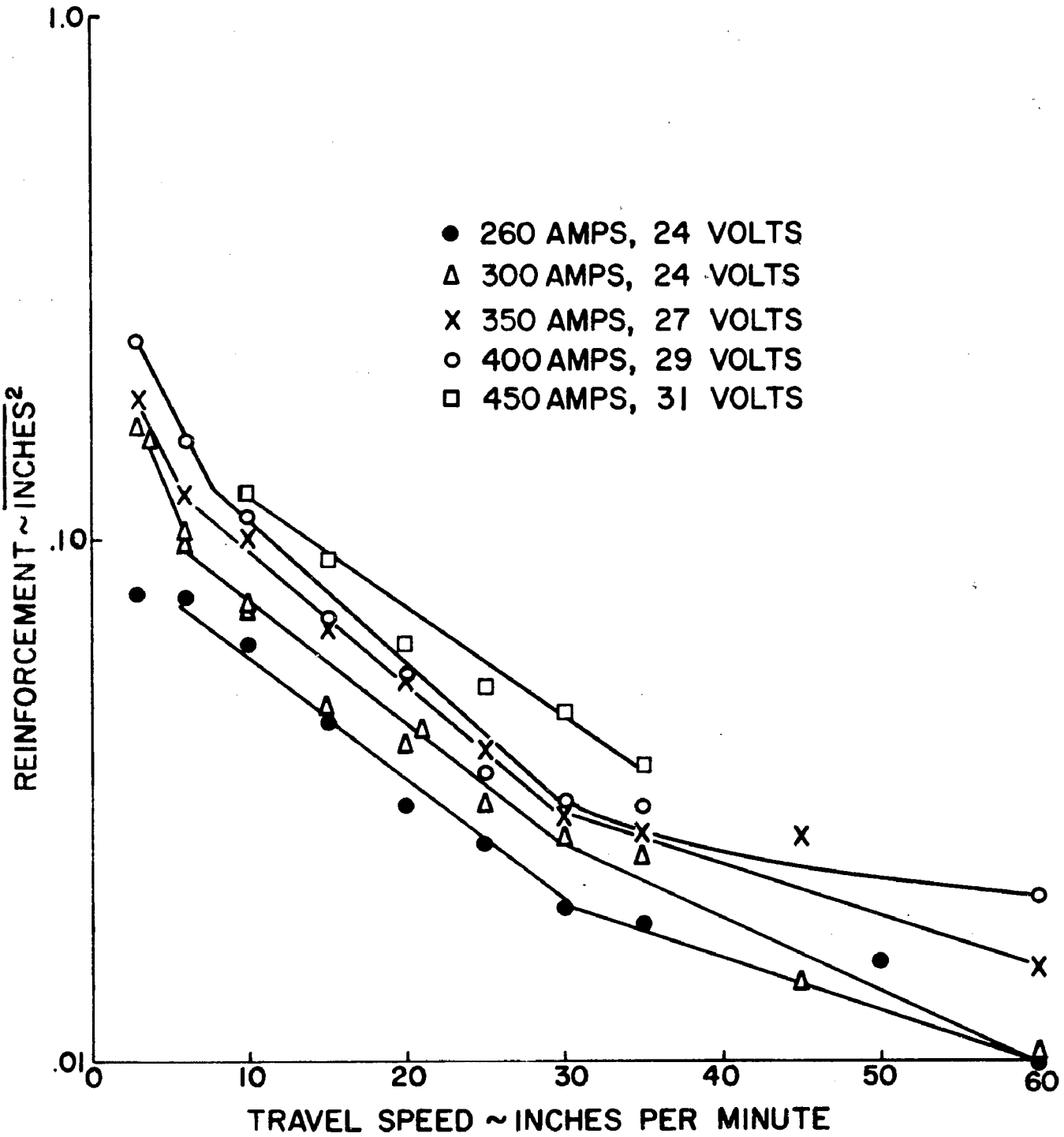

FIG. 23. REINFORCEMENT VOLUME (per inch of weld) AS A FUNCTION OF TRAVEL SPEED.

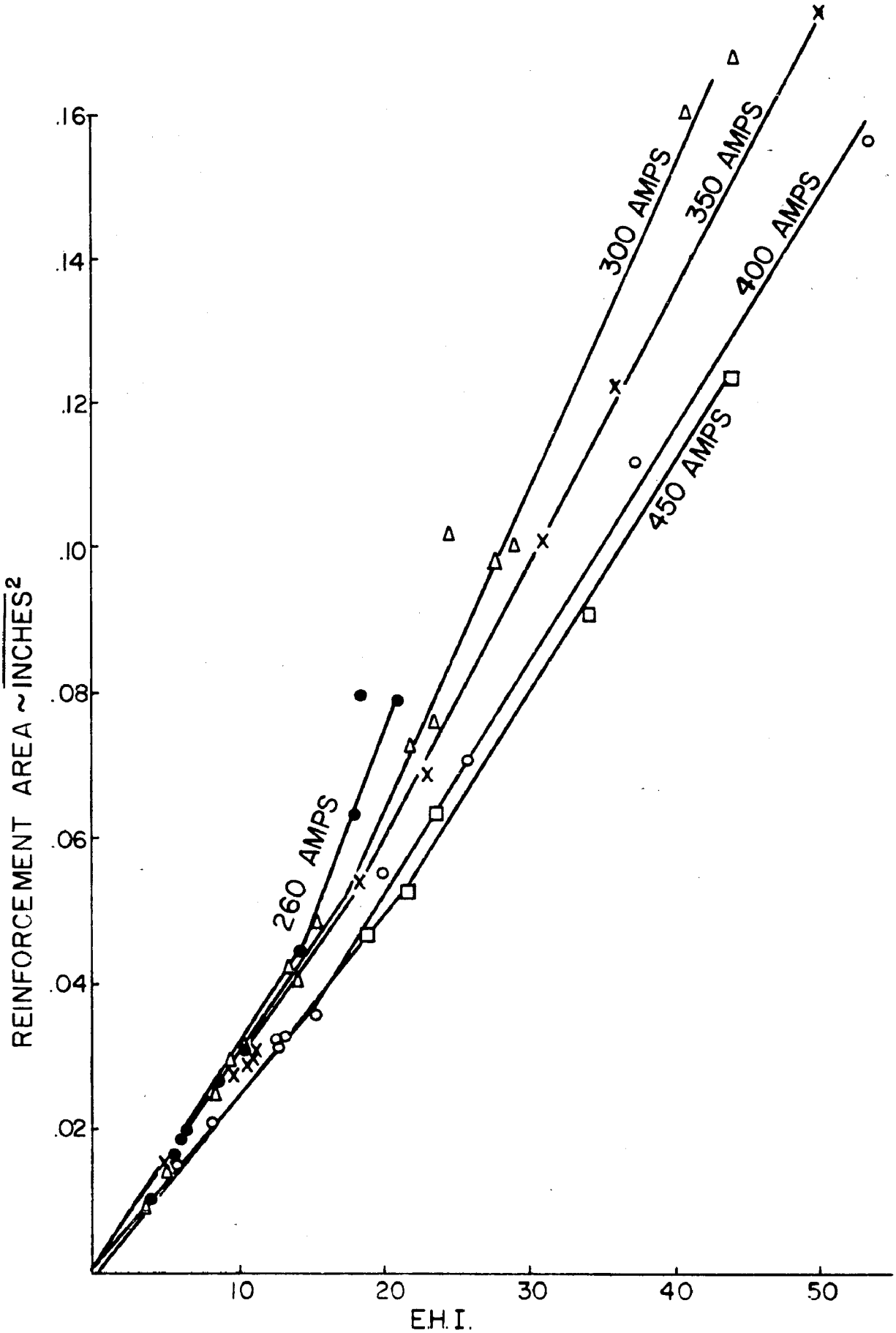

FIG. 24. REINFORCEMENT AREA AS A FUNCTION OF EFFECTIVE HEAT INPUT.

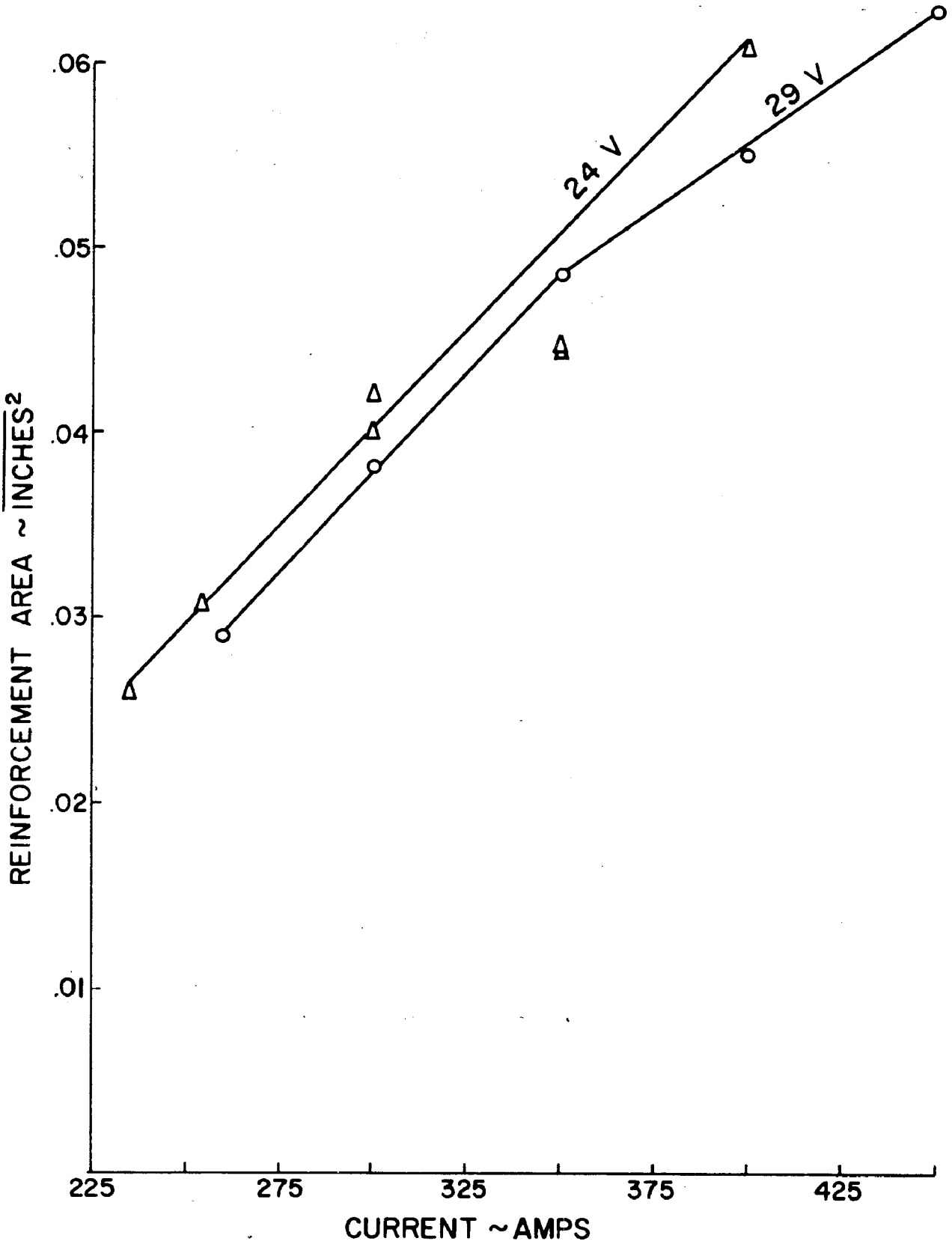

FIG. 25. REINFORCEMENT AREA AS A FUNCTION OF CURRENT LEVEL.

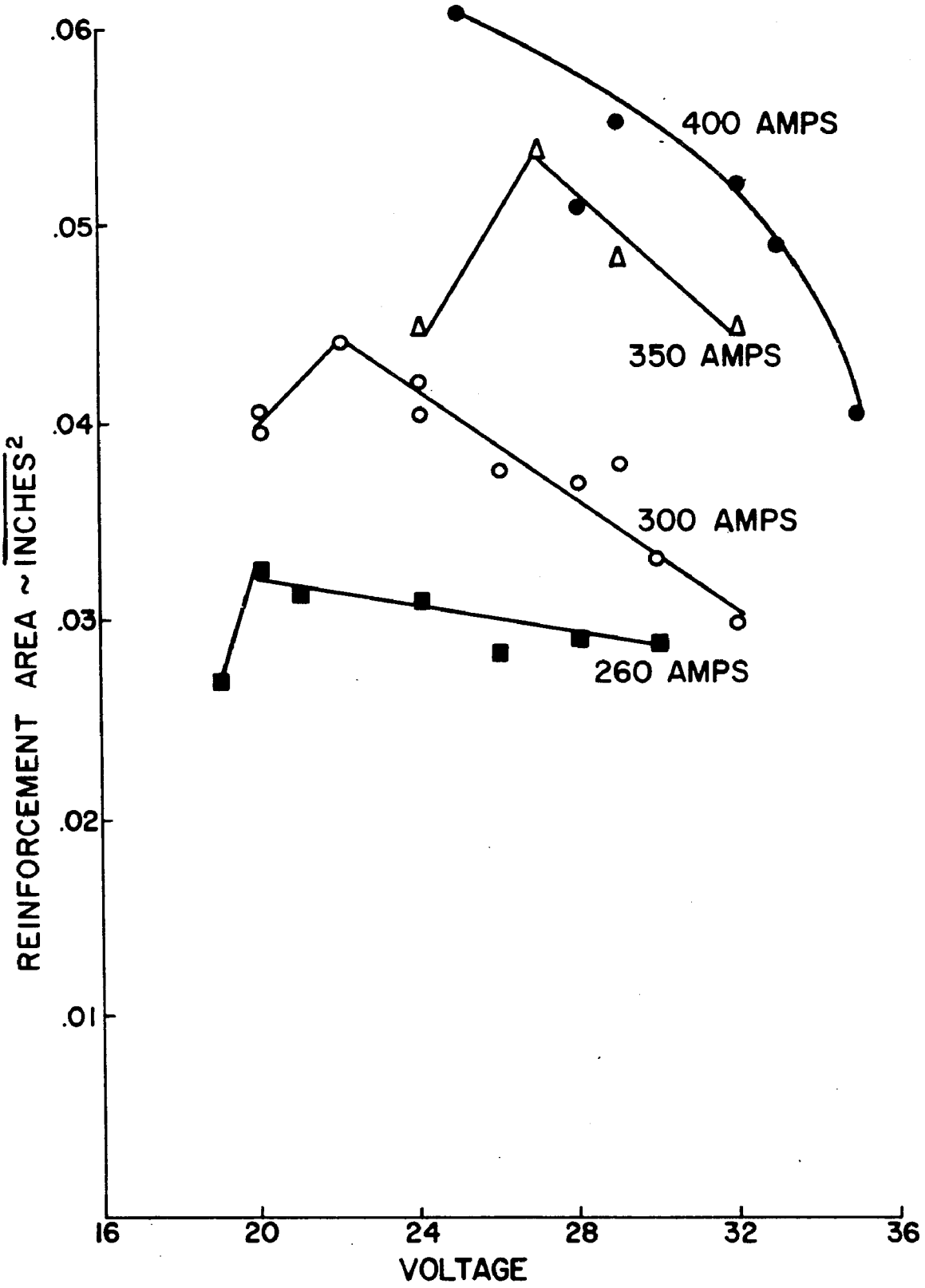

FIG. 26. REINFORCEMENT AREA AS A FUNCTION OF WELDING VOLTAGE AT 20 INCHES PER MINUTE.

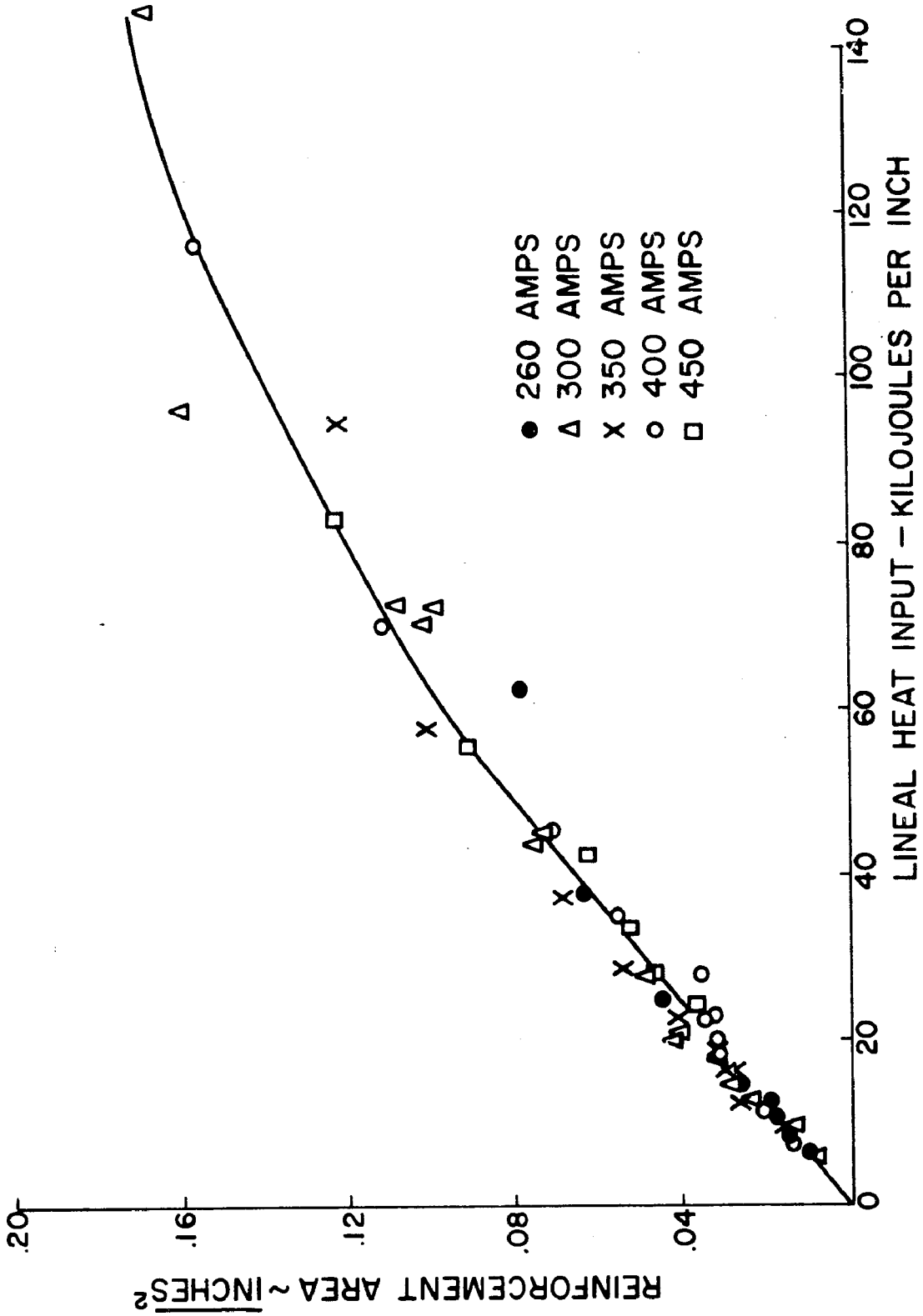

FIG. 27. REINFORCEMENT AREA AS A FUNCTION OF LINEAL HEAT INPUT.

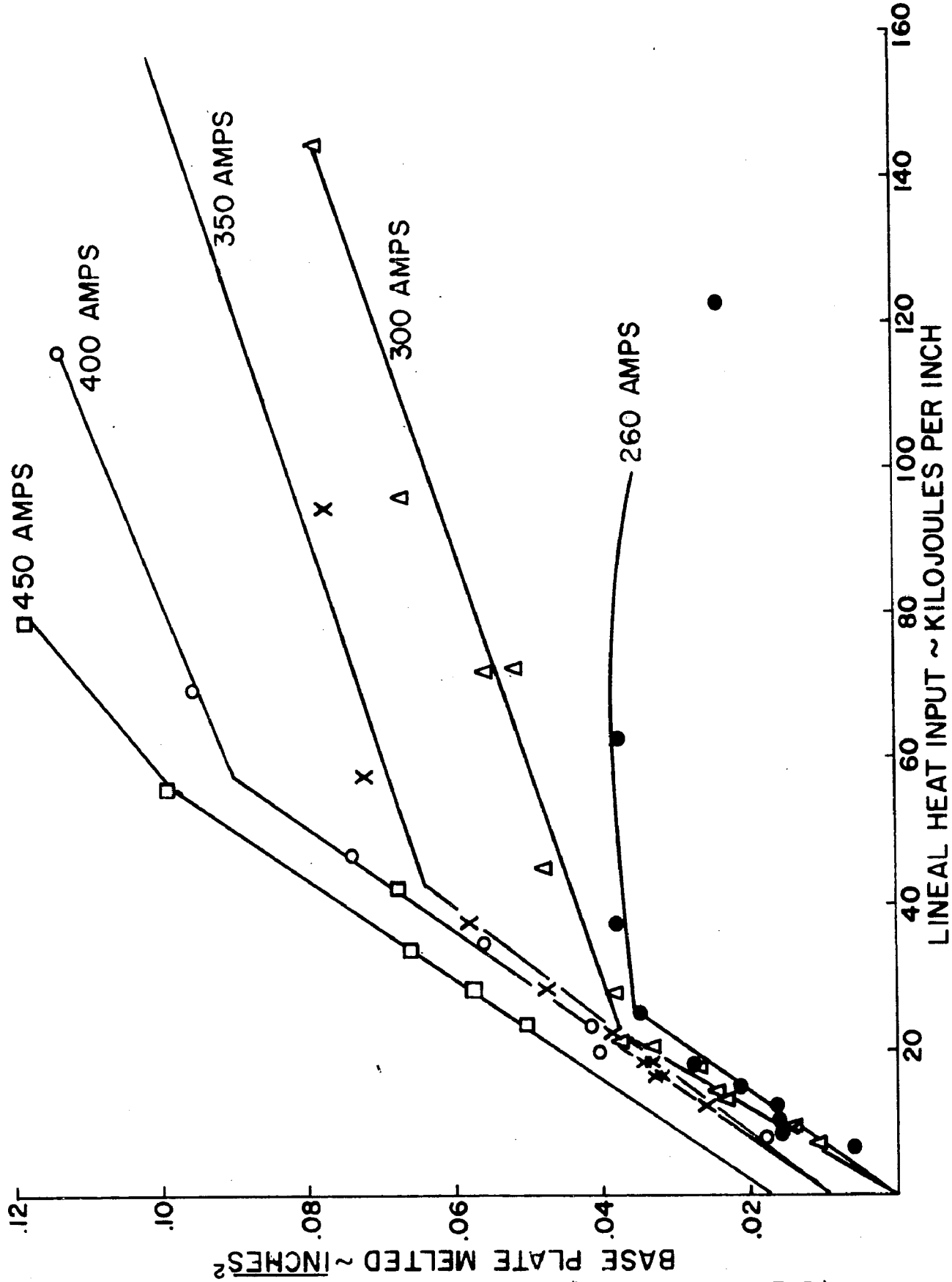

FIG. 28 VOLUME OF BASE PLATE MELTED (PER INCH OF WELD) AS A FUNCTION OF LINEAL HEAT INPUT.

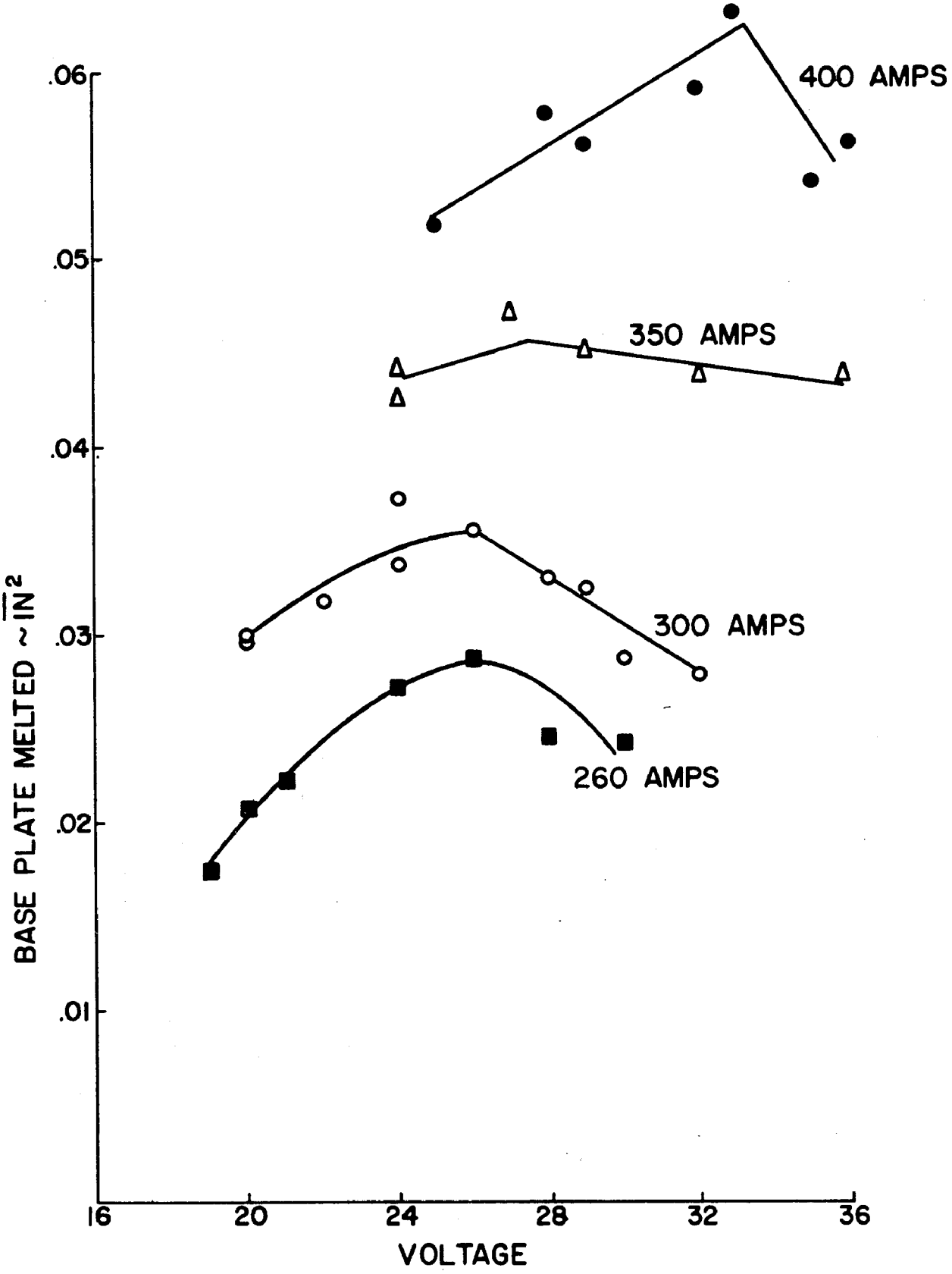

FIG. 29. BASE PLATE AREA MELTED AS A FUNCTION OF WELDING VOLTAGE AT 20 INCHES PER MINUTE.

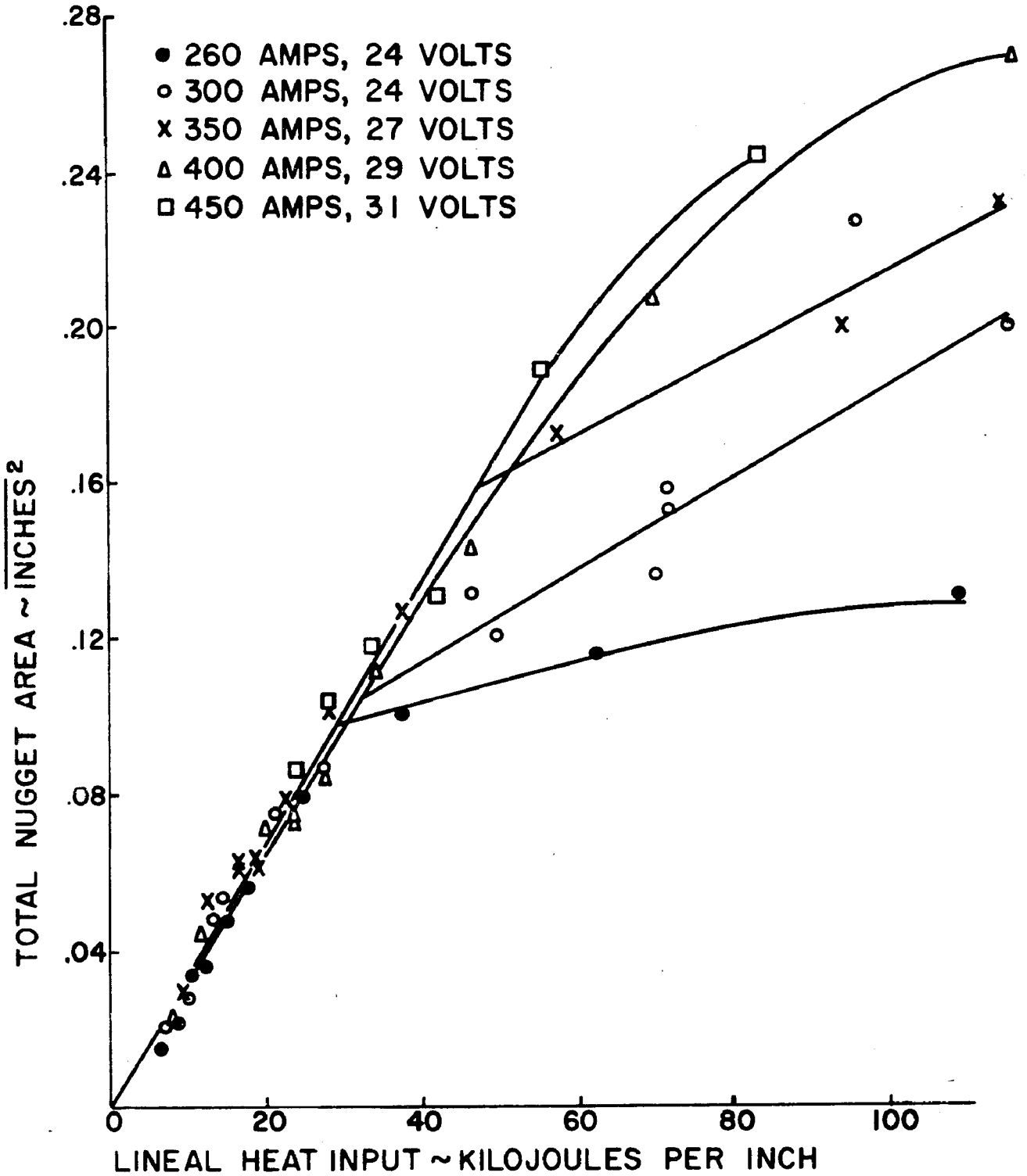

FIG. 30. TOTAL AREA OF WELD NUGGET AS A FUNCTION OF LINEAL HEAT INPUT.

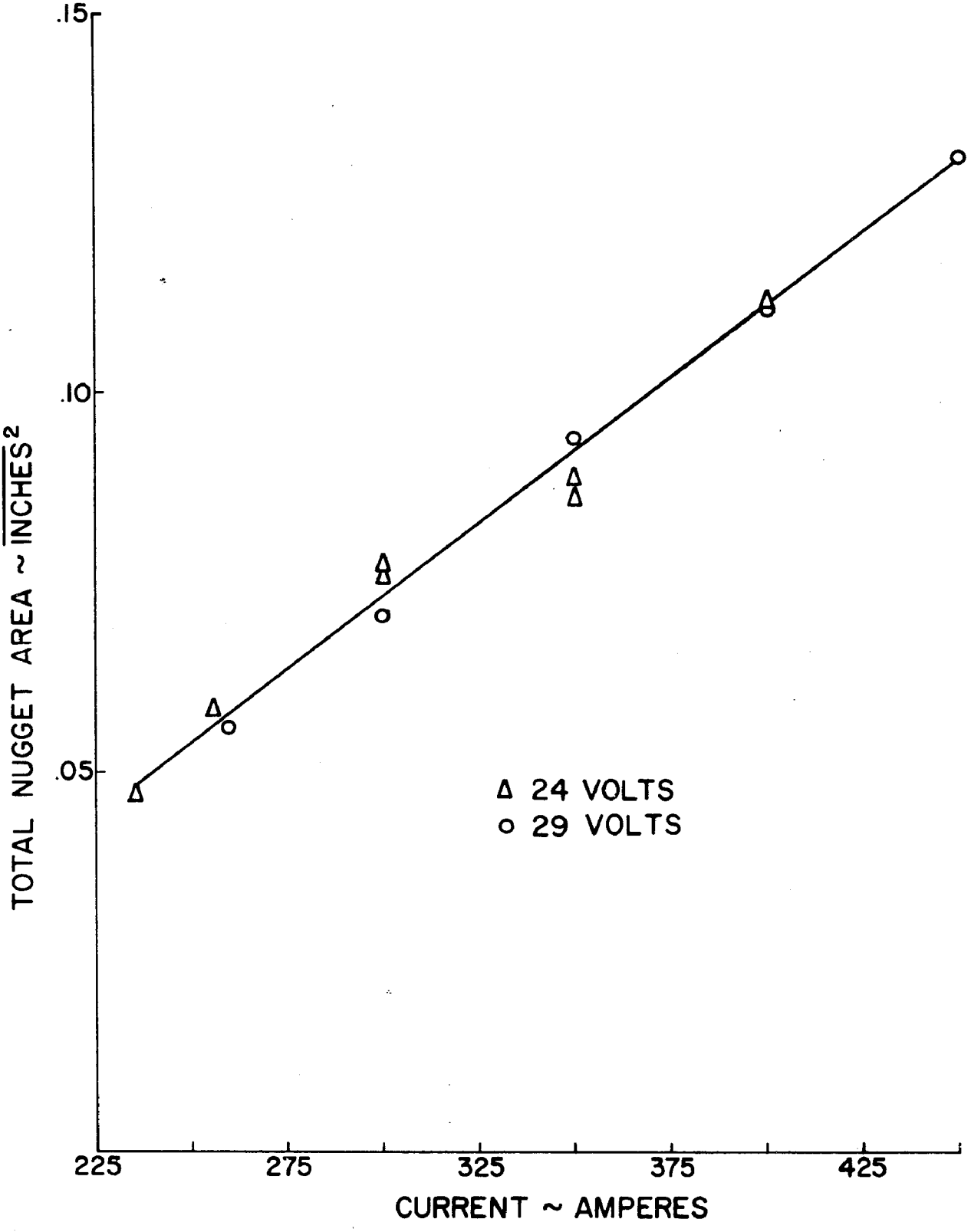

FIG. 31. NUGGET AREA AS A FUNCTION OF CURRENT LEVEL.

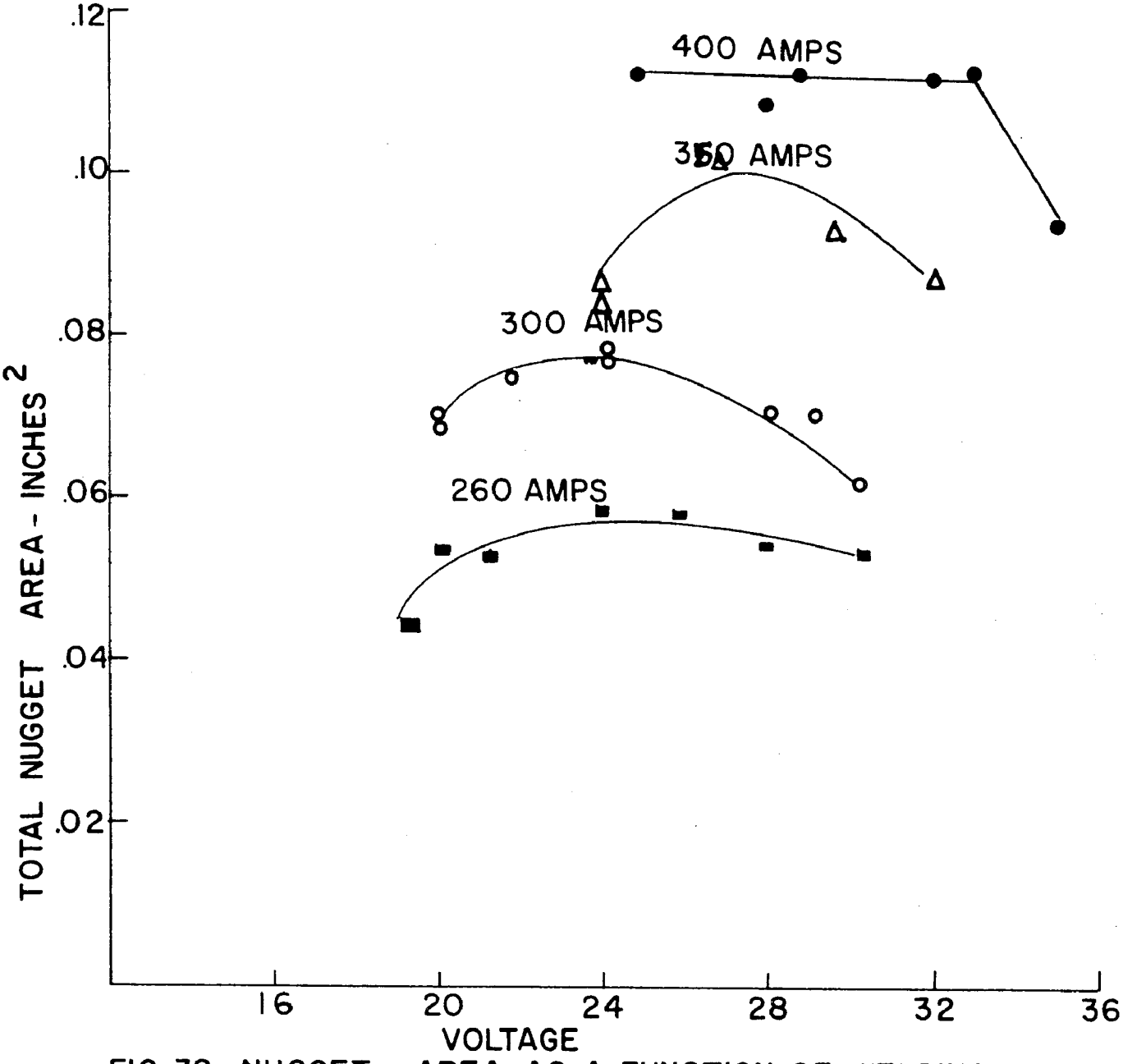

FIG. 32. NUGGET AREA AS A FUNCTION OF WELDING VOLTAGE AT 20 INCHES PER MINUTE.

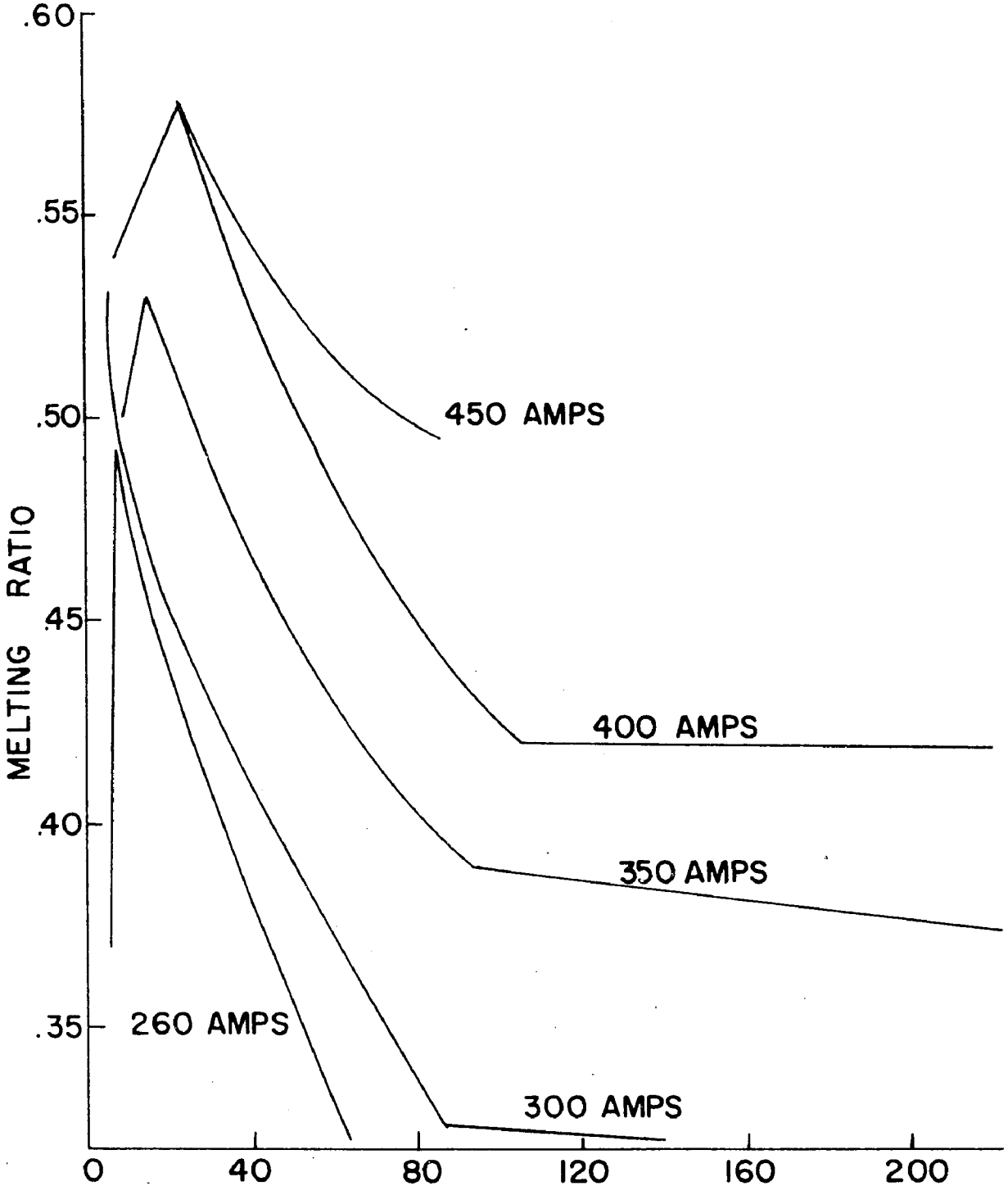

FIG. 33. MELTING RATIO (BASE PLATE MELTED/TOTAL NUGGET AREA) AS A FUNCTION OF LINEAL HEAT INPUT.

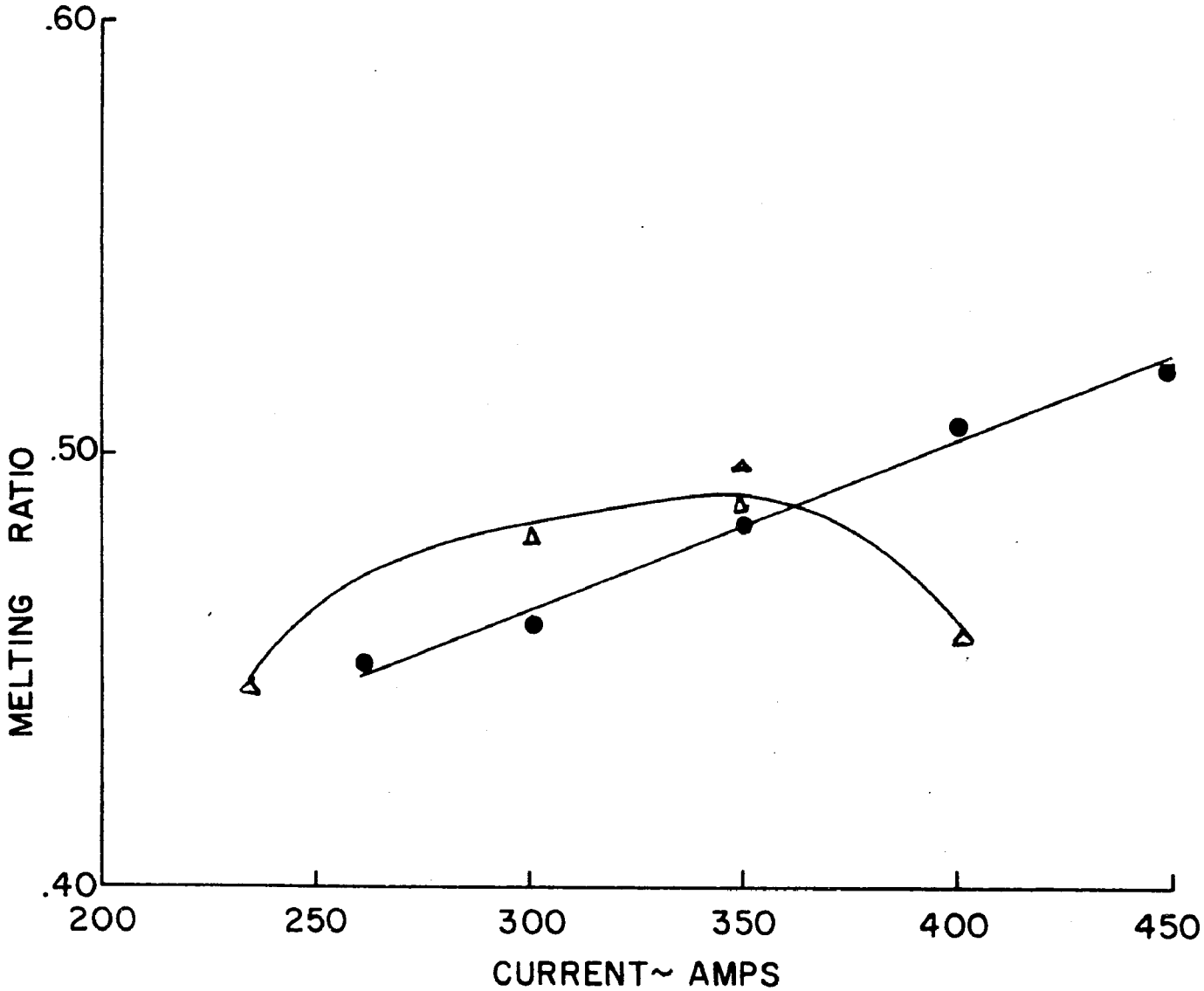

FIG. 34. MELTING RATIO AS A FUNCTION OF WELDING CURRENT.

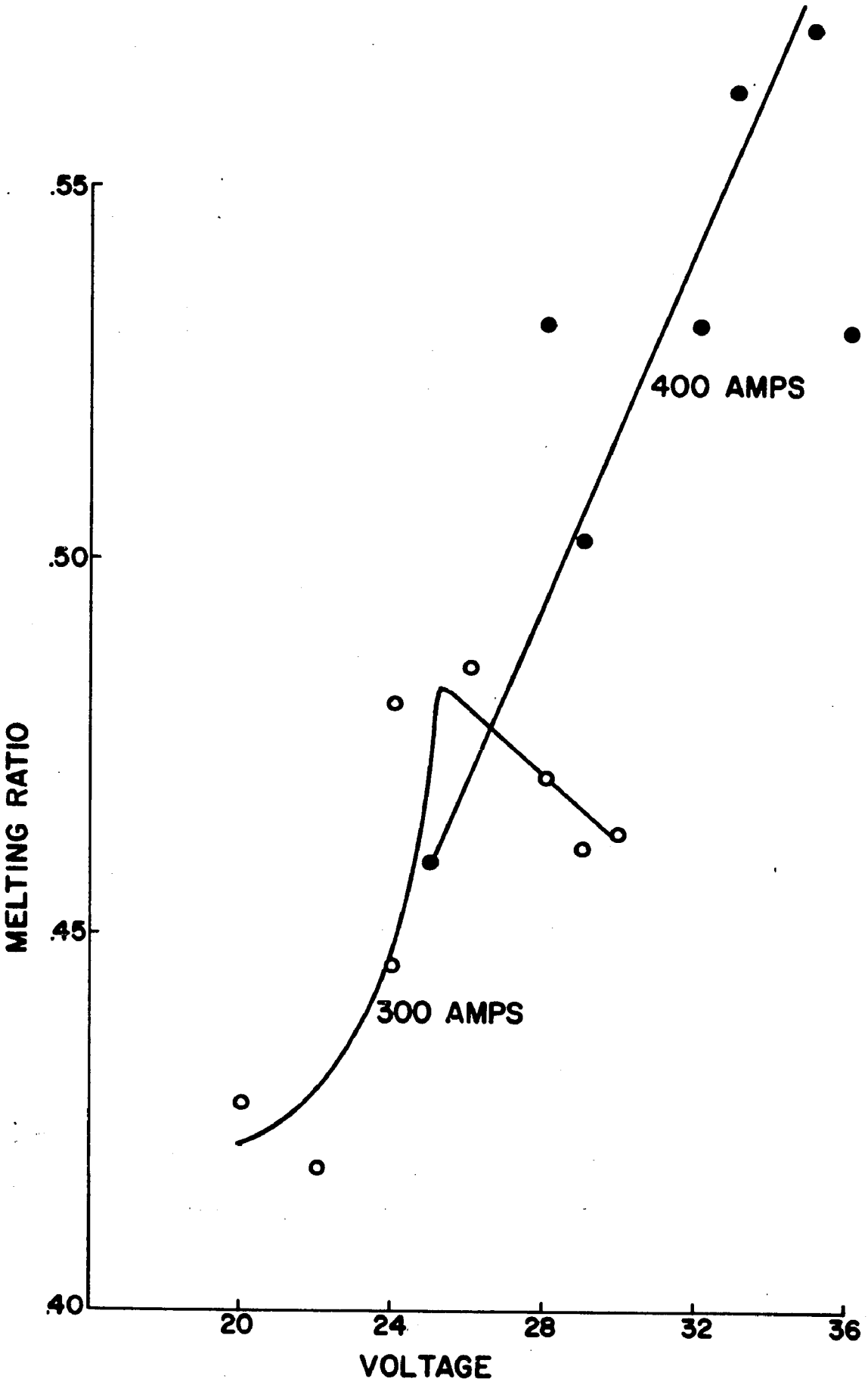

FIG. 35. MELTING RATIO AS A FUNCTION OF VOLTAGE.

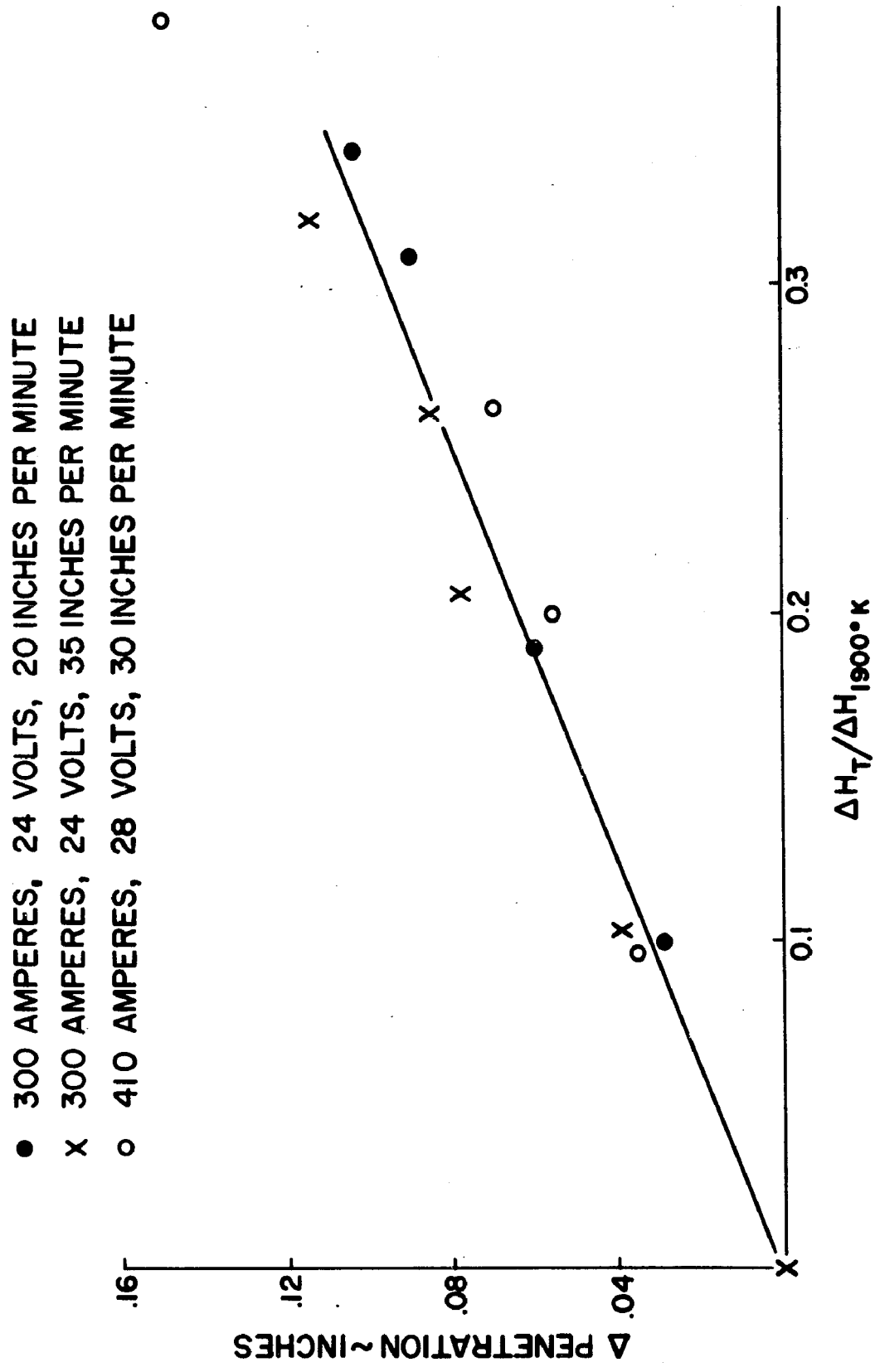

FIG. 36. INCREASE IN PENETRATION AS A FUNCTION OF $\Delta H_T/\Delta H_{1900°K}$ (RATIO OF ENTHALPY SUPPLIED BY PREHEAT TO ENTHALPY REQUIRED TO MELT AND SUPERHEAT WELD METAL.)

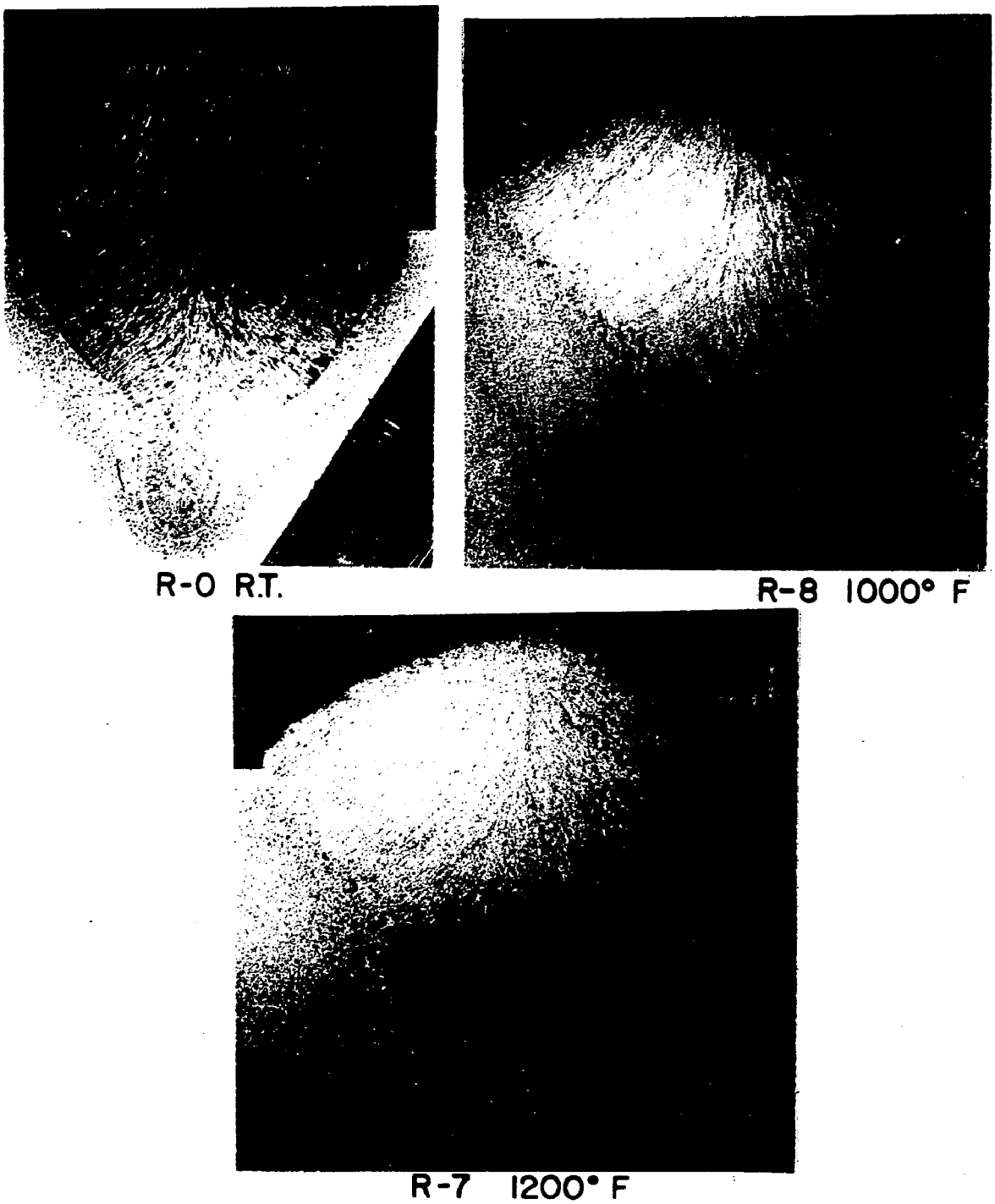

FIG. 37. EFFECT OF PREHEAT TEMPERATURE ON WELD CONTOURS PRODUCED AT 410 AMPERES, 28 VOLTS, 30 INCHES PER MINUTE. (~7X, NITAL ETCH)

● 300 AMPS, 24 VOLTS, 20 INCHES PER MINUTE
X 300 AMPS, 24 VOLTS, 35 INCHES PER MINUTE
o 410 AMPS, 28 VOLTS, 30 INCHES PER MINUTE

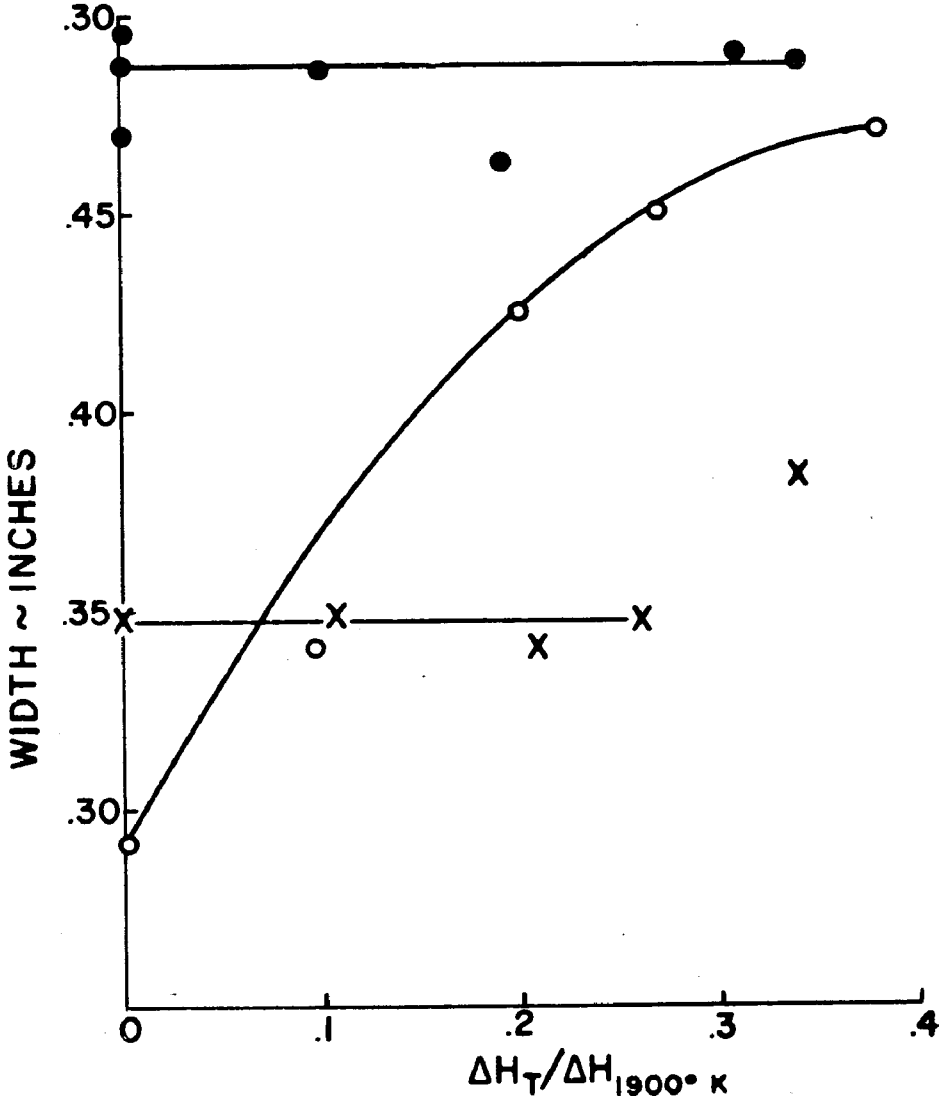

FIG. 38. WELD BEAD WIDTH AS A FUNCTION OF PREHEATING ENTHALPY PARAMETER.

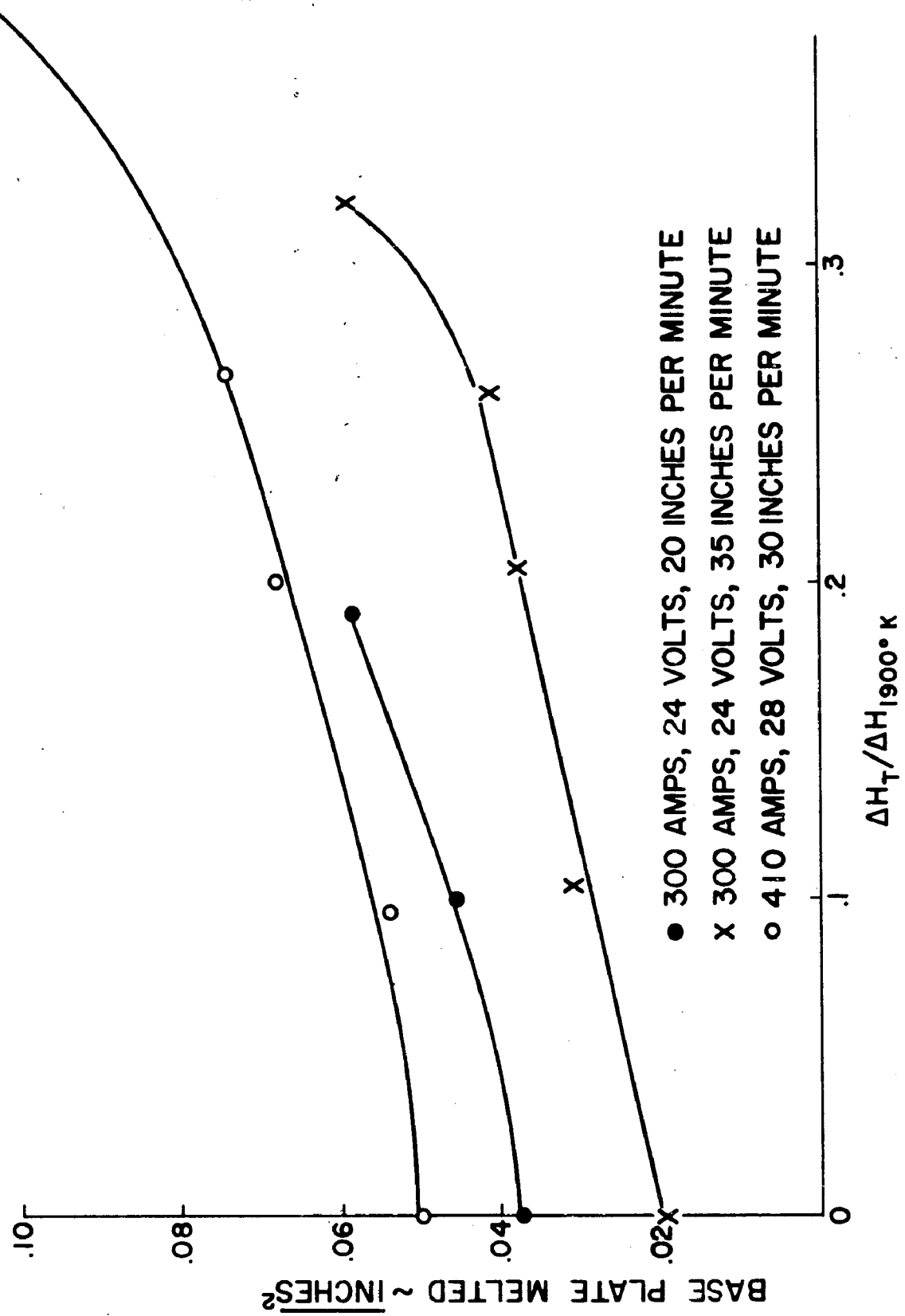

FIG. 39. BASE PLATE AREA MELTED AS A FUNCTION OF PREHEAT ENTHALPY PARAMETER.

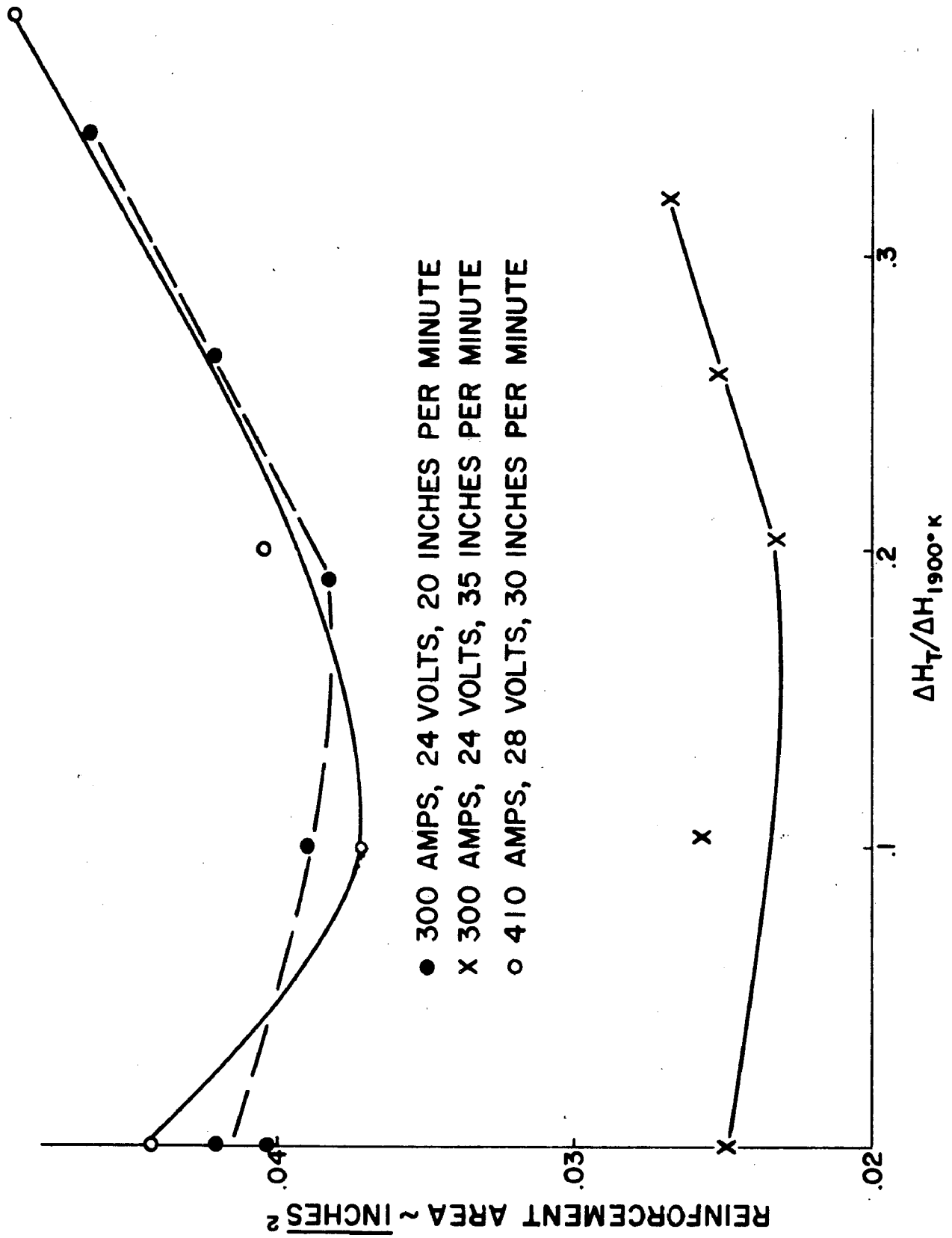

FIG. 40. REINFORCEMENT AREA AS A FUNCTION OF PREHEAT ENTHALPY PARAMETER.

● 300 AMPS, 24 VOLTS, 20 INCHES PER MINUTE

X 300 AMPS, 24 VOLTS, 35 INCHES PER MINUTE

○ 410 AMPS, 28 VOLTS, 30 INCHES PER MINUTE

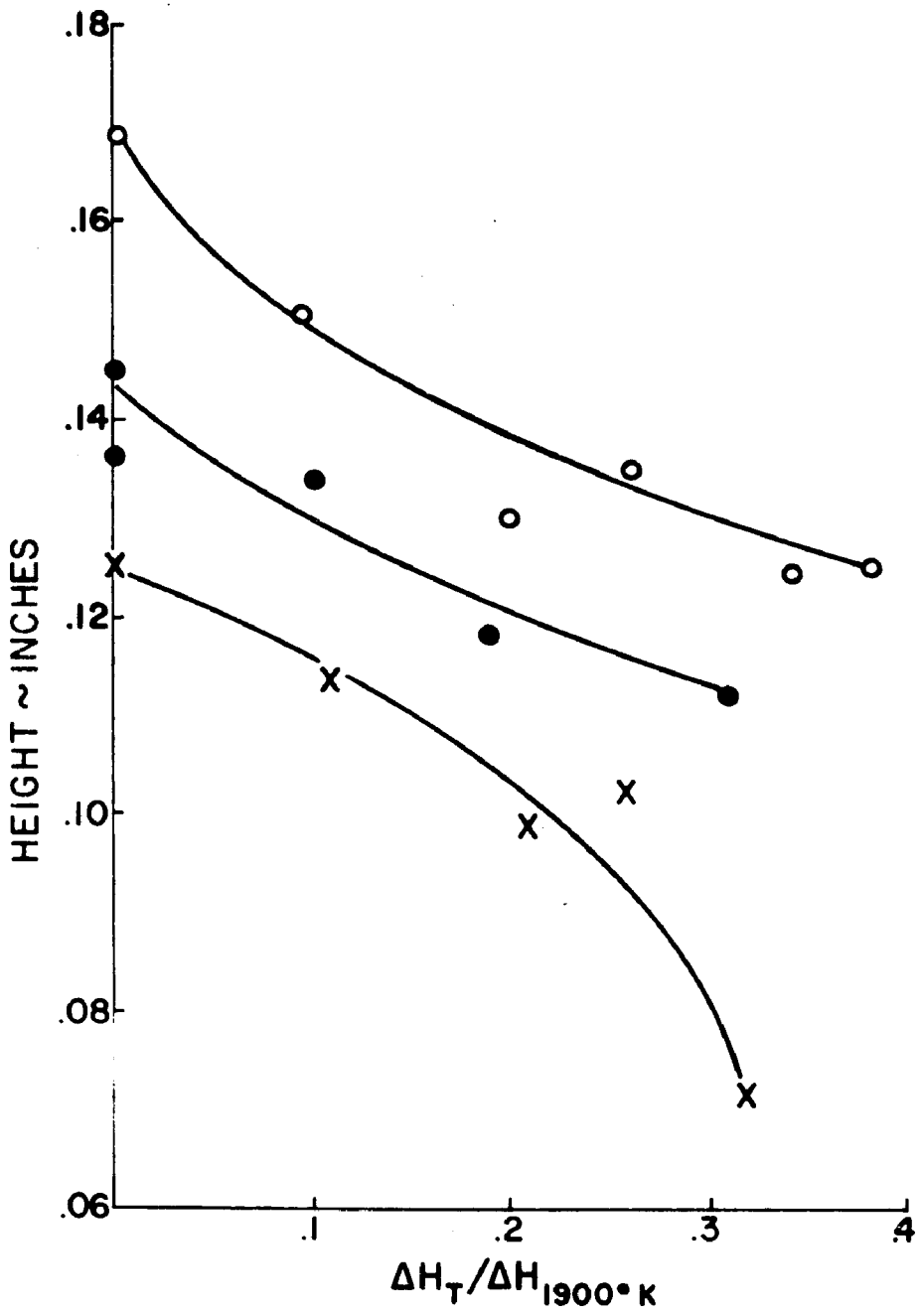

FIG. 41. WELD REINFORCEMENT HEIGHT AS A FUNCTION OF PREHEAT ENTHALPY PARAMETER.

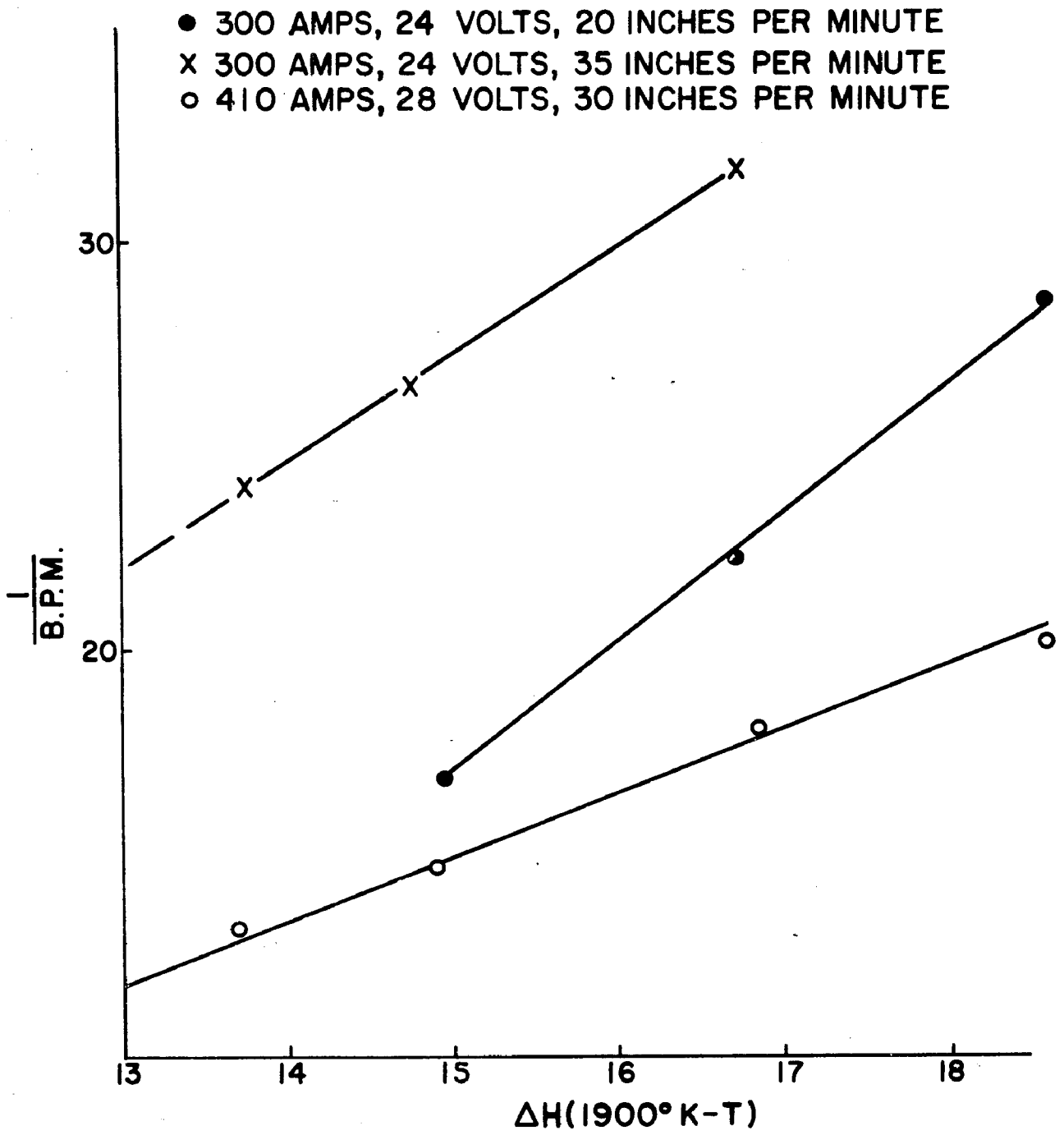

FIG. 42. RECIPROCAL OF BASE PLATE AREA MELTED AS A FUNCTION OF $\Delta H_{1900°K} - \Delta H_{\text{PREHEAT TEMPERATURE}}$ TO INDICATE HYPERBOLIC RELATION BETWEEN B.P.M. AND $\Delta H_{1900°K-T}$

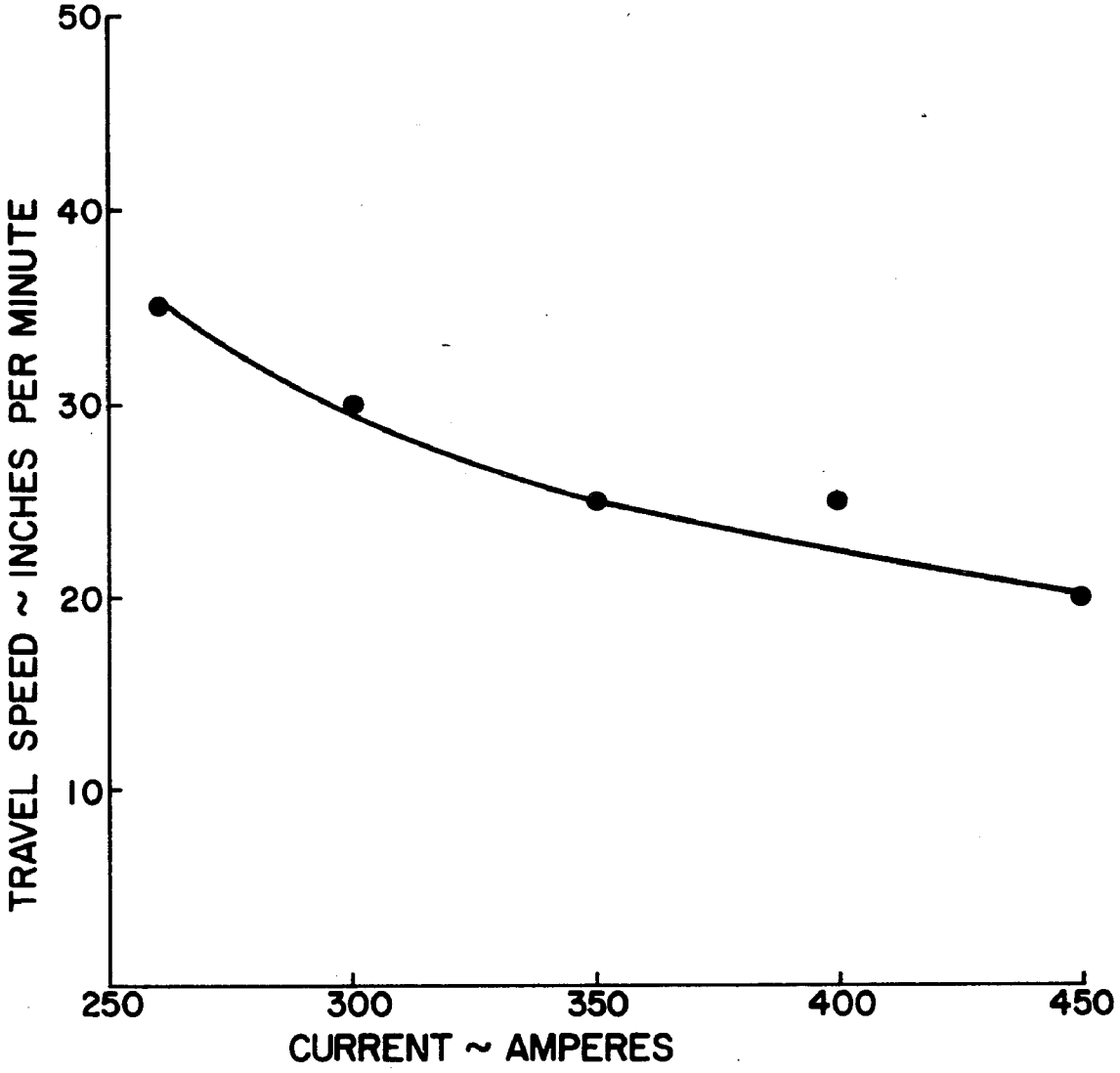

FIG. 43. MAXIMUM TRAVEL SPEED PRODUCING WELD BEAD FREE OF UNDERCUTTING AS A FUNCTION OF CURRENT LEVEL EMPLOYED.

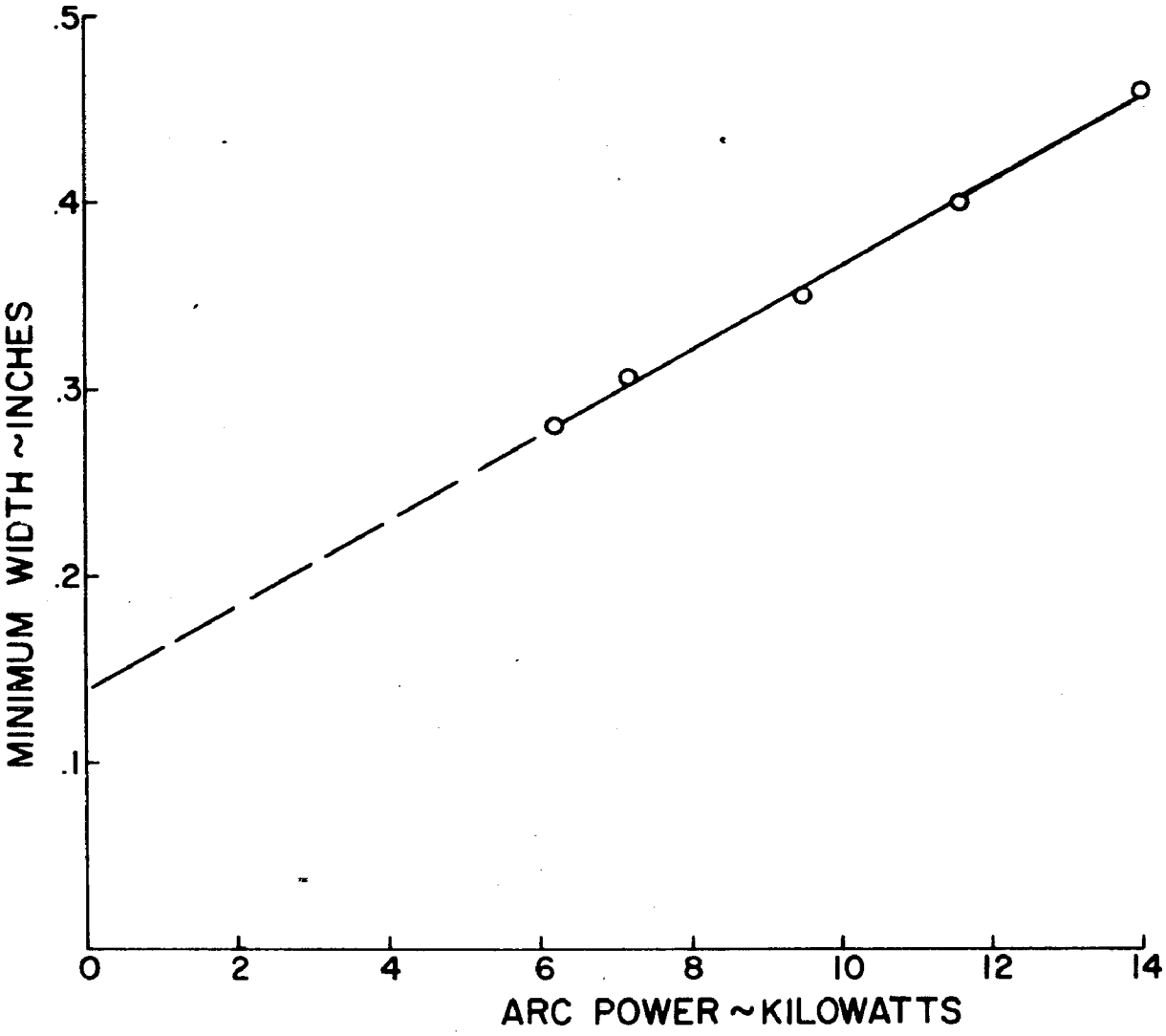

FIG. 44. MINIMUM WIDTH OF BASE PLATE MELTED AS A FUNCTION OF ARC POWER.

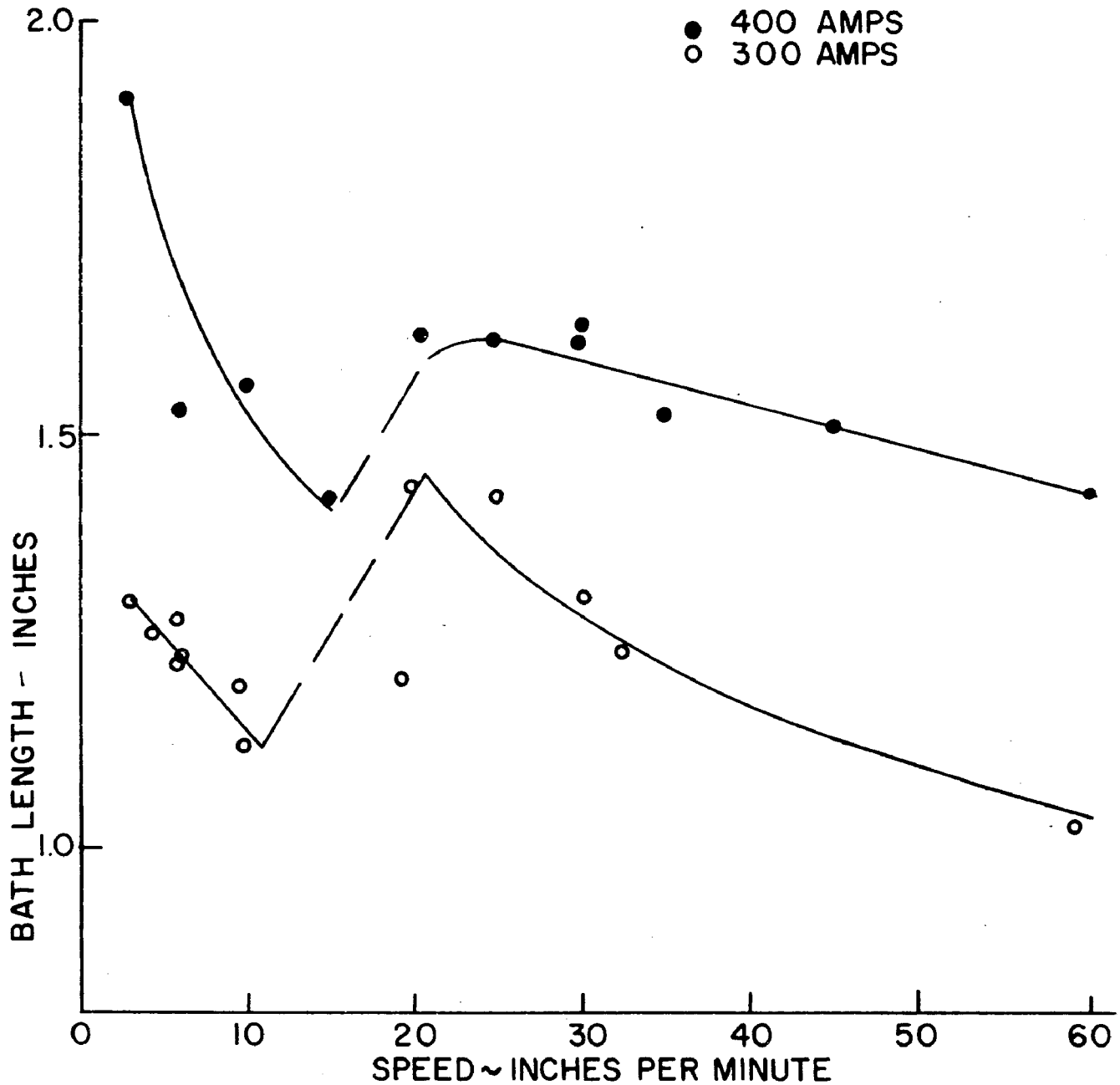

FIG. 45. BATH LENGTH, AS MEASURED IN CRATER, AS A FUNCTION OF TRAVEL SPEED.

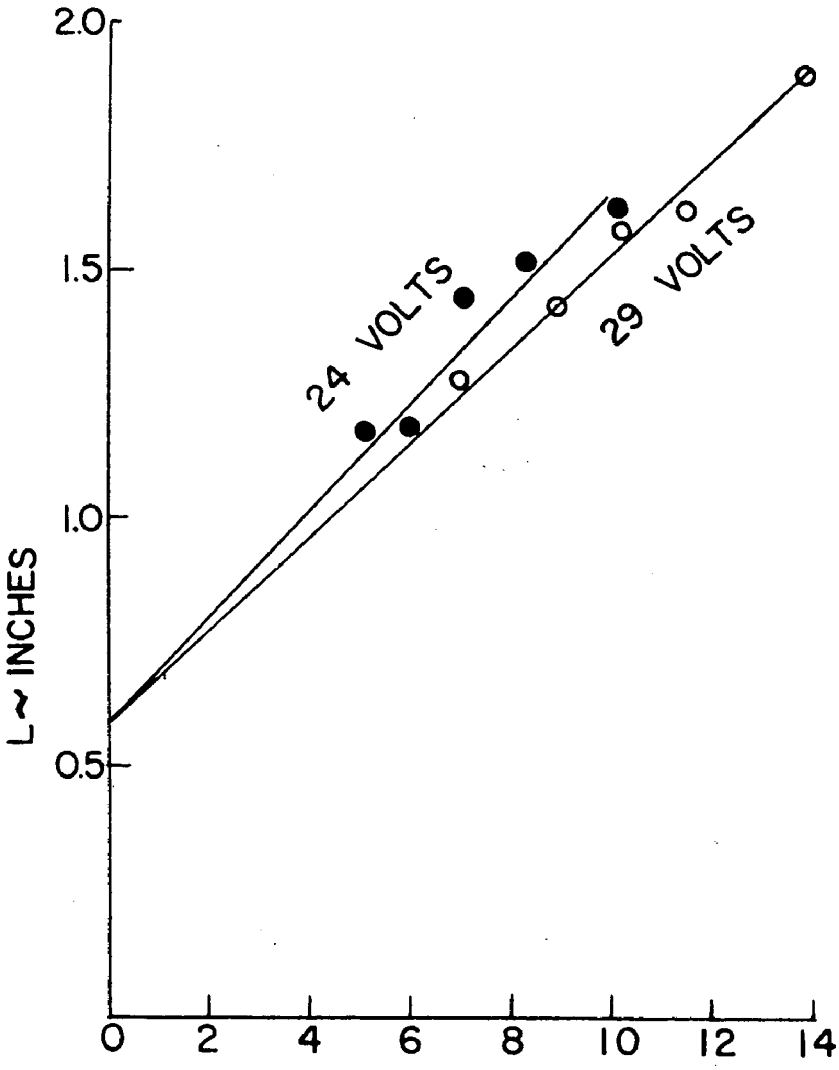

FIG. 46 BATH LENGTH, L, AS A FUNCTION OF ARC POWER AT TWO VOLTAGE LEVELS.

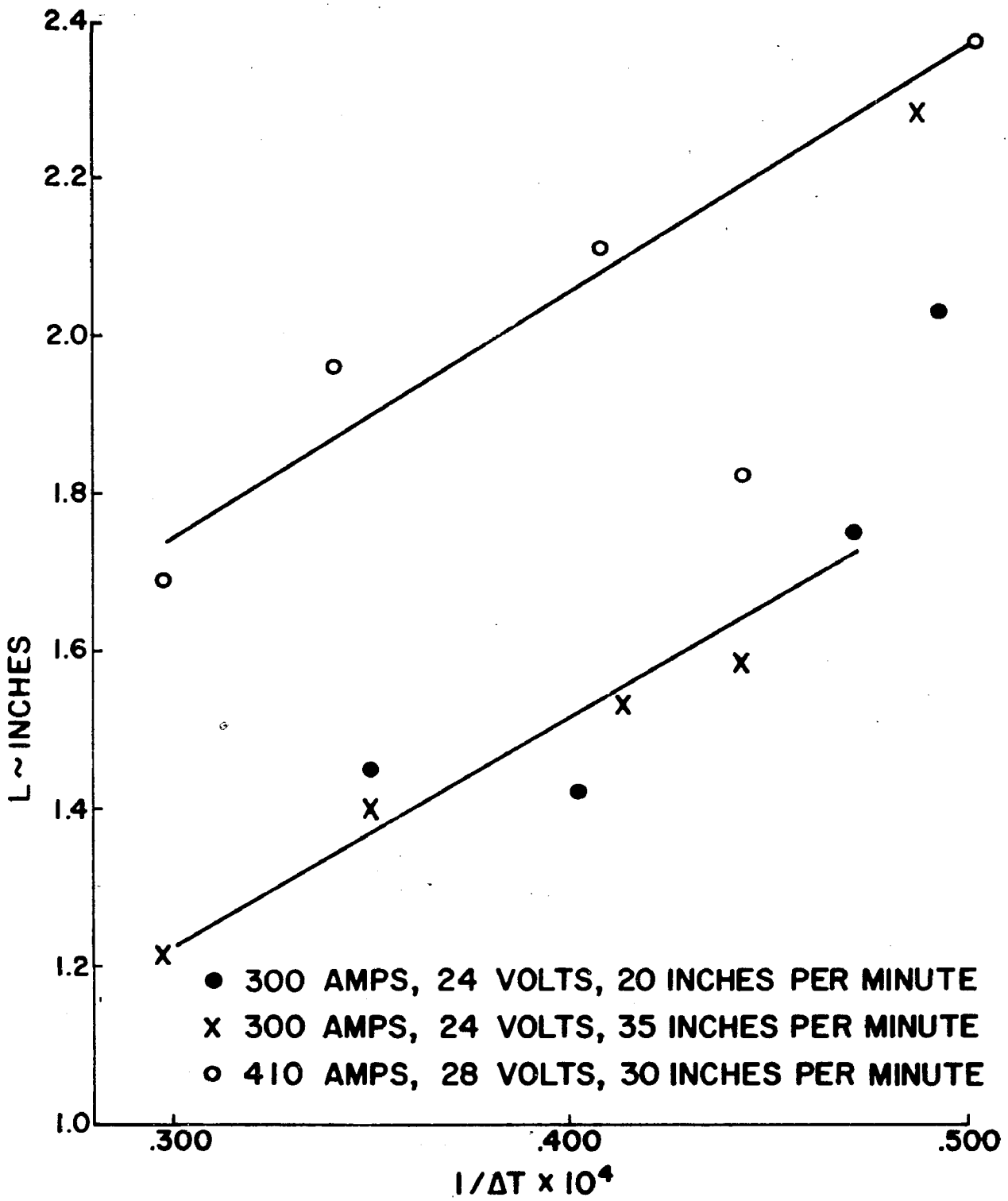

FIG. 47. BATH LENGTH AS A FUNCTION OF PREHEAT TEMPERATURE PARAMETER—

$$\frac{1}{[\text{Fe-C LIQUIDUS TEMP. (°K)} - \text{PREHEAT TEMP. (°K)}]} = \frac{1}{\Delta T}$$

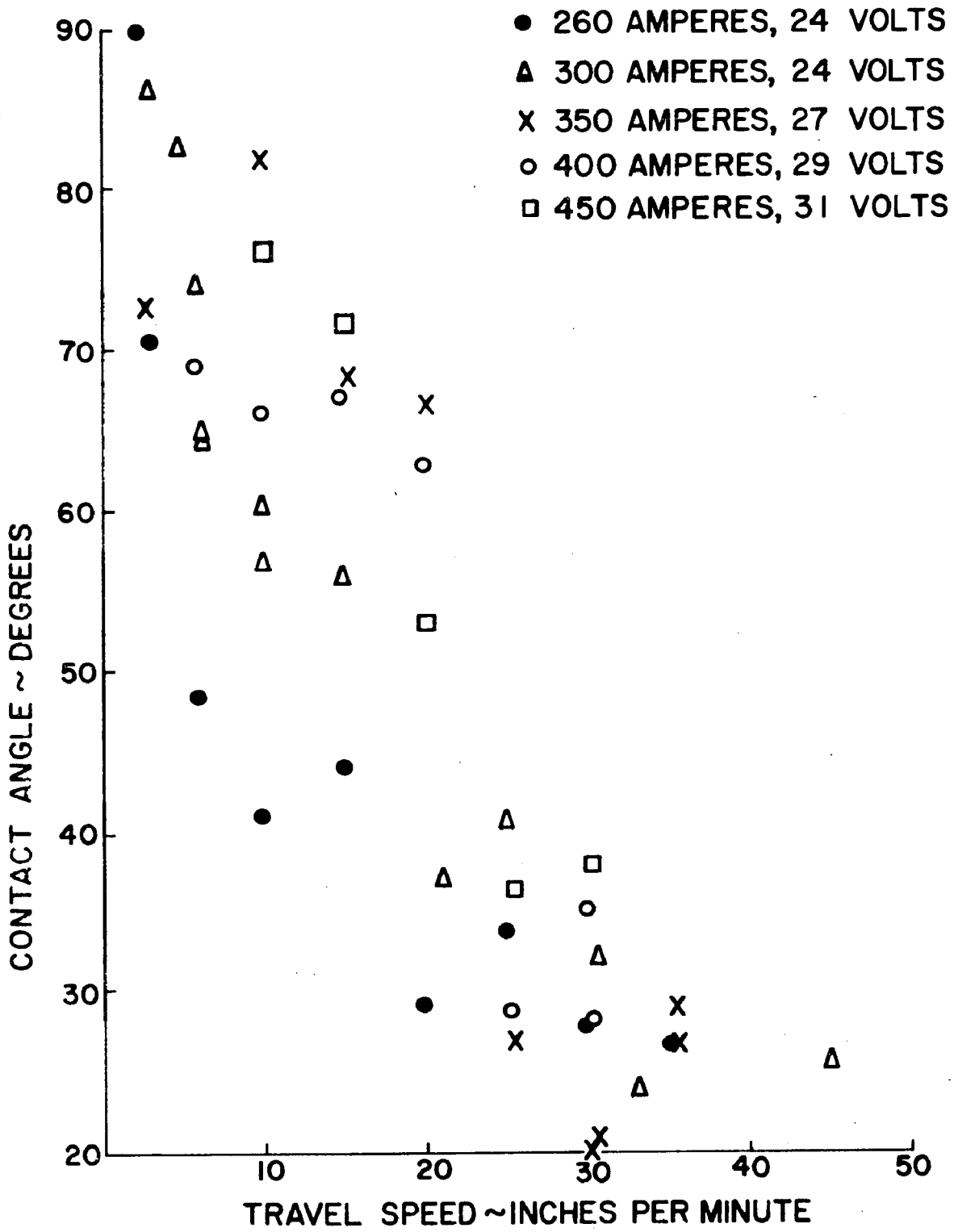

FIG. 48. AVERAGE WELD BEAD-BASE PLATE CONTACT ANGLE θ AS A FUNCTION OF TRAVEL SPEED.

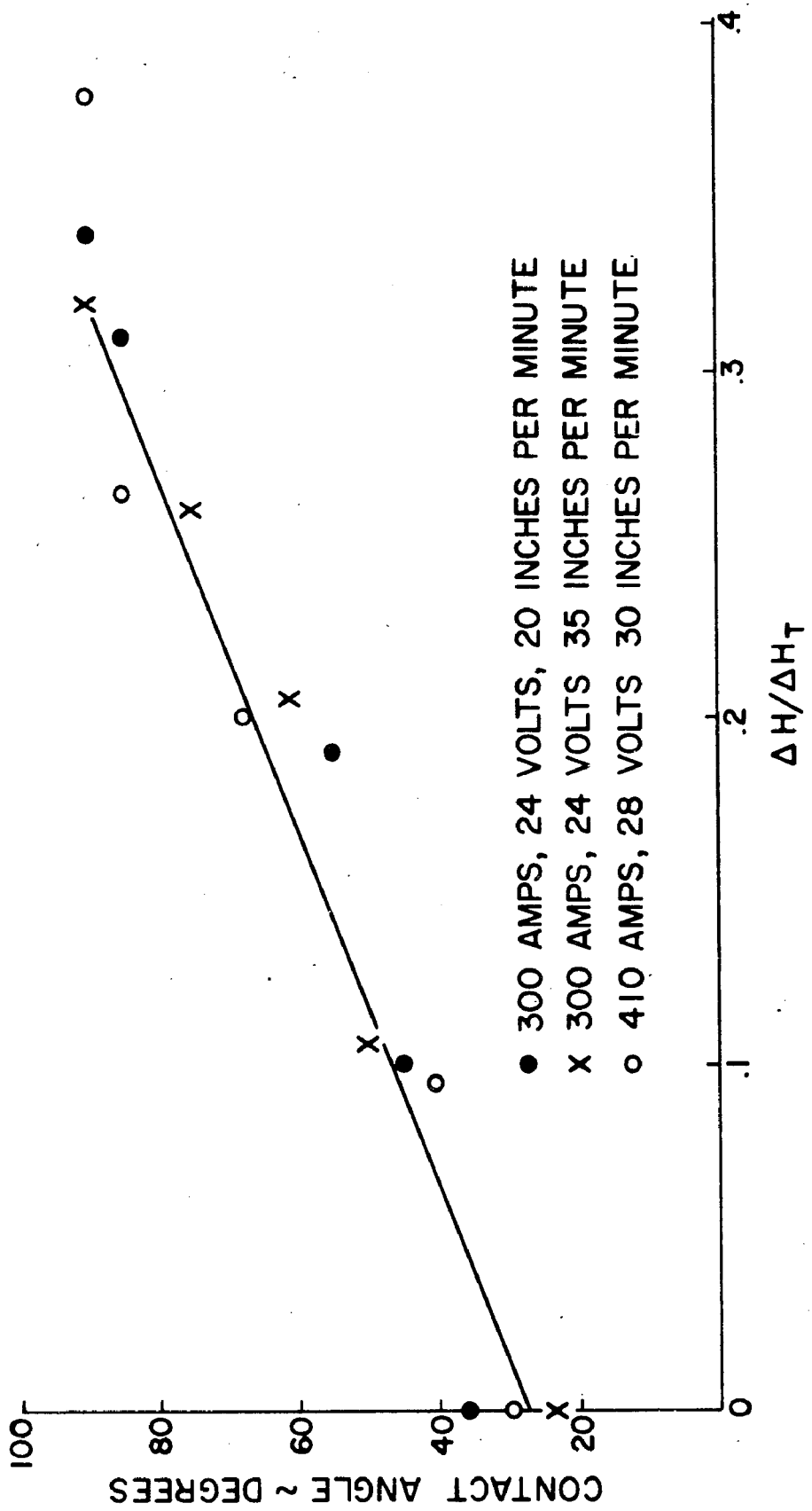

FIG. 49. WELD BEAD CONTACT ANGLE θ AS A FUNCTION OF PREHEAT ENTHALPY PARAMETER.

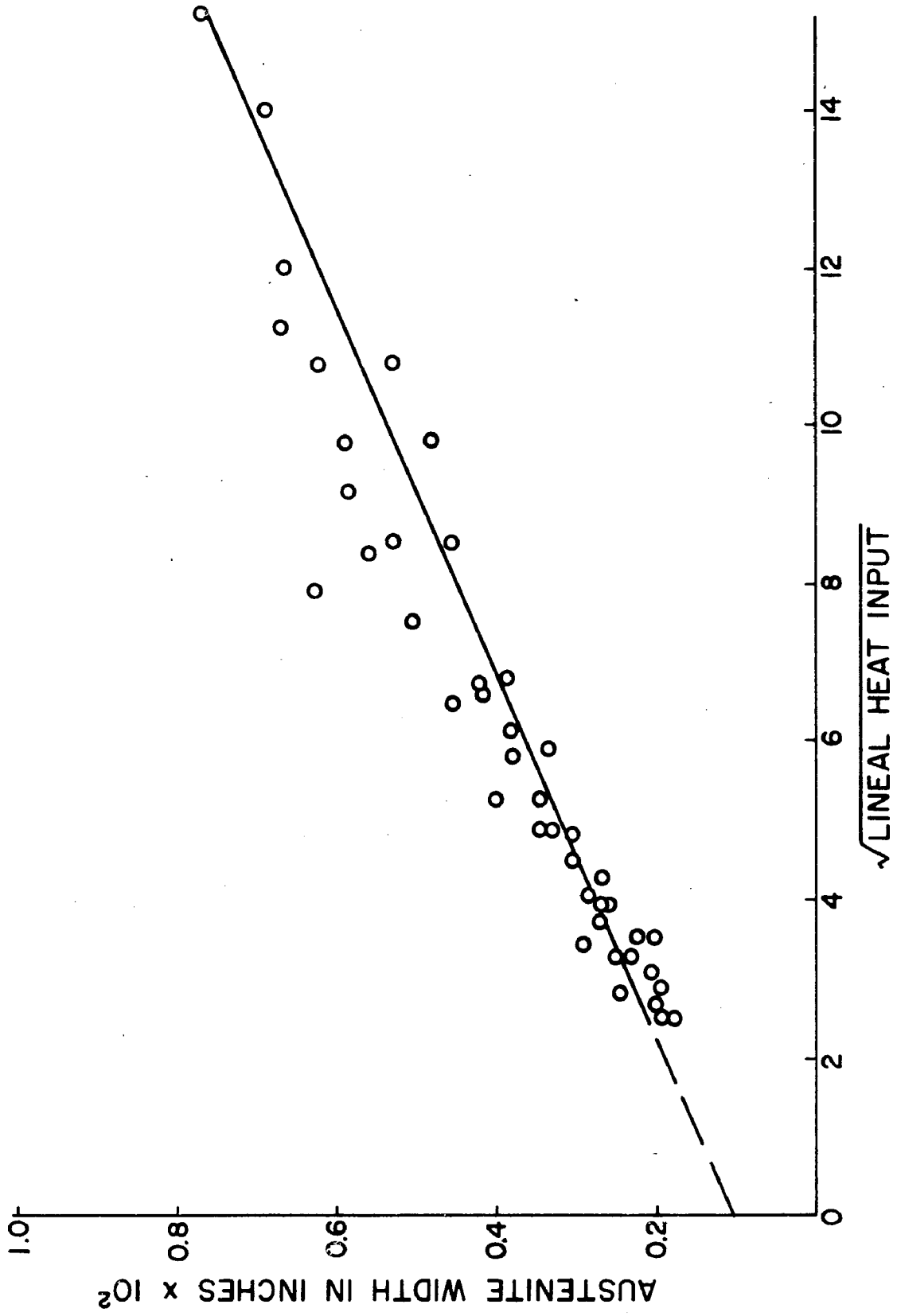

FIG. 50. AUSTENITE GRAIN SIZE, AS MEASURED AT LATERAL EXTREMITIES OF WELD IN DIRECTIONS ⊥ TO HEAT FLOW, AS FUNCTION OF $\sqrt{\text{HEAT INPUT}}$.

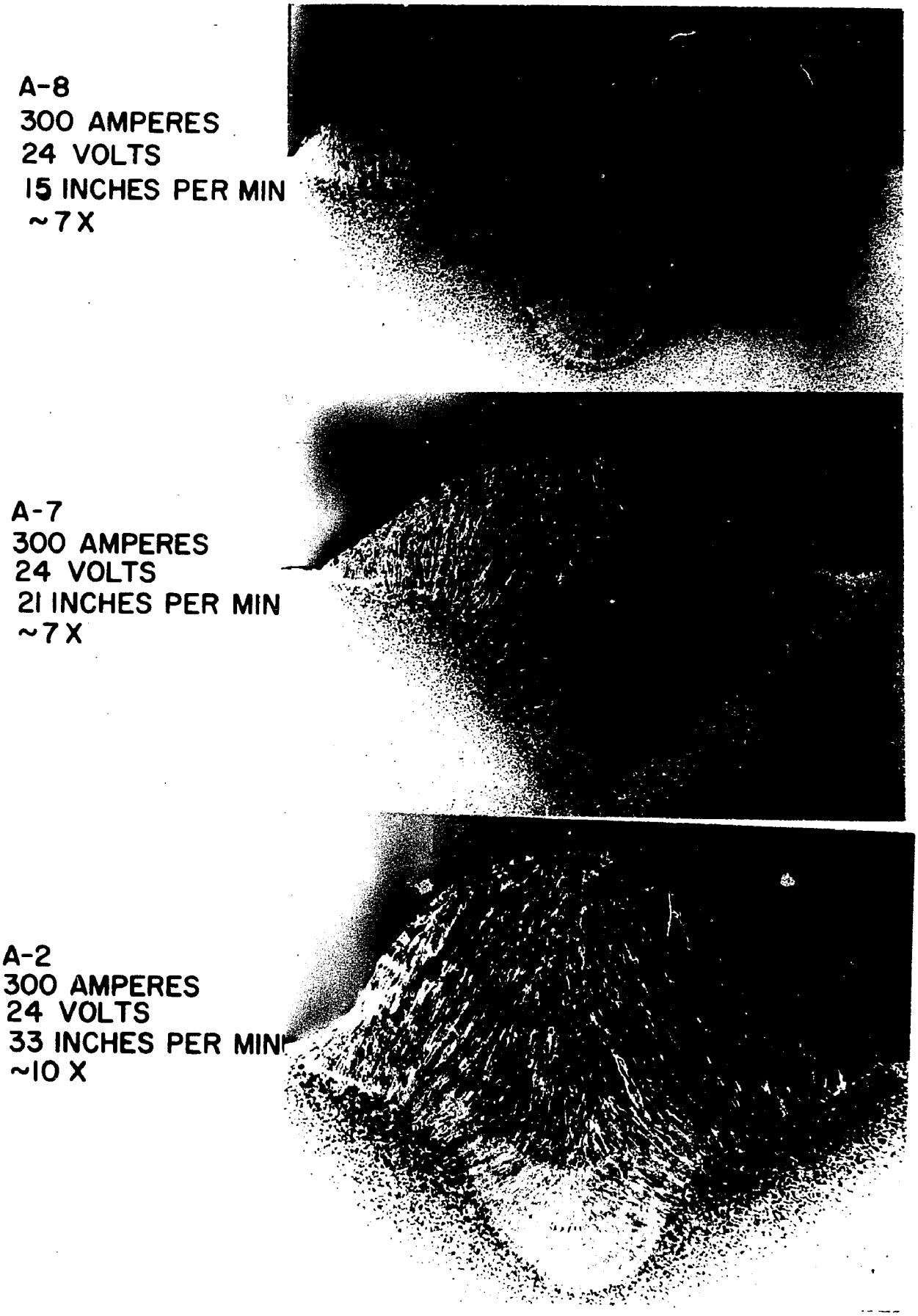

FIG. 51. REPRESENTATIVE TRANSVERSE AND LONGITUDINAL MACROGRAPHS.

A-8

TRAVEL DIRECTION

A-7

A-2

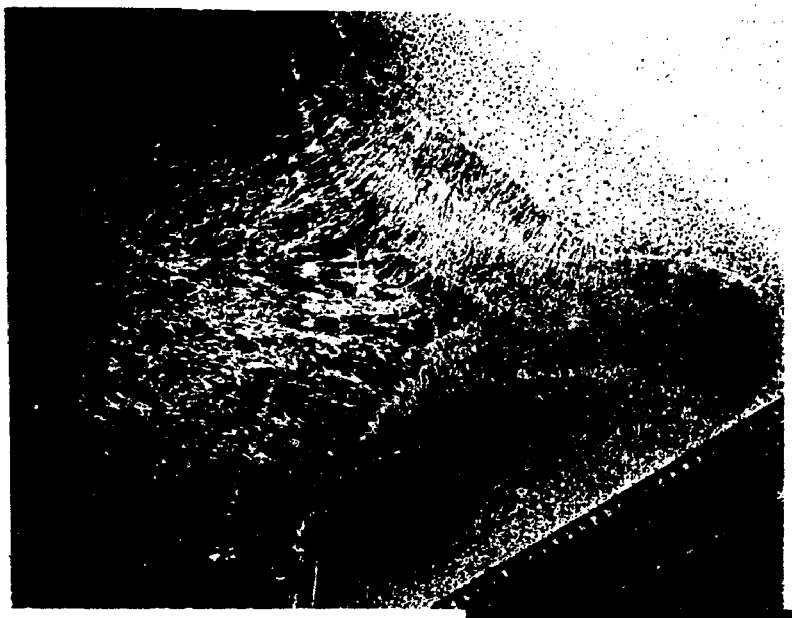

L-4
400 AMPERES
25 VOLTS
20 INCHES PER MINUTE
~8X

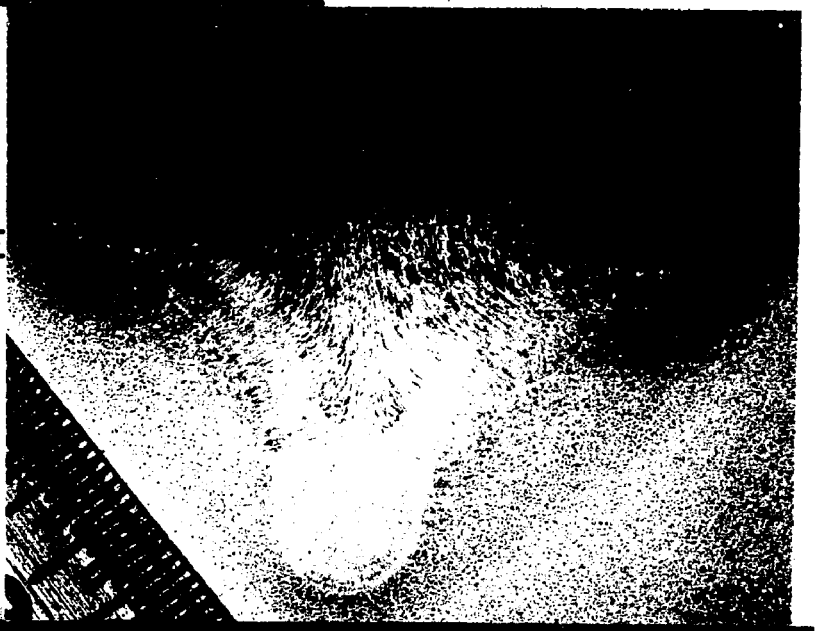

L-5
400 AMPERES
28 VOLTS
20 INCHES PER MINUTE
~7X

L-1
400 AMPERES
32 VOLTS
20 INCHES PER MINUTE
~7X

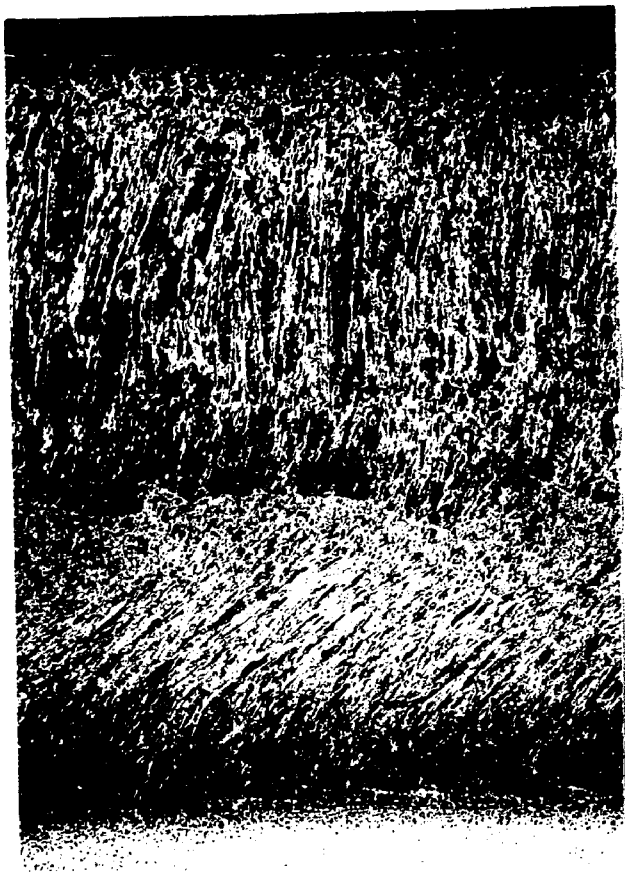

L-4 →

L-5

←

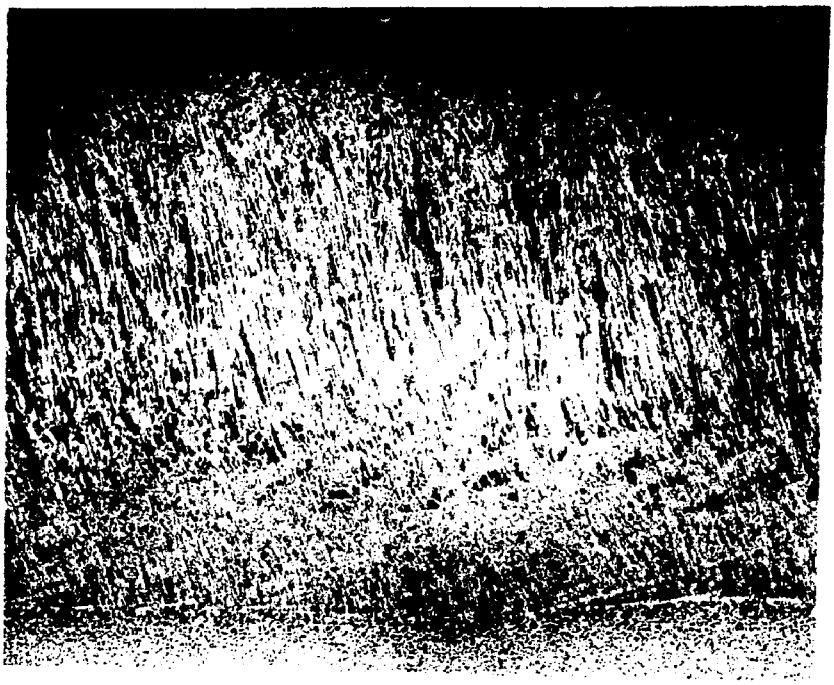

L-1

←

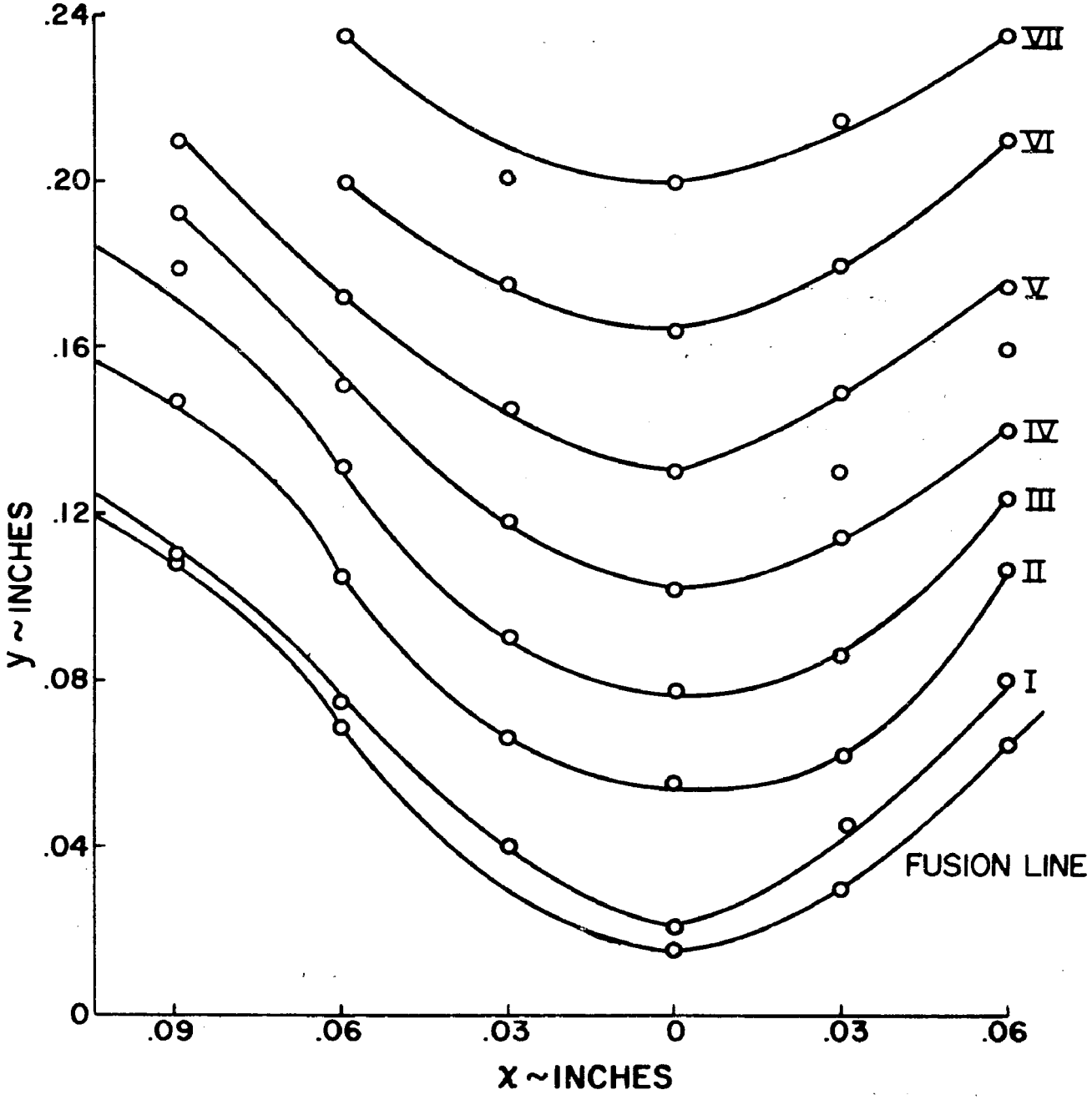

FIG. 52. MAP LOCATIONS OF MINIMA NOTED IN MICROHARDNESS TRAVERSES OF WELD A-2. X PARAMETER IS HORIZONTAL DISTANCE FROM WELD CENTER LINE-WHILE Y IS VERTICAL DISTANCE FROM ARBITRARY ORIGIN APPROXIMATELY 0.015" BELOW FUSION LINE. MINIMA INDICATED ARE GROUPED IN CONTOUR LINES I....VII WHOSE PERIODICITY AND SPACING STRONGLY RESEMBLE LAYER LINES NOTED IN THIS WELD BEAD. (SEE FIG. 51.)

FIG. 53. MACROSTRUCTURE OF WELD M32, PREPARED BY WELDING OVER 4% C IRON POWDER. NOTE WIDE VARIATION IN STRUCTURE FROM TOP TO BOTTOM OF WELD. (10 X – NITAL ETCHANT)

← TRAVEL DIRECTION

M-81
300 AMPERES, 24 VOLTS
15 INCHES PER MINUTE

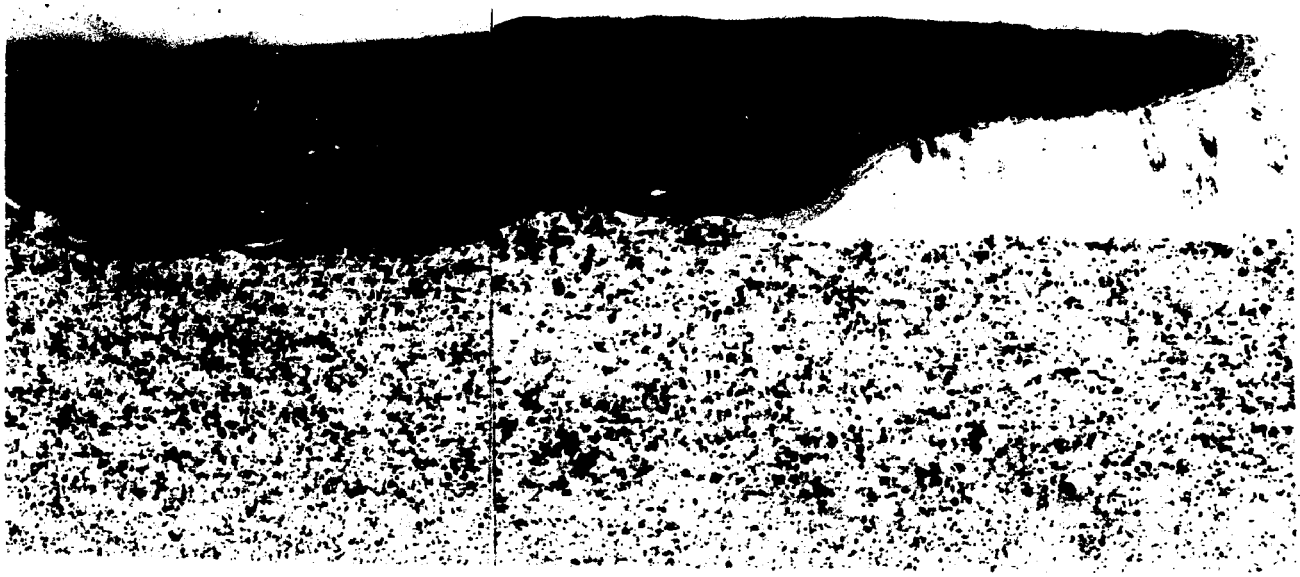

←

S-62
300 AMPERES, 24 VOLTS
6 INCHES PER MINUTE

FIG. 54. SULPHUR PRINTS OF WELDS PREPARED BY WELDING OVER IRON SULPHIDE POWDER. (ENLARGED 2 X)

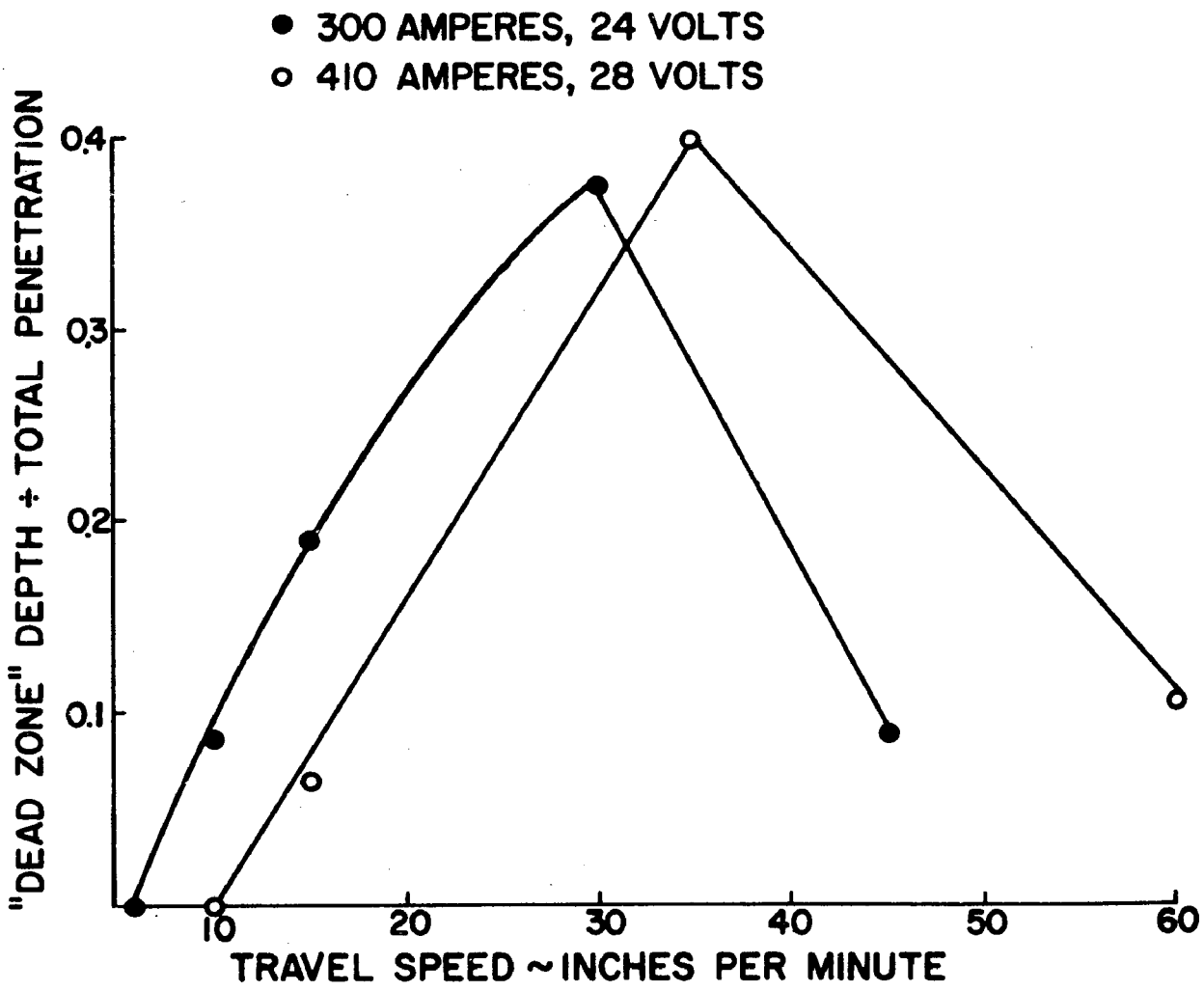

FIG. 55. EFFECT OF TRAVEL SPEED ON PROPORTION OF PENETRATION WHICH IS SULPHUR-FREE "DEAD ZONE".

References:

1. D. Rosenthal, Welding Journal, 17, (1938), 2s-83.
2. N. N. Rykalin, Die Warmegrundlagen des Schweissvorgantes, (The Theory of Heat Distribution in Arc Welding), Verlag Technik Berlin, (1952).
3. A. A. Wells, Welding Journal, 31, (1952) 263s-266s.
4. A. A. Erokhin, Izvestiia Akademii Nauk SSSR, 9, (1955), 125-136.
5. C. E. Jackson, Welding Journal, 39, (1960), 124s-145s.
6. N. Christensen, J. Chipman, Welding Research Bulletin, No. 15, Am. Welding Society, (1953).
7. N. Christensen, Distribution of Heat around Finite Moving Sources, Final Report, Contract DA 91-508-EUC-378, (1960).
8. D. M. Rabkin, British Welding Journal, 6, (1959), 132-137.
9. I. I. Frumin, Avtomiticheskaya Svarka, 5, (1955), 39-44.
10. L. S. Livshits et al, Metallovedenie i Obratotka Metallov, (1958), 26-28.
11. B. Bruk et al, "A Study of Element Redistribution in Metal Alloys and Welds by Autoradiographic and Radiometric Methods", Peaceful Uses of Atomic Energy-Second Geneva Conference, 19, The Use of Isotopes-Industrial Uses, 219-237.

12. G. L. Petrov, Trud Leningr. Politekh. Inst. 199, (1958), 143-156.

13. S. M. Makin et al, British Welding Journal, 7, (1960), 595-599.

14. A. M. Makara and A. A. Rossoshinskii, Avtomaticheskaya Svarka, 9, (1956), 65-76.

15. B. A. Movchan, Avtomaticheskaya Svarka, 10, (1957) 75-82.

16. L. A. Poznyak, Avtomaticheskaya Svarka, 11, (1958) 65-71.

17. A. R. Muir, British Welding Journal, 4, (1957) 323-330.

18. A. Lesnewich, Welding Journal, 37, (1958) 418-425.

19. C. E. Jackson, A. E. Shrubsall, Welding Journal, 32 (1953), 172s-178s.

20. R. T. Breymeier, Welding Journal, 31, (1952), 393-399.

21. B. H. Baker et al, British Welding Journal, 8, (1961) 151-168.

22. P. E. Brown, C. M. Adams, Jr., Welding Journal, 39, (1960), 520-524s.

23. A. Lesnewich, Welding Journal, 34, (1955), 1167-1179.

Vita:

Harold S. Gurev was born in Cleveland, Ohio, on March 28, 1935, the son of Mr. and Mrs. Elias Gurev. He was educated in the Cleveland Heights public school system and received his Bachelor of Science from Case Institute of Technology in metallurgical engineering in 1957. The degree of Master of Science was earned from Case Institute of Technology in 1959 in the field of physical metallurgy. The author married the former Evelyn Olkes in 1957.

Graduate study in metallurgy at Lehigh University was conducted while the author was the Linde Company Fellow and an instructor in the metallurgy department. The author is a member of Tau Beta Pi and Sigma Xi.